THESIS

Submitted in fulfillment of the requirements for the

Diploma of Doctorate

by:

Kacem ZEREG

Theme:

EVALUATION OF AEROSOLS' EFFECT ON THE EFFICIENCY OF SOLAR TOWER POWER PLANTS IN ALGERIA

Domain: Matter Sciences
Branch: Physics
Specialty: Physics of Energetics
Title of the Formation: Fluid Dynamics and Energetics

Defended on 02 /11 / 2023.

In front of the jury:

President:	Belkacem ADOUANE	Professor	University of Batna 1
Supervisor:	Mounir AKSAS	Professor	HNSREESD
Co-supervisor:	Amor GAMA	Research Director	URAER-CDER
Examiners:	Saadi BOUGOUL	Professor	University of Batna 1
	Abdelmoumene Hakim BENMACHICHE	Professor	University of Batna 1

Abstract

The environmental concerns about greenhouse gases and the consequent climate change urge the transition towards cleaner, renewable energy sources. Solar energy applications are promising to play an important role in energy transition, especially photovoltaics (PV) and concentrated solar power (CSP) technologies. CSP plants are of interest, particularly solar tower plants, thanks to the possibility of reaching high temperatures, and thus more important efficiencies. The Algerian Sahara has a high potential to host solar projects in general and CSP ones in particular thanks to its high annual levels of incident, direct solar irradiance, and there already are pilot projects to assess this potential, however, the environmental hostility of the Sahara requires the prior evaluation of the possible optical losses suffered by solar mirrors due to the presence of high aerosols' loads and dust particles. Such particles would attenuate considerably the incident solar energy, either by atmospheric extinction due to suspended particles, or due to the deposition of these soiling particles on the surfaces of solar mirrors.

In the present thesis, we make a first step towards the evaluation of reflectivity losses of solar tower's heliostats under Saharan climate (since this issue has never been studied in Algeria), and this through the first outdoor heliostats' soiling campaign at a CSP-suitable site in the province of Laghouat, we also explore soiling mitigation approaches that are water-economic such as coatings. To do so, we used an experimental setup to expose several solar mirrors to outdoor arid climate conditions of Laghouat city. The trends of the measured reflectivity are consistent with the theoretical and bibliographic background. Also, the physical and chemical properties of dust particles -deposited on the mirrors- are investigated through the characterization by scanning electron microscopy (SEM), energy dispersive X-ray spectroscopy (EDX), and X-rays diffraction (XRD), the desired properties were investigated in the Technical Platform for Physical and Chemical Analysis (CRAPC-PTAPC) located in Laghouat as well, next to where the experimental setup was installed. Another important contribution of the present thesis is publishing the first paper to review the literature of dust-related problems for CSP, unlike photovoltaic technology which benefited from multiple reviews. In our future work, we plan to geographically extend the present study for the purpose of assessing the potential of different Algerian regions to host concentrated solar power plants in general, and solar tower projects in particular.

Key words: Aerosols, Concentrated solar power (CSP), Extinction, Reflectivity loss, Soiling, Atmospheric turbidity.

ملخص

إن المخاوف البيئية بشأن الغازات الدفيئة وما يترتب على ذلك من تغير مناخي تحث على الانتقال نحو مصادر طاقة متجددة ونظيفة. تطبيقات الطاقة الشمسية تعد بلعب دور مهم في الانتقال الطاقي، خاصةً تقنيات الخلايا الكهروضوئية والطاقة الشمسية المركزة. تحظى محطات الطاقة الشمسية المركزة بالاهتمام، خاصة محطات الأبراج الشمسية، وذلك بفضل إمكانية الوصول إلى درجات حرارة عالية، وبالتالي مردود عال. تتمتع الجزائر بإمكانيات عالية لاستضافة مشاريع الطاقة الشمسية بشكل عام ومشاريع الطاقة الشمسية المركزة بشكل خاص بفضل المستويات العالية الواردة سنويا من الإشعاعات الشمسية الناظمة، وهناك بالفعل مشاريع تجريبية لتقييم هذه الإمكانات، ومع ذلك، فإن البيئة الصحراوية القاسية تتطلب التقييم المسبق للخسائر البصرية المحتملة التي قد تتعرض لها المرايا الشمسية بسبب وجود نسب عالية من الهباء الجوي وجسيمات الغبار. ستضعف هذه الجسيمات إلى حد كبير الطاقة الشمسية، إما بسبب طريق الاندثار الجوي الناجم عن جسيمات الهباء الجوي، أو بسبب ترسب هذه الجسيمات على أسطح المرايا الشمسية.

في هاته الأطروحة، نتخذ خطوة أولى نحو تقييم خسائر الانعكاسية للمرايا الشمسية -التي تعد عنصرا حيويا لمحطات الأبراج الشمسية- في ظل المناخ الصحراوي (حيث لم يتم دراسة هذه المسألة من قبل في الجزائر)، وذلك من خلال أول حملة -في الهواء الطلق- لدراسة أثر المناخ الصحراوي على انعكاسية المرايا الشمسية، الحملة التجريبية كانت في بيئة مناسبة لمحطات الطاقة الشمسية في ولاية الأغواط، نستكشف أيضًا طرق أكثر اقتصادا للموارد البشرية والمائية لتخفيف تلوث أسطح المرايا كالأطلية. للقيام بذلك، استخدمنا نظاما تجريبيًا لتعريض العديد من المرايا الشمسية للظروف المناخية الجافة لمدينة الأغواط. تتوافق الانعكاسية المقاسة مع الخلفية النظرية والمرجعية للموضوع. أيضًا، تفحصنا الخصائص الفيزيائية والكيميائية لجزيئات الغبار ـ المترسبة على المرايا ـ عن طريق نتائج المسح المجهري الإلكتروني (SEM)، والتحليل الطيفي للأشعة السينية المشتتة للطاقة (EDX)، وحيود الأشعة السينية (XRD)، وتم فحص الخصائص المرغوبة في المنصة التقنية للتحليلات الفيزيائية والكيميائية (CRAPC-PTAPC) الموجودة في الأغواط أيضًا، بجوار مكان تثبيت النظام التجريبي. مساهمة مهمة أخرى للأطروحة الحالية هي نشر الورقة الأولى لمراجعة الأبحاث المتعلقة بالمشاكل الناجمة عن الغبار في محطات الطاقة الشمسية المركزة، على عكس التكنولوجيا الكهروضوئية التي استفادت من مراجعات عديدة. نخطط مستقبلا لتوسيع الدراسة الحالية جغرافيًا بغرض تقييم إمكانات مختلف المناطق الجزائرية لاستضافة محطات الطاقة الشمسية المركزة بشكل عام، ومشاريع الأبراج الشمسية بشكل خاص.

الكلمات المفتاحية: الهباء، الطاقة الشمسية المركزة، الاندثار، خسائر الانعكاسية، التلوث، الكدر الجوي.

*"Over every knowledgeable person is **One** who knows."*

Holy Quran, 12:76.

This thesis is dedicated to my very precious parents, for their unconditioned support and unlimited love, and to my dearest brothers and sisters.

Acknowledgments

Table of Contents

List of Figures

List of Tables

Nomenclature

Symbols

A	Area (m^2)
A_{ij}	Hamaker constant (J)
A_{nr}	Total non-reflective mirror area (m^2)
A_{block}	Blocked mirror area (m^2)
A_{shad}	Shaded mirror area (m^2)
B	Boltzmann constant (SI)
C_a	Geometric concentration ratio (-)
C_c	Correction coefficient for slip (-)
C_D	Drag coefficient (-)
C_{Dm}	Drag coefficient for momentum (-)
C_d	Concentration of dust ($\mu g/m^3$)
C_f	Energetic concentration ratio (-)
C_s	Correction factor for sticking particles (-)
c_r	Concentration ratio (-)
D_{iff}	Diffusivity (m^2/s)
D_p	Dust particle diameter (microns)
d_s	Minimum distance of separation in vacuum (nm)
E_{br}	Brownian diffusion factor (-)
E_{imp}	Inertial impaction factor (-)
F	Dust deposition flux ($\mu g/m^2/s$)
F_{adh}	Adhesion force (N)
F_d	Aerodynamic drag force (N)
F_g	Gravitational force (N)
h	Height (m)
I_0	Normal incident extraterrestrial irradiance (W/m^2)
I_{0C}	Solar constant (W/m^2)
$I_\lambda(I_{\lambda,b})$	Spectral (blackbody) intensity of solar radiation ($W/m^2/microns$)
$I_{\lambda,rec}$	Spectral intensity of the received solar radiation ($W/m^2/microns$)

K	Von Karman constant (-)
Kn	Knudsen number (-)
l	Path traversed through the atmosphere by the DNI (m)
M	Mass of dust particles (kg)
m	Optical mass
N_j	Julien day (-)
n	Refraction index (-)
$\hat{n}$	Normal (-)
Q_s	Radiative solar energy (J)
$\dot{Q}_s$	Radiative solar power (W)
$\dot{Q}_{rec}$	Received radiative power (W)
$\dot{q}_{\lambda,s}$	Spectral flux of solar radiation (W/m^2/microns)
P	Local pressure (mbar)
Re	Reynolds number (-)
$\vec{r}$	Position (m)
r_a	Aerodynamic resistance (s/m)
r_b	Quasi-laminar boundary resistance (s/m)
r_s	Radius of contact at separation (microns)
Sc	Schmidt number (-)
St	Stokes number (-)
$\hat{s}$	Direction (-)
T_{air}	Air temperature (K)
T_L	Linke's turbidity factor (-)
t	Time (s)
U_W	Undisturbed wind velocity (m/s)
u_*	Velocity of friction (m/s)
W_{adh}	Adhesion work (J)
Z	Solar zenith angle (-)
z	Reference height (m)
z_0	Height of homogenous atmosphere (m)

z_r	Surface roughness (m)

Greek symbols

α	Angstrom's exponent (-)
β	Angstrom's coefficient (microns$^{\alpha}$)
β_{λ}	Coefficient of spectral extinction (-)
δ_{CDA}	Optical depth of the clean dry atmosphere (-)
ε_0	Empirical constant (-)
η	Efficiency (-)
θ	Tilt angle (-)
κ_{λ}	Coefficient of spectral absorption (-)
λ	Wavelength (microns)
λ_p	Mean free path (microns)
μ_{air}	Dynamic viscosity of air (kg/m/s)
ϑ_{air}	Kinematic viscosity of air (m^2/s)
v_d	Deposition velocity of dust (m/s)
v_g	Deposition velocity due to gravity (m/s)
v_t	Deposition velocity due to turbulence and Brownian motion (m/s)
ρ	Reflectivity of the soiled mirror (-)
ρ_0	Density of the homogenous atmosphere (kg/m^3)
ρ_{air}	Density of air (kg/m^3)
ρ_{atm}	Density of the atmosphere (kg/m^3)
ρ_c	Reflectivity of the clean mirror (-)
ρ_p	Density of dust particles (kg/m^3)
$\rho_{\lambda,mir}$	Spectral bi-directional reflection function
$\sigma_{s,\lambda}$	Coefficient of spectral scattering (-)
τ	Optical depth (-)
τ_{aer}	Aerosols' optical depth (-)
τ_{wall}	Wall shear stress (N/m^2)
Φ_{λ}	Phase function for scattering
φ	Angle between the incident beam radiation and the surface's normal

Ω	Solid angle (-)	

Subscripts

d	Dust	
g	Gravity	
h	Height	
i	Incidence	
r	Reflection	
rec	Receiver	
$refs$	Reflectors	
s	Solar	
sfc	Surface	
TOA	Top of atmosphere	
λ	Spectral	

Glossary

A

AM	Air Mass
AOD	Aerosols' Optical Depth

C

CSP	Concentrating Solar Power

D

DNI	Direct Normal Irradiance

L

LF	Linear Fresnel

P

PD	Parabolic Dish
PM	Particulate Matter
PT	Parabolic Trough
PV	Photovoltaic(s)

S

ST	Solar Tower

INTRODUCTION

Research motivation

Critical environmental impacts of global climate change urge the transition towards cleaner renewable energy sources, especially after the reported 1% increase -reflecting the historical record of 37.5 billion tones- in global carbon dioxide emissions (CO_2) following the unexpected decrease imposed by the COVID-19 pandemic. In fact, these numbers announced by scientists at the United Nations Climate Change Conference of the Parties 2022 (COP27) in Sharm El-Sheikh, Egypt, are due to, among other factors, the increased European consumption of coal in an attempt to fix their energy shortage, consequent to the geopolitical situation in Ukraine. Another contributing factor is the spike in oil consumption caused by the resumption of air traffic after the lift of governmental travel restrictions (Tollefson, 2022). The 2015 Paris Agreement aimed to limit the climate change by keeping the global warming below 2 °C in comparison to pre-industrial levels, and this as a first step towards the ideal -yet still possible- goal of limiting the global warming to 1.5 °C by reaching net-zero and, furthermore, net-negative CO_2 emissions; the deployment of sustainable power plants that use renewable energy resources is required to achieve needed global warming limits (Park and Kug, 2022; Slamersak et al., 2022).

Solar energy is the most available renewable energy resource, and solar technologies and systems are being investigated, deployed, and improved in order to lighten the increasing environmental concerns; photovoltaic (PV) and Concentrating Solar Power (CSP) technologies are among the promising solar applications (Behar et al., 2013; Hachicha et al., 2019; Yettou et al., 2014). CSP technologies are based on the intense concentration of solar radiation by large fields of different configurations of reflectors (more details in the next section), which allows the conversion of the radiative energy of sunlight into thermal energy, and thus replace the process of hydro carburants' combustion (Avilat-Marin, 2011; Pérez-Burgos et al., 2017), up to 2021, CSP technologies lowered CO_2 emissions by 12 Mt/year (Shahabuddin et al., 2021). Among CSP technologies, solar tower (or central receiver) plants are the most promising and of particular interest due to the possibility of reaching high temperatures of the working fluid as a result of the punctual concentration of the beam solar radiation, commonly known as Direct Normal Irradiance (DNI, Roldan et al., 2016; Shahabuddin et al., 2021).

Algeria has an immense potential for harvesting solar energy projects thanks to its important solar resources, mainly in the southern region of Algeria according to recent research that studied sites'

suitability to host CSP projects in Algeria basing on multiple criteria such as the intensity of DNI and proximity (access) to the electricity grid (Haddad et al., 2021). However, the Saharan desert of Algeria does not host only high insolation levels, but also high aerosols and dust loads, which would often result in the occurrence of sand storms, not to mention soiling problems and the rare precipitations thus the rarity of natural cleaning (Benkaciali et al., 2018; Boudghene Stambouli, 2011; Memiche et al., 2020). These soiling issues (generally accompanying high insolation, not only in Algeria but also worldwide as will be discussed in Chapter III) are of serious concerns to solar energy projects, especially CSP technologies which suffer more serious losses in the yielded energy when compared to photovoltaics (Bellmann et al., 2020; Hachicha et al., 2019).

Even though the expected negative consequences of soiling on photovoltaic panels in Algeria were evaluated and confirmed by many previously published studies (such as: Memiche et al., 2020; Mostefaoui et al., 2019), no work that studies dusting issues and consequences on CSP (let alone solar tower) systems figures in the literature.

In this context, we try in the present PhD thesis to present an evaluation of the optical losses suffered by solar heliostats due to soiling and dust deposition. The present study is, to our knowledge, the first assessment of solar mirrors' soiling under Algerian climate conditions. Please note that since the optical mechanisms of reflection and solar reflectors' soiling are the same for all four CSP technologies (Arnaoutakis and Katsaprakakis, 2021), the present study is applicable also to the other three technologies (the description of all CSP systems is presented hereafter). Also, due to the similarity of dust deposition process on CSP mirrors and PV modules (Sarver et al. 2013), the results of the evaluation of dust deposition on solar reflectors' surfaces -that will be reported in the present work- are valid for solar panels as well.

Research objectives

The attenuation of solar radiation by atmospheric aerosols and the deposition of dust causes serious losses to all solar energy applications, however, it can be realized that the scientific literature has not given much attention to soiling problems of CSP when compared to PV.

An evident proof of that is the fewer number of papers studying optical losses suffered by CSP technologies comparing to the much richer and more extended research data of PV soiling (Costa et al., 2018). Consequently to this unbalance, many papers reviewed soiling-related issues for PV

systems (such as Figgis et al., 2017 and Maghami et al., 2016), while no literature review was dedicated to CSP soiling. Similarly, there are multiple studies evaluating soiling effect on PV in Algeria, while no research papers studied this problem for CSP.

In the light of these constatations, the focus of the research work done in the context of our thesis will be on the following objectives:

1) Providing a detailed literature review dedicated to dusting-related issues for CSP technologies.
2) Evaluating the optical losses suffered by solar reflectors in general (and heliostats in particular) due to dust deposition under climatic conditions of Algerian Sahara, and this through outdoor exposure of solar mirrors at an arid CSP-candidate site.
3) Assessing economic soiling mitigation in remote arid sites, the chosen approach is the dry mitigation through the application of an anti-soiling coating to the reflective surface of selected exposed mirrors.

Thesis outline

The present thesis is structured as follows:

In *Chapter I*, a brief background is presented to explain, concisely, notions needed to understand the context of our thesis.

After the general notions, we provide in *Chapter II* the basic theory explaining major physical phenomena taking place, namely optical losses due to the deposition of dust on solar reflectors and atmospheric extinction of incident solar irradiance through scattering and absorption. These theoretical concepts will be necessary for the understanding of the chapters to follow.

The essence of the first literature review of dust impact on concentrated solar power will be presented in *Chapter III*. Both sources of optical losses will be covered, which are dusting of solar mirrors resulting in reflectivity losses and atmospheric extinction of solar irradiance due to the presence of -suspended- aerosols' particles.

In *Chapter IV*, the methodology of our work is detailed, starting with the climatologic and geologic description of the exposure site (Laghouat city), as well as the description of the experimental set-up on which the mirrors are mounted for outdoor exposure. After that, the protocol followed to

evaluate, quantify, and characterize the optical losses (and related parameters) through multiple measurements is explained.

In *Chapter V*, we present the results of the first soiling campaign under Algerian climate. The effects of two factors on the intensity of dust deposition on solar mirrors are discussed, namely the inclination angle of solar mirrors and coating their reflective surfaces as a mitigation approach. Also, we provide the physical and chemical properties of Laghouat's soil, obtained after random collection of dust particles and their characterization through X-ray diffraction and scanning electron microscopy.

Last but not least, the conclusions and the future perspectives of the work are presented.

References of Introduction

Arnaoutakis, G.E., Katsaprakakis, D.A., 2021. Concentrating Solar Power Advances in Geometric Optics, Materials and System Integration. *Energies* 14, 6229. https://doi.org/10.3390/en14196229

Avilat-Marin, A.L., 2011. Volumetric receivers in Solar Thermal Power Plants with Central Receiver System technology: A review. *Solar Energy* 85, 891. https://doi.org/10.1016/j.solener.2011.02.002

Behar, O., Khellaf, A., Mohammedi, K., 2013. A review of studies on central receiver solar thermal power plants. *Renewable and Sustainable Energy Reviews* 23, 12. http://dx.doi.org/10.1016/j.rser.2013.02.017

Bellmann, P., Wolfertstetter, F., Conceição, R., Silva, H. G., 2020. Comparative modeling of optical soiling losses for CSP and PV energy systems. *Solar Energy* 197, 229–237. https://doi.org/10.1016/j.solener.2019.12.045

Benkaciali, S., Haddadi, M., Khellaf, A., 2018. Evaluation of direct solar irradiance from 18 broadband parametric models: Case of Algeria. *Renewable Energy* 125, 694-711. https://doi.org/10.1016/j.renene.2018.02.108

Boudghene Stambouli, A., 2011. Promotion of renewable energies in Algeria: Strategies and perspectives. *Renewable and Sustainable Energy Reviews* 15, 1169-1181. https://doi.org/10.1016/j.rser.2010.11.017

Costa, S.C.S., Diniz, A.S.A.C., Kazmerski, L.L., 2018. Solar energy dust and soiling R&D progress: Literature review update for 2016. *Renewable and Sustainable Energy Reviews* 82, 2504-2536. https://doi.org/10.1016/j.rser.2017.09.015

Figgis, B., Ennaoui, A., Ahzi, S., Remon, Y., 2017. Review of PV soiling particle mechanics in desert environments. *Renewable and Sustainable Energy Reviews* 76, 872-881. https://doi.org/10.1016/j.rser.2017.03.100

Hachicha, A.A., Al-Sawafta, I., Hamadou, D.B., 2019. Numerical and experimental investigations of dust effect on CSP performance under United Arab Emirates weather conditions. *Renewable Energy* 143, 263-276. https://doi.org/10.1016/j.renene.2019.04.144

Haddad, B., Diaz-Cuevas, P., Ferreira, P., Djebli, A., Perez, J.P., 2021. Mapping concentrated solar power site suitability in Algeria. *Renewable Energy* 168, 838-853. https://doi.org/10.1016/j.renene.2020.12.081

Maghami, M.R., Hizam, H., Gomes, C., Radzi, M.A., Rezadad, M.I., Hajighorbani, S., 2016. Power loss due to soiling on solar panel: A review. *Renewable and Sustainable Energy Reviews* 59, 1307-1316. https://doi.org/10.1016/j.rser.2016.01.044

Memiche, M., Bouzian, C., Benzahia A., Moussi, A., 2020. Effects of dust, soiling, aging, and weather conditions on photovoltaic system performances in a Saharan environment—Case study in Algeria. *Global Energy Interconnection* 3, 60-67. https://doi.org/10.1016/j.gloei.2020.03.004

Mostefaoui, M., Ziane, A., Bouraoui, A., Khelifi, S., 2019. Effect of sand dust accumulation on photovoltaic performance in the Saharan environment: southern Algeria (Adrar). *Environmental Science and Pollution Research* 26, 259-268. https://doi.org/10.1007/s11356-018-3496-7

Park, S., Kug, J., 2022. A decline in atmospheric CO_2 levels under negative emissions may enhance carbon retention in the terrestrial biosphere. *Communications Earth & Environment* 3, 289. https://doi.org/10.1038/s43247-022-00621-4

Pérez-Burgos, A., Díez-Mediavilla, M., Alonso-Tristán, C., Rodríguez-Amigo, M., 2017. Analysis of solar direct irradiance models under clear-skies: evaluation of the improvements for locally adapted models. *Journal of Renewable and Sustainable Energy* 9, 023703. http://dx.doi.org/10.1063/1.4981798

Roldan, M.I., Fernandez-Reche, J., Ballestrin, J., 2016. Computational fluid dynamics evaluation of the operating conditions for a volumetric receiver installed in a solar tower. *Energy* 94, 844. http://dx.doi.org/10.1016/j.energy.2015.11.035

Sarver, T., Al-Qaraghuli, A., Kazmerski, L.L., 2013. A comprehensive review of the impact of dust on the use of solar energy: History, investigations, results, literature, and mitigation approaches. *Renewable and Sustainable Energy Reviews* 22, 698-733. http://dx.doi.org/10.1016/j.rser.2012.12.065

Shahabuddin, M., Alim, M.A., Alam, T., Mofijur, M., Ahmed, S.F., Perkins, G., 2021. A critical review on the development and challenges of concentrated solar power technologies. *Renewable and Sustainable Energy Reviews* 47, 101434. https://doi.org/10.1016/j.seta.2021.101434

Slamersak, A., Kallis, G., O'Neil, D.W., 2022. Energy requirements and carbon emissions for a low-carbon energy transition. *Nature Communications* 13, 6932. https://doi.org/10.1038/s41467-022-33976-5

Tollefson, E., 2022. Carbon emissions hit new high: warning from COP27. *Nature*. https://doi.org/10.1038/d41586-022-03657-w

Yettou, F., Azoui, B., Malek, A., Gama, A., Panwar, N.L., 2014. Solar cooker realizations in actual use: An overview. *Renewable and Sustainable Energy Reviews* 37, 288-306. http://dx.doi.org/10.1016/j.rser.2014.05.018

CHAPTER I – GENERAL NOTIONS

I. 1. Concentrating solar power technologies

Among CSP systems, there are four configurations that have the most techno-economic maturity, which are distinguished according to the type of reflectors (mobile/static) and receptor (punctual/linear) into (Arnaoutakis and Katsaprakakis, 2021; Gonzalo et al., 2019; Zhang et al., 2013):

- Solar Tower (ST): Hundreds of reflective mirrors, called heliostats, concentrate the reflected DNI onto a single punctual receiver.

- Parabolic Dish (PD): Parabolic-shaped large mirrors are used to focus the beam radiation onto a single point of reception and power generation, the whole system has the possibility of double-axis-sun-tracking, and heat transfer fluids aren't required. This technology is the least mature one, and is still not competitive with the other ones yet, mainly due to the following reasons: low compatibility with thermal storage systems, most expensive cost, and low power generation capacities of individual parabolic dishes, which implies the need of large plants, similarly to other more economically feasible CSP systems.

- Linear Fresnel (LF): linearly-arranged plane mirrors focus the DNI onto linear receivers. When compared to the other three technologies, the main advantage of LF technology is the very reduced costs and required investments due to their much simpler design, and fix receivers that enable steam generation directly and thus eliminate the need of heat exchangers and heat transfer fluids. However, this advantage is constrained with an equally important disadvantage, which is the reduced efficiency of this technology, the lowest among all four technologies.

- Parabolic Trough (PT): most mature CSP commercial application, parabolic trough reflectors are used to concentrate beam radiation onto a linear absorber placed within the focal line of the parabola, this system has the possibility of single-axis-sun-tracking which allows reaching temperatures higher than those obtained through LF technology. The linear absorber is composed of a glass-enveloped metal tube. For the sake of minimizing thermal losses, a selective coating is applied to the absorber, the coating is highly absorbent of DNI and has reduced thermal remittance; also, the glass envelop is either filled with air or voided from it.

As can be seen in Figure 1.1, in terms of reflectors' mobility, ST & LF technologies have static reflectors, while PD & PT technologies have mobile ones; as to the receiver's type, ST & PD have punctual receivers, and LF & PT have linear ones, as clarified in Table. 1.1.

Table 1.1: Classification of CSP technologies.

Shape Mobility	Fix	Mobile
Punctual	ST	PD
Linear	LF	PT

Typically, CSP plants are composed of the following main components: i) the solar field including reflectors and receivers where the heat is either transferred directly to the power block, or via a heat transfer fluid, generally steam or molten salts, which receives the concentrated heat by the mean of heat exchangers; ii) the power block (which converts the collected heat into electrical power), and iii) the optional thermal storage system (Li et al., 2016; Zhang et al., 2013).
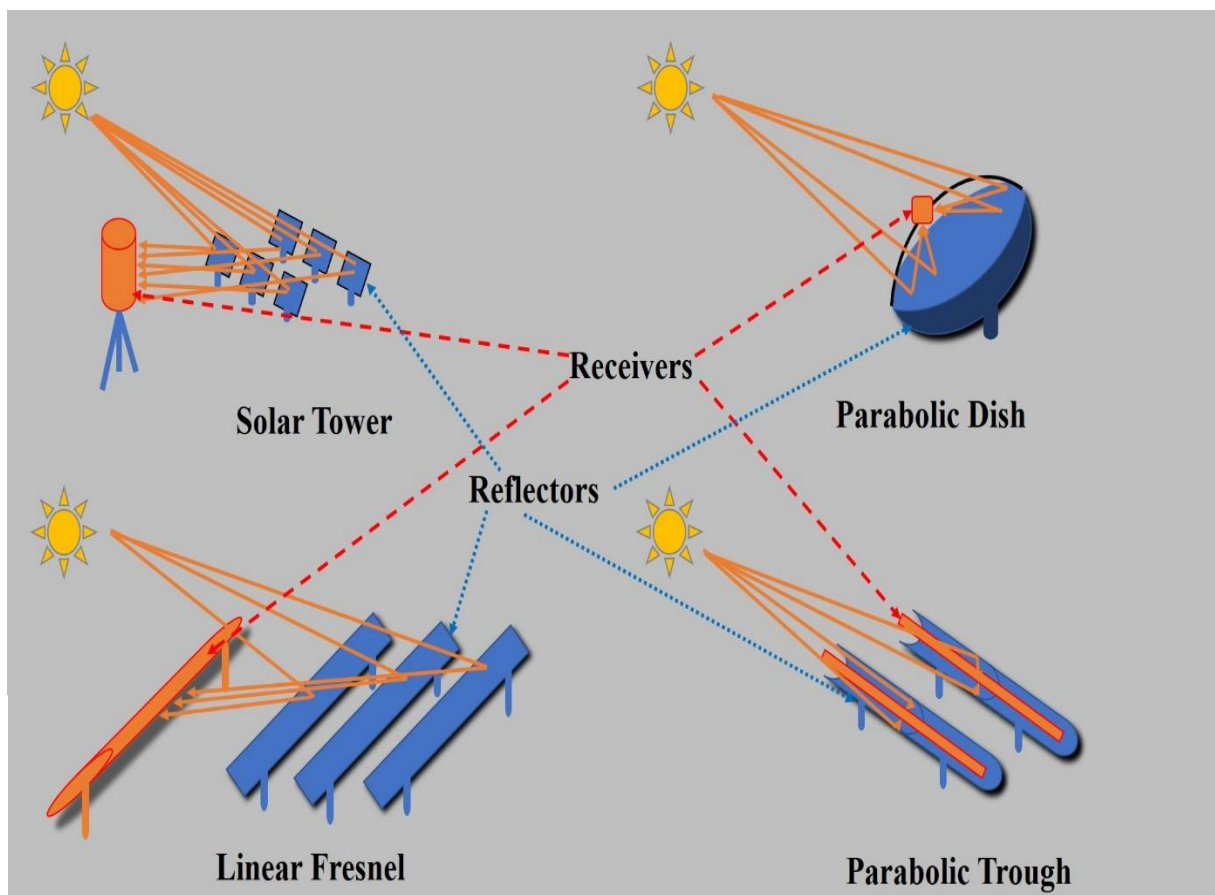
Figure 1.1: The four most mature CSP technologies.

One of the main characteristics of CSP plants is the *concentration ratio* which is the ratio of the area of the integrity of the reflectors to the area of the receiver (Equation1. 1.):

$$c_r = {A_{refs}} \Big/ {A_{rec}} \qquad\qquad (1.1),$$

this factor is proportional to the reachable temperature of the heat transfer fluid, higher concentration ratios of the punctual-receiver systems (greater than 1000) result in working temperatures higher than 1000 °C, while lower concentration ratios of the linear-receiver systems (60 to 100) result in temperatures up to 500 °C; these temperatures result in the following typical efficiencies: 25 to 28% for ST, 30% for PD, 12% for LF, 18% for PT. As for the typical capacity, it's around 10 to 200 MW for ST, 0.010 to 0.025 MW for PD, 10 to 200 MW for LF, and 10 to 300 MW for PT (Arnaoutakis and Katsaprakakis, 2021; Duffie and Beckman, 2013; Shahabuddin et al., 2021).

To conclude this section, when compared to other renewable energy technologies candidates for a sustainable development, CSP have multiple advantages such as: optional thermal storage which results in higher overall efficiency (by insuring heat supply during nighttime/ cloudy passages, or by backing up during periods of shortage between the energy supply and demand), integrability with fossil fuel power plants (by hybridization, thus offering the possibility of gradual transition towards zero-emission), the relatively low cost of operation which would lower more the already competitive cost of per-unit electricity production (Khamlich et al., 2021; Shahabuddin et al., 2021). Among the different CSP technologies, central receiver system (ST) is the most promising one thanks to the high reachable temperatures and its important potential for cost reduction and efficiency improvements (Behar et al., 2013; Roldan et al., 2016).

I. 2. Solar tower technology

I. 2. 1. Generalities

Similarly to other CSP technologies, a solar tower plant (or central receiver solar plant, Figure 1.2) is composed mainly of the reflectors' field (heliostats in this case), the receiver (a central punctual one, on top of the tower), and the power conversion system. The receivers are usually made up of materials that can resist intense radiative energy density and important changes of temperature (e.g., ceramic). According to their geometry and function, three types of receivers can be distinguished, namely cavity receivers, volumetric receivers, and particle receivers. The beam radiation reflected by heliostats and absorbed afterwards by the receiver is transferred to the working fluid, the heat transfer fluids that are generally used in solar tower plants are steam and molten salts, the right association of receiver and working fluid can boost

the heat transfer by minimizing thermal losses, thus even higher working temperatures are reached (Behar et al., 2013).

Even though heliostats were basically conceptualized as static reflectors, one of the main improvements that were applied to solar tower is the individual smart double-axis sun-tracking by each of the heliostats, thus allowing to increase furthermore more the concentration of the beam radiation; another advantage of solar tower technology, besides tracking and high reachable temperatures, is the economic feasibility thanks to the easily manufactured heliostats, which are plane reflectors, simpler to produce and to improve in terms of reflective materials' development, unlike the currently most mature CSP technology of trough collectors which has such manufacturing limitations due to the parabolic shape of the solar reflectors (Behar et al., 2013; Malwad and Tungikar, 2021).

Figure 1.2: Solar tower plants PS10 (foreground) and PS20 (background) in Sevilla, Spain (Behar et al., 2013).

I. 2. 2. Reflective materials

The proper selection of the reflective material for solar mirrors is crucial for the economic feasibility of CSP plants, it has decisive impacts on the optical efficiency (thus the overall efficiency), the lifetime, and the operation and management costs of the solar field (Azouzoute et al., 2019). Four main classes of solar mirrors can be found in the literature,

namely silvered-glass reflectors, silvered-polymer reflectors, aluminum reflectors, and stainless-steel reflectors (Malwad and Tungikar, 2021):

Glass reflectors: silvered glass -as a reflective material- answers to the conditions of good optical performance for CSP technologies, however, if longer lifetime is desired, the manufacturing cost increases, which limits the economic feasibility of glass mirrors for CSP plants, this limitation is essentially due to the low resistance of glass to degradation consequent to outdoor exposure, mainly under some weather conditions (e.g., sandstorms). Still, glass remains a popular reflector, thanks to its compatibility with protective coatings. Also, because it's hard to shape, glass suits better CSP technologies which have plane reflectors (solar tower (heliostats) and linear Fresnel) more than those with curved reflectors (parabolic trough and parabolic dish, Malwad and Tungikar, 2021).

Polymer reflectors: compared to glass, silver-coated polymer mirrors are light in weight, and -furthermore- are much more flexible in design. However, despite the good resistance to outdoor conditions, polymer reflectors have shorter lifetime, and some of them have poor adhesion with the silver coat after being exposed to water which indicates their poor washability. The development of adequate materials to be added as a protective film of polymer reflectors could promote the durability of polymer reflectors (Malwad and Tungikar, 2021; Qi and Zhang, 2019).

Aluminum reflectors: aluminum is the frequently exploited solar reflector in CSP industry. Without a suitable treatment, the reflectivity of aluminum reflectors drops rather rapidly because of environmental conditions. The treatment usually applied consists of multilayer coatings. The research and development of aluminum reflectors considerably contributed to the reduction of their cost and to the enhancement of their durability, not to mention that among metals, aluminum is the most abundant, and is considerably inexpensive (Malwad and Tungikar, 2021; Mishra et al., 2016).

Stainless-steel reflectors: stainless-steel does not require high thickness thanks to its rigidity, however, its low reflectance makes it less attractive for CSP technologies when compared with other reflective materials. Attempts to enhance the reflectivity of stainless-steel failed to make it competitive within CSP markets. The good resistance of stainless-steel and the much higher reflectivity of the aluminum lead to the combination of the two advantages through aluminum-on-steel materials which showed excellent outdoor durability (Hussain et al., 2017; Malwad and Tungikar, 2021).

I. 3. Chemical nature of aerosols

Aerosols are fundamental components of the atmosphere and have crucial impact on the climate, energy balance of earth, and public health. An aerosol is usually perceived, in atmospheric knowledge, as a suspension of particles (whether solid or liquid) in a gas, with their diameter in the range of 10^{-3} to 10^2 µm. In scientific literature, the appellation Particulate Matter "PM" relates to aerodynamic equivalent diameters less than or equal to 1 micron (PM1), 2 microns (PM2), or 10 microns (PM10, Hinds, 1999; Seinfeld and Pandis, 1998; Poschl, 2005), while ultrafine particles (or nanoparticles) are particles with an aerodynamic equivalent diameter less than or equal to 0.1 micron (Shao et al., 2022). Many parameters determine the impact of aerosols on the environment, climate, and public health, such as size, chemical composition, mass and number concentration, as well as structure. In the troposphere (lower atmosphere), the concentrations of the mass and number of particles range from 1 to 100 $\mu g.m^{-3}$ and from 10^2 to 10^5 particle per cm^3 respectively (Poschl, 2005). Aerosols vary extensively in terms of composition due to the diversity in their origin (natural and anthropogenic):

Carbonaceous aerosols consist of black carbon and organic carbon. Organic carbon is resulted from biomass scorching (such as forest fires) and transport of biological materials (eg: waste of animals & plants). Black -inorganic- carbon (also known as elemental carbon) results principally from the combustion of fossil fuels (Poschl, 2005). Also, Sulfur is a result -as well as an indication- of industrial activity and the combustion of hydrocarbons, it's the consequence of the transport and conversion to secondary particulate sulfur (secondary particles are the result of gas-to-particle atmospheric conversion, in contrast to direct primary particles, Elminir et al., 2006; Poschl, 2005)

Dust -as a specie of atmospheric aerosols- is frequently given due consideration when simulating atmospheric attenuation (eg: Hanrieder et al., 2019; Singh et al., 2005), the existence of atmospheric dust particles results in the attenuation of the incident solar energy and the reduction of CSP plants' efficiency (Carra et al., 2020; Yadav et al., 2014). Desert dust is principally composed of quartz -rich in silicon- and calcite -rich in calcium- (eg: Egypt, Elminir et al., 2006; Morocco, Alami Merrouni et al., 2015), the presence of silicon is because of the disturbed desert soil either by human activity (e.g., agriculture) or by windy weather, while calcium comes from building and/or industrial activeness (such as cement plants, Elminir et al., 2006; Shao et al., 2022).

The very dynamic nature of aerosols due to the continuous variations in size, composition and concentration requires multiple technologies in order to characterize it (Moorchilot et al., 2022). Usually, atmospheric aerosols are characterized by means of the techniques to follow (among others, for further details please refer to: Poschl, 2005; Shao et al., 2022): scanning/transmission electron microscopy, inertial separation, Mie's light scattering, nephelometry for absorption and scattering coefficients, photoacoustic spectroscopy differential mobility analysis, and spectrophotometry.

In our thesis, we are interested in solar irradiance attenuation -especially the direct component- by natural aerosols (cited also as soiling or -rural- dust).

I. 4. Summary

In the present chapter, we provided the background of the research work that will be conducted in our thesis. Concentrated solar power technologies, especially solar tower which we highlighted, are promising and could play a significant role in energy transition towards renewable, cleaner sources. However, regions blessed with important potential of solar irradiance -such as Algeria- also host significant loads of aerosols, it was highlighted that the consequent optical losses should be evaluated in order to avoid the overestimation of the yielded energy. For this purpose, multiple parameters that need to be taken into consideration -among others- were underlined, such as the reflective materials of the solar mirror and the chemical nature of dust particles at the hosting site.

In the next chapter, we present the basic theory that rules the different physical phenomena of soiling of the reflective surfaces of solar mirrors, as well as the different formalisms of atmospheric turbidity due to aerosols.

References of Chapter I

Alami Merrouni, A., Wolfertstetter, F., Mezrhab, A., Wilbert, S., Pitz-Paal, R., 2015. Investigation of soiling effect on different solar mirror materials under Moroccan climate. *Energy Procedia* 69, 1948–1957. https://doi.org/10.1016/j.egypro.2015.03.194

Arnaoutakis, G.E., Katsaprakakis, D.A., 2021. Concentrating Solar Power Advances in Geometric Optics, Materials and System Integration. *Energies* 14, 6229. https://doi.org/10.3390/en14196229

Azouzoute, A., Merrouni, A. A., Garoum, M., Bennouna, E. G., 2019. Comparison of soiling effect of two different solar mirrors in mid-south of Morocco. *AIP Conference Proceedings* 2126, 190002. https://doi.org/10.1063/1.5117699

Behar, O., Khellaf, A., Mohammedi, K., 2013. A review of studies on central receiver solar thermal power plants. *Renewable and Sustainable Energy Reviews* 23, 12. http://dx.doi.org/10.1016/j.rser.2013.02.017

Carra, E., Marzo, A., Ballestrin, J., Polo, J., Barbero, J., Alonso-Montesinos, J., Monterreal, R., Abreu, E.F.M., Fernández-Reche, J., 2020. Atmospheric extinction levels of solar radiation using aerosol optical thickness satellite data. Validation methodology with measurement system. *Renewable Energy* 149, 1120–1132. https://doi.org/10.1016/j.renene.2019.10.106

Duffie, J.A., W.A., Beckman, 2013. *Solar engineering of thermal processes (4th edition)*. John Wiley & Sons, Inc.

Elminir. H.K., Ghitas, A.E., Hamid, R.H., El-Hussainy, F., Beheary, M.M., Abdel-Mouneim. 2006. Effect of dust on the transparent cover of solar collectors. *Energy Conversion and Management* 47, 3192-3203. https://doi.org/10.1016/j.enconman.2006.02.014

Gonzalo, A.P., Marugán, A.P., Márquez, F.P.G., 2019. A review of the application performances of concentrated solar power systems. *Applied Energy* 255, 113893. https://doi.org/10.1016/j.apenergy.2019.113893

Hanrieder, N., Ghennioui, A., Merrouni, A. A., Wilbert, S., Wiesinger, F., Sengupta, M., Zarzalejo, L., Schade, A., 2019. Atmospheric Transmittance Model Validation for CSP Tower Plants. *Remote Sensing* 11, 1083. https://doi.org/10.3390/rs11091083

Hinds, W.C., 1999. *Aerosol Technology.* Wiley, New York.

Hussain, M. I., Hyun, J., Kim, J., 2017. Experimental validation of mathematical models of identical aluminum and stainless steel engineered conical solar collectors. *Renewable Energy* 112, 44-52. https://doi.org/10.1016/j.renene.2017.05.035

Khamlich, I., Zeng, K., Flamant, G., Baeyens, J., Zou, C., Li, J., Yang, X., He, X., Liu, Q., Yang, H., Yang, Q., Chen, H., 2021. Technical and economic assessment of thermal energy storage in concentrated solar power plants within a spot electricity market. *Renewable and Sustainable Energy Reviews* 139, 110583. https://doi.org/10.1016/j.rser.2020.110583

Li, L., Coventry, J., Bader, R., Pye, J., Lipinski, W., 2016. Optics of solar central receiver systems: a review. *Optics Express* 24, A985-A1007. https://doi.org/10.1364/OE.24.00A985

Malwad, D., Tungikar, V., 2021. Development and performance testing of reflector materials for concentrated solar power: A review. *Materials Today: Proceedings* 46, 539-544. https://doi.org/10.1016/j.matpr.2020.10.744

Mishra, S. K., Kumar, V., Tiwari, S. K., Mishra, T., Angula, G., Adhikari, S., 2016. Development and degradation behavior of protective multilayer coatings for aluminum reflectors for solar thermal applications. *Thin Solid Films* 619, 202-207. https://doi.org/10.1016/j.tsf.2016.10.067

Moorchilot, V.S., Aravind, U.K., Menacherry, S.P.M., Aravindakumar, C.T., 2022. Single-Particle Analysis of Atmospheric Aerosols: Applications of Raman Spectroscopy. *Atmosphere* 13, 1779. https://doi.org/10.3390/atmos13111779

Poschl, U., 2005. Atmospheric Aerosols: Composition, Transformation, Climate and Health Effects. *Angewandte Chemie International* 44, 7520-7540. https://doi.org/10.1002/anie.200501122

Qi, Y., Zhang, J., 2019. Chemically modified Sb_2O_3, a new member of high solar-reflective material family, incorporating with ASA (acrylonitrile-styrene-acrylate copolymer) for fabrication of cooling composite with lower wetting behavior. *Composites Part B* 162, 112-121. https://doi.org/10.1016/j.compositesb.2018.11.014

Roldan, M.I., Fernandez-Reche, J., Ballestrin, J., 2016. Computational fluid dynamics evaluation of the operating conditions for a volumetric receiver installed in a solar tower. *Energy* 94, 844. http://dx.doi.org/10.1016/j.energy.2015.11.035

Seinfeld, J.H., Pandis, S.N., 1998. *Atmospheric Chemistry and Physics*. Wiley, New York.

Shahabuddin, M., Alim, M.A., Alam, T., Mofijur, M., Ahmed, S.F., Perkins, G., 2021. A critical review on the development and challenges of concentrated solar power technologies. *Renewable and Sustainable Energy Reviews* 47, 101434. https://doi.org/10.1016/j.seta.2021.101434

Shao, L., Liu, P., Jones, T., Yang, S., Wang, W., Zhang, D., Li, Y., Yang, C.X., Xing, J., Hou, C., Zhang, M., Feng, X., Li, W., Berube, K., 2022. A review of atmospheric individual particle analyses: Methodologies and applications in environmental research. *Gondwana Research* 110, 347-369. https://doi.org/10.1016/j.gr.2022.01.007

Singh, S., Nath, S., Kohli, R., Singh, R., 2005. Aerosols over Delhi during pre-monsoon months: Characteristics and effects on surface radiation forcing. *Geophysical Research Letters* 32, L13808. https://doi.org/10.1029/2005GL023062

Yadav, N.K., Pala, D., Chandra, L., 2014. On the understanding and analyses of dust deposition on heliostat. *Energy Procedia* 57, 3004-3013. https://doi.org/10.1016/j.egypro.2014.10.336

Zhang, H.L., Baeyens, J., Degrève, J., Cacères, G., 2013. Concentrated solar power plants: Review and design methodology. *Renewable and Sustainable Energy Reviews* 22, 466-481. http://dx.doi.org/10.1016/j.rser.2013.01.032

CHAPTER II – BASIC THEORY AND PHYSICS

II. 1. General concepts

One can use the quasi-steady form of the radiative transfer equation to model the spatial difference in radiative intensity among the direction of incidence, reflectors, and a receiver during the atmospheric transfer of radiation. The quasi-steady form of the radiative transfer equation is the following (equation 2.1, Azad and Modest, 1981; Lie et al., 2016; Modest, 2013):

$$\frac{dI_\lambda(\vec{r},\lambda,\hat{s})}{ds} + \beta_\lambda I_\lambda(\vec{r},\lambda,\hat{s}) = \kappa_\lambda I_{\lambda,b}(\vec{r},\lambda) + \frac{\sigma_{s,\lambda}}{4\pi} \int_{\Omega_i=0}^{4\pi} I_\lambda(\vec{r},\lambda,\hat{s}_i)\Phi_\lambda(\vec{r},\lambda,\hat{s}_i,\hat{s})d\Omega_i \qquad (2.1)$$

Where $I_\lambda(I_{\lambda,b})$ is the spectral (blackbody) intensity of solar radiation, λ is the wavelength, $\vec{r}$ is the position, and $\hat{s}$ the direction of incidence. Also, κ_λ and $\sigma_{s,\lambda}$ are, respectively, the coefficients of spectral absorption and scattering, of which the sum gives β_λ, the spectral extinction coefficient; Φ_λ is the phase function for scattering of radiation from direction of incidence $\hat{s}_i$ to direction $\hat{s}$, and Ω_i is the solid angle.

The use of the quasi-steady form of the radiative transfer equation is appropriate due to the short characteristic time of the propagation of radiation, which takes for the radiation to spread across the length-scales of solar thermal systems (Lie et al., 2016).

The spectral intensity of solar radiation that comes from a direction $\hat{s}$ on a particular area element dA which has a normal $\hat{n}$ and is situated at a position $\vec{r}$ is (Lie et al., 2016):

$$I_{\lambda,s}(\vec{r},\lambda,\hat{s},t) = \frac{dQ_s(\vec{r},\lambda,\hat{s},t)}{|\hat{n}.\hat{s}|dAd\lambda d\Omega dt} \qquad (2.2)$$

Where $dQ_s(\vec{r},\lambda,\hat{s},t)$ is the radiative solar energy received by the area element dA within the elemental interval of wavelength $d\lambda$ around the wavelength λ.

By introducing the radiative solar power $d\dot{Q}_s$, equation (2.2) becomes:

$$I_{\lambda,s}(\vec{r},\lambda,\hat{s},t) = \frac{d\dot{Q}_s(\vec{r},\lambda,\hat{s},t)}{|\hat{n}.\hat{s}|dAd\lambda d\Omega} \qquad (2.3)$$

Based on the preceding equation, the spectral flux of solar radiation is:

$$\dot{q}_{\lambda,s}(\vec{r}, \lambda, t) = \int\limits_{\Omega=0}^{2\pi} I_{\lambda,s}(\vec{r}, \lambda, \hat{s}, t) \, |\hat{n}.\hat{s}| d\Omega \qquad (2.4)$$

The considerations made to obtain equations 2.1-4 are the following (Lie et al., 2016; Modest, 2013):

- The air mass $AM = 1.5$ spectral distribution is typically used as spectrum of reference for optical spectral models in CSP projects (please refer to subsection II.3.1 for more information on the air mass), locally modified parameters should be introduced when needed.

- Sun is considered a black body at an effective temperature of 5780 K for the solar spectral distribution.

- The solar disk is at solid and half-cone angles of $6.79 \times 10^{-5} \, sr$ and $4.65 \, mrad$ (0.27°) respectively due to the sun-earth geometry. Apart from the sun-earth geometry, the directional distribution of the incident solar irradiation is also consequent to the sunshape effect, which is the observed (from earth) distribution of solar radiation within solar disk and the circumsolar aureole.

For solar mirrors, the spectral bi-directional reflection function is (Lie et al., 2016):

$$\rho_{\lambda,mir}(\vec{r}, \lambda, \hat{s}_i, \hat{s}_r) = \frac{dI_\lambda(\vec{r}, \lambda, \hat{s}_i, \hat{s}_r)}{I_\lambda(\vec{r}, \lambda, \hat{s}_i)|\hat{n}.\hat{s}_i|d\Omega_i} \qquad (2.5)$$

Subscripts i and r are for incidence and reflection respectively.

The total radiative power arriving on the aperture of the receiver is (equation 2.6, same previous reference):

$$\dot{Q}_{rec}(\vec{r}) = \int\limits_{\lambda=0}^{\infty} \int\limits_{A_{rec}} \int\limits_{\Omega=0}^{2\pi} I_{\lambda,rec}(\vec{r}, \lambda, \hat{s}) \, |\hat{n}.\hat{s}| \, d\Omega \, dA \, d\lambda \qquad (2.6)$$

Where $I_{\lambda,rec}(\vec{r}, \lambda, \hat{s})$ is the spectral intensity of the solar radiation intercepted by the receiver.

Optical performance metrics:

The performance of concentrated solar power plants can be assessed according to two categories of performance metrics: optical metrics, and thermodynamic metrics which are beyond the scope of the present work.

The main usually considered metrics of optical performance in CSP are (Lie et al., 2016):

- Optical efficiency: the overall optical efficiency is expressed as the ratio of the total received radiative energy to the maximal reflected radiative energy (equation 2.7):

$$\eta_{opt} = \frac{\int_{\Delta t} \dot{Q}_{rec} dt}{DNI \times A_{mirrors} \times \Delta t} \qquad (2.7)$$

  The overall optical efficiency accounts for multiple efficiencies according to the source of optical losses, namely efficiency losses due to: reflection, atmospherics attenuation, blockage, cosine, shading, and spillage (equation 2.8):

$$\eta_{opt} = \boldsymbol{\eta_{refl}} \times \boldsymbol{\eta_{atm}} \times \eta_{block} \times \eta_{cos} \times \eta_{shad} \times \eta_{spill} \qquad (2.8)$$

  In our thesis, we are interested in the optical losses due to reflection losses and atmospheric attenuation, as these losses result from the environmental conditions surrounding CSP plants. The first optical parameter is of particular interest (since it can be mitigated) and will be evaluated following an experimental campaign as will be explained in Chapters IV and V.

- Concentration ratio: Another important parameter, it indicates the potential reachable temperature and differs from one CSP technology to another. The concentration ratio has two forms: the geometric form and the energetic one. The geometric concentration ratio is defined as the ratio of the total area of solar mirrors $A_{mirrors}$ to the area of the receiver A_{rec} (equation 2.9). While the energetic (area-averaged flux) concentration ratio is the ratio of area-averaged incident flux of radiation intercepted by the receiver's aperture to the one intercepted by the totality of solar mirrors' area (equation 2.10):

$$C_a = \frac{A_{mirrors}}{A_{rec}} \qquad (2.9)$$

$$C_f = \frac{\dot{Q}_{rec}}{DNI \times A_{mirrors}} \qquad (2.10)$$

Note that since $\dot{Q}_{rec}$ is the instantaneous area-averaged received power, the time-averaged energetic concentration ratio equals to the optical efficiency ($\overline{C_f} = \eta_{opt}$).

II. 2. Process of soiling and consequent reflectivity losses

As can be seen in equation (2.8), the reflection efficiency is an optical loss factor, furthermore a major one that needs to be continuously assessed because it is consequent to environmental conditions of soiling, unlike most of other factors which are due to the design of the power plant and nothing can be done about them once the plant is installed (Zereg et al., 2022). Soiling of solar mirrors is a complicated process that depends on numerous factors which we will try to provide hereafter:

II. 2. 1. Dust deposition on solar mirrors

The first step of soiling is the dry deposition of dust particles on the reflective surfaces of solar mirrors; since wet deposition is simultaneous to precipitations which result in cleaning the reflectors much more than soiling them (Mejia and Kleissl, 2013).

The most characteristic parameter of the dry deposition of airborne dust (aerosols) particles is the dust deposition flux F (in µg/m^2/s, equation 2.11):

$$F = C_d \times v_d \qquad\qquad (2.11)$$

Where C_d and v_d are, respectively, the concentration and deposition velocity of dust (in µg/m^3 and m/s). F speaks for the quantity of dust that vertically falls in the direction of the reflectors (Picotti et al., 2018).

Note that for θ-tilted surfaces:

$$F = C_d \times v_d \times cos\theta \qquad\qquad (2.12)$$

For the sake of the development to follow, dust particles will be considered as rigid (non-deformable), homogenous spheres that are made of silica of which the density is $\rho_p \cong 2000 \ kg/m^3$. The dynamic viscosity μ_{air} and density ρ_{air} of air are considered under ambient conditions and equal to their standard values. Under these assumptions, the dust deposition velocity is assumed to be the sum of two components according to the driving physical phenomena: v_g, the velocity of deposition due to gravity and drag, and v_t, the velocity of deposition due to turbulence and Brownian motion (equation 2.13, Seinfeld and Pandis, 1998; Zhang et al., 2001):

$$v_d = v_g + v_t \qquad\qquad (2.13)$$

Determination of v_g:

For particles larger than few microns, the settling velocity v_g is the most important term in equation 2.13. The gravitational settling is assured by a balance between the gravitational pull F_g and aerodynamic drag F_d forces applied on dust particles immersed in air, according to the law of Newtonian dynamics:

$$M\frac{dv_g}{dt} = F_g + F_d \qquad (2.14)$$

The gravitational force is equal to:

$$F_g = \frac{1}{6}g\rho_p\pi D_p^3 \qquad (2.15)$$

Where M is the mass of dust particles, g the acceleration of gravity, and D_p is the dust particle diameter.

As for the aerodynamic drag F_d force, its formulation depends on the assumptions made to solve the equations that rule the behavior of the air, the fluid in which the particles are immersed, in other words the continuity and Navier-Stokes equations.

Let λ_p be the mean free path, which is the mean distance that a molecule travels between two successive collisions ($\lambda_p^{air} = 0.065\ \mu m$), if the dust particle is greater than the mean free path of the gas ($D_p \geq \lambda_p$), the latter behaves as a continuum with regards to the suspended particles. For the other case ($D_p \leq \lambda_p$), the (kinetic) regime of the free molecule is applied (Seinfeld and Pandis, 1998).

The Knudsen number (Kn, equation 2.16) is the key dimensionless group to determine the nature of particles, when $Kn \rightarrow 0$, the medium is considered as a continuum, for $Kn \gg 0$, this consideration cannot be applied and the medium is a non-continuum (Picotti et al., 2018).

$$Kn = \frac{2\lambda_p}{D_p} \qquad (2.16)$$

Another required dimensionless group is the Reynolds number (Re, equation 2.17), which compares the inertial and viscous forces acting on a body during its motion in a fluid.

$$Re = \frac{\rho_{air} v D_p}{\mu_{air}} \qquad (2.17)$$

Where v is the fluid-body relative velocity.

Depending on Knudsen number and Reynolds number, the force of aerodynamic drag is as follows (Picotti et al., 2018):

- $Kn \to 0$ (continuum) and $Re \ll 1$: Stokes regime for a rigid sphere is applied to get Stokes' law (equation 2.18):

$$F_d = 3\pi\mu_{air} D_p v_g \qquad (2.18)$$

- $Kn \to 0$ (continuum) and $Re \gg 1$: The drag coefficient C_D is introduced to consider the effects of regimes of higher velocities, because Stokes' law neglects the effects of inertial forces in Navier-Stokes equation.

$$F_d = \frac{1}{2} C_D \pi \frac{D_p^2}{4} \rho_{air} v_g^2 \qquad (2.19)$$

- $Kn \gg 0$: The assumption of non-slip cannot be strictly applied and a slip correction factor C_c must be introduced to take into consideration non-continuum effects.

$$F_d = \frac{3}{C_c} \pi\mu_{air} D_p v_g \qquad (2.20)$$

For the drag coefficient C_D and the slip correction factor C_c, please refer to equations 12-16 in (Picotti et al., 2018).

And thus, the determination of the velocity of deposition due to gravity and drag v_g comes down to the resolution of a fist order differential equation, which -depending on the formulation of the aerodynamic drag force- is non-linear when combining equations 2.14, 2.15, and 2.19, and linear in the two other cases (equations 2.18 and 2.20 instead of 2.19). It should be noted that the former non-linear equation is a Bernoulli equation that can be linearized.

Determination of v_t:

In order to determine the velocity of deposition due to turbulence and Brownian motion v_t, it is expressed through the electric analogy of the deposition velocity as the inverse of the sum of two

resistances (equation 2.21, figure 2.1), representative of the effects of atmospheric turbulence (aerodynamic resistance, r_a) and diffusion and impaction (quasi-laminar boundary resistance, r_b).

$$v_t = \frac{1}{r_a + r_b}$$ (2.21)
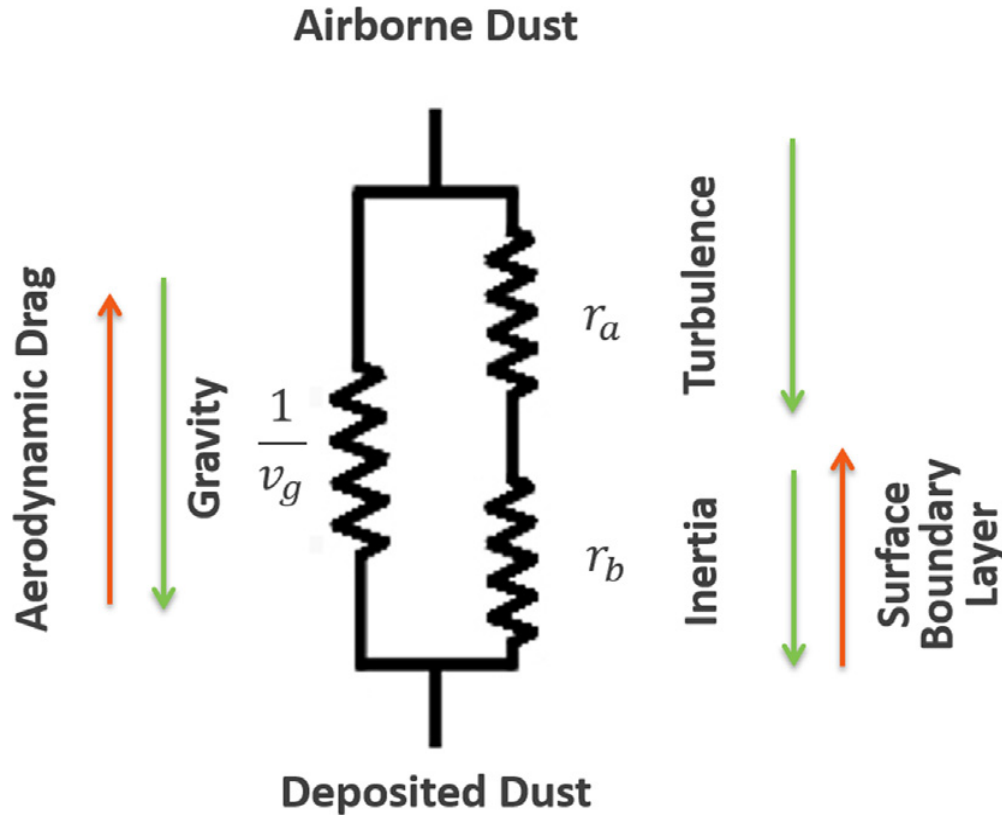
Figure 2.1: Electric analogy of the deposition velocity (Picotti et al., 2018).

The aerodynamic resistance r_a is expressed as follows:

$$r_a = \frac{1}{C_{Dm}U_W}$$ (2.22)

Where $C_{Dm} = \frac{K^2}{ln^2(z/z_r)}$ is the drag coefficient for momentum and U_W is the undisturbed wind velocity. C_{Dm} is a function of Von Karman constant K, the reference height z, and the (usually tabulated) surface roughness z_r, which is the height above which the logarithmic wind speed profile extrapolates to zero. In equation (2.22), the product $C_{Dm}U_W$ expresses the wind's capacity to pass on its kinetic energy to the particles of dust (Jacobson, 2005).

Brownian diffusion and inertial impaction are the processes of predominance in the surface boundary layer at lower altitudes. The expression of the quasi-laminar boundary resistance is (Zhang et al., 2001):

$$r_b = \frac{1}{u_*(E_{br} + E_{imp})\varepsilon_0 C_s} \qquad (2.23)$$

Where u_* is the velocity of friction, ε_0 an empirical constant, C_s a correction factor for sticking particles, E_{imp} and E_{br} two factors accounting for the effects of inertial impaction and Brownian diffusion, respectively.

The Brownian diffusion factor is an exponential function of the Schmidt number (equations 2.24 and 2.25 respectively):

$$E_{br} = Sc^{-\frac{2}{3}} \qquad (2.24)$$

$$Sc = \frac{\vartheta_{air}}{D_{iff}} \qquad (2.25)$$

Where ϑ_{air} and D_{iff} are respectively the kinematic viscosity of the air and the diffusivity, the latter is expressed as following:

$$D_{iff} = \frac{BT_{air}C_c}{3\pi\mu_{air}D_p} \qquad (2.26)$$

Where B is the constant of Boltzmann and T_{air} is the temperature of the air (Picotti et al., 2018).

The inertial impaction factor is dependent upon the Stokes number as will follow in equation 2.27, the Stokes number expresses the ratio of stop distance (crossed by a dragged particle) to the length that characterizes the flow (Seinfeld and Pandis, 1998):

$$E_{imp} = \frac{St^2}{400 + St^2} \qquad (2.27)$$

$$St = \frac{u_*^2 v_g}{\vartheta_{air}g} \qquad (2.28)$$

The friction velocity u_* expresses the change in the horizontal component of air's velocity with the height consequently to the effects of the near-wall shear stress. The friction velocity u_* is defined

by the equation 2.29 (in which τ_{wall} is the wall shear stress), and is evaluated by different approximation with different levels of precision, as we have followed the model of (Picotti et al., 2018), the chosen approximation of u_* will be the following equation 2.30:

$$u_* = \sqrt{\frac{\tau_{wall}}{\rho_{air}}} \qquad (2.29)$$

$$u_* = \frac{KU_W}{\ln\left(\frac{Z}{Z_r}\right)} \qquad (2.30)$$

Of which all terms have already been named.

Finally:

$$v_d = v_g + \frac{1}{r_a + r_b} \qquad (2.31)$$

II. 2. 2. Adhesion of dust particles to solar mirrors

The major forces that cause the adhesion of dust particles to the reflective surfaces of solar mirrors are van der Waals, capillary, and electrostatic forces. Electrostatic forces are related only to highly charged particles, while capillary forces depend on the wetting of the surface and require high levels of humidity, usually correlated with the formation of superficial water layers that have removal consequences more than adhesive ones, especially for tilted surfaces. Thus, the only adhesive force that will be considered is van der Waals interactions, being always present whenever an object (particles in our case) gets close to a surface (Hinds, 1999; Picotti et al., 2018).

The expression of the adhesive force F_{adh} as a function of the adhesion work W_{adh} and the particle diameter D_p is then:

$$W_{adh} = \frac{3}{4}\pi F_{adh} D_p \qquad (2.32)$$

The adhesion work W_{adh} is the free change in energy to detach unit areas of two media (with subscripts i and j) from juxtaposition to infinity in vacuum. Its expression, per unit of surface, is the following:

$$W_{adh} = \frac{A_{ij}}{12\pi d_s^2} \qquad\qquad (2.33)$$

Where A_{ij} is the constant of Hamaker and d_s is the minimum distance of separation in vacuum.

In vacuum $A_{ij} = \sqrt{A_{ii}A_{jj}}$, while across a medium $A_{izj} = (\sqrt{A_{ii}} - \sqrt{A_{zz}})(\sqrt{A_{jj}} - \sqrt{A_{zz}})$, yet, as the fluid in which dust particles are immersed is air, the approximation of A_{izj} with A_{ij} is possible. The phenomena of our interest involve two materials: quartz (dust) and glass (mirrors), for which the respective values of Hamaker constant are $A_{quartz} = 8.5 \times 10^{-20} J$ and $A_{glass} = 6.5 \times 10^{-20} J$. While the distance of separation is assumed to be equal to its common value of $d_s = 0.4\ nm$ (Ahmadi, 2004; Lefevre and Jolivet, 2009; Picotti et al., 2018).

The detachment of dust particles off the surfaces of tilted mirrors is possible when the following condition is satisfied (Picotti et al., 2018):

$$F_g sin\theta \sqrt{(\frac{D_p^2}{4} - r_s^2)} \geq (F_g cos\theta - F_{adh})r_s \qquad\qquad (2.34)$$

r_s is the radius of contact at separation, which is the radius of the particle area flattened by the superficial contact right before the particle's detachment. The formulation of r_s can be found in (Ahmadi and Guo, 2007; Picotti et al., 2018).

II. 2. 3. Reflectivity losses due to soiling of solar mirrors

The reflectivity of the soiled mirror is expressed as:

$$\rho = \rho_c \frac{A_{clean}}{A_{mirror}} = \rho_c \frac{A_{mirror} - A_{soil}}{A_{mirror}} = \rho_c \left(1 - \frac{A_{soil}}{A_{mirror}}\right) \qquad\qquad (2.35)$$

Where ρ and ρ_c are the reflectivity values of the mirror in its soiled and clean states respectively, A_{mirror} is the total area of the mirror, A_{soil} is the area covered by dust, and A_{clean} is the remaining area.

Under the assumptions that deposited dust particles do not collide with each other, and that their deposition forms a monolayer of dust, the soiled mirror area can be expressed as in equation 2.36 (Picotti et al., 2018):

$$A_{soil} = \sum_i A_{soil,i} = \sum_i \frac{3M_i}{2\rho_p D_{p,i}} \tag{2.36}$$

M_i is the mass of every single dust particle, the latter is indicated by the subscript i.

For deeper analysis, the total non-reflective area A_{nr} of the solar mirror can be considered as the sum of two components according to the mechanism of optical losses, namely blocking A_{block} and shading A_{shad}. Shading is a consequence of the opacity of dust particles, while blocking occurs when DNI is not perpendicular to the surface of the mirror (Al-Hasan and Ghonaim, 2005; Al-Hasan, 1998).

$$A_{block} = \frac{3Mtan(\varphi)}{2\rho_p D_p} \tag{2.37}$$

$$A_{shad} = \frac{3M}{2\rho_p D_p \cos(\varphi)} \tag{2.38}$$

Where φ is the angle between the incident beam radiation (DNI) and the normal of the reflective surface. It can be noticed that $A_{block}(\varphi = 0) = 0$, which is logical since when the DNI hit perpendicularly the surface, and consequently the particles, no blocking occurs and the only cause of non-reflectance is the opacity of the particles. At the same angle, it is also remarked that $A_{shad}(\varphi = 0) = A_{soil}$, which is the area obtained after the projection of a spherical particle. The last two mathematical consequences are an assurance of the validity of the model. For the detailed assumptions and geometrical analysis, the reader is referred to (Picotti et al., 2018).

Then, the total non-reflective area is:

$$A_{nr} = \frac{3M}{2\rho_p D_p}\left(\frac{1 + \sin(\varphi)}{\cos(\varphi)}\right) \tag{2.39}$$

Finally, the reflectivity of the soiled mirror is as in the following equation 2.40:

$$\rho = \eta_{refl} = \rho_c \frac{A_{mirror} - A_{nr}}{A_{mirror}} \tag{2.40}$$

II. 3. Atmospheric extinction of solar irradiance

After penetrating the atmosphere, the solar irradiance suffers multiple losses due to various phenomena, a part of the irradiance is absorbed, another scattered either towards the earth (diffuse irradiance) or towards the outer space, and a part reaches directly the terrestrial surface arriving from the solar disk. At any altitude or height, the DNI is expressed as a function of the DNI at top of the atmosphere DNI_{TOA} (before penetrating it), the optical depth τ (sometimes confused with transmittance), the solar zenith angle Z, and the height h (Molineaux et al., 1995; Sengupta and Wagner, 2012):

$$DNI(h) = DNI_{TOA} \times \exp\left(\frac{-\tau(h)}{cosZ}\right) \qquad (2.41)$$

It is possible to express the DNI between two heights, or at the borders of an atmospheric layer, dependently on the optical depth of that atmospheric layer as follows:

$$DNI(h_1) = DNI(h_2) \times \exp\left(\frac{-(\tau_{h1} - \tau_{h2})}{cosZ}\right) = DNI(h_2) \times \exp\left(\frac{-(\tau_{\Delta h})}{cosZ}\right) \qquad (2.42)$$

Where $\tau_{\Delta h}$ is the optical depth of that atmospheric layer.

Similarly, at the surface:

$$DNI_{sfc} = DNI_{\Delta h} \times \exp\left(\frac{-(\tau_{\Delta h})}{cosZ}\right) \qquad (2.43)$$

$$\eta_{atm} = \frac{DNI_{sfc}}{DNI_{\Delta h}} = \exp\left(\frac{-(\tau_{\Delta h})}{cosZ}\right) \qquad (2.44)$$

Which gives the possibility of determining the optical depth at a particular location by means oof two pyrheliometers installed at different heights, in addition to other required devices (Tahboob et al., 2014).

II. 3. 1. Formalisms of extinction due to aerosols

To determine the attenuation by extinction due to atmospheric aerosols, multiple attempts can be found in the literature, the most famous, developed, and -relatively- practical are Angstrom's formalism (Angstrom, 1929) and Linke's one (Linke, 1922).

II. 3. 1. a. Formalism of Angstrom

Angstrom proposed to express the optical depth characterizing the attenuation due to atmospheric aerosols through the Aerosols' Optical Depth (AOD) as in equation 2.45 (Angstrom, 1929):

$$\tau_{aer} = AOD = \beta\lambda^{-\alpha} \qquad (2.45)$$

Where α and β are respectively Angstrom's exponent and coefficient. The coefficient of Angstrom β represents the quantity of aerosols' particles that are present in the atmospheric column (vertical atmospheric direction), usually, β variates within the range $[0; 0.5]$ and for values greater than 2.5 ($\beta > 2.5$) it is reasonable to consider the atmosphere as hazy. The exponent of Angstrom α has an inverse proportionality to the particle size of aerosols. The habitual value of α for most normal atmospheres is $\alpha = 1.3 \pm 0.2$ and its range of variation is $\alpha \in [0; 4]$. For values greater than 2.5 of Angstrom's exponent, the presence of more small particles than large ones is confirmed (Khalil and Shaffie, 2016).

The major drawback to the formalism of Angstrom is the obtention of precise experimental evaluation of Angstrom's exponent and coefficient.

II. 3. 1. b. Formalism of Linke

In his formalism, Linke expresses the total atmospheric optical depth (called interchangeably optical thickness) as the product of two terms: the optical depth of the clean dry atmosphere δ_{CDA} (which is mainly due to Rayleigh scattering and accounts for the gaseous components except for ozone), and the well-known Linke's turbidity factor T_L (accounting for scattering and absorption due to aerosols and precipitations, Linke, 1922). In equation 2.46, the term of the relative air mass AM (accounting for ozone) is almost equivalent to the inverse of the cosine of the zenith angle in equation 2.41, more precise formula for $AM(Z)$ are available in the literature, such as the frequently used Kasten's formula that will be provided by the end of this subsection (Kasten, 1965). The formalism of Linke is the following:

$$DNI_{sfc} = I_0 \times \exp(-\delta_{CDA} \times T_L \times AM) \qquad (2.46)$$

$$\eta_{atm} = \frac{DNI_{sfc}}{I_0} = \exp(-\delta_{CDA} \times T_L \times AM) \qquad (2.47)$$

I_0 is the normal incident extraterrestrial irradiance, function of the solar constant I_{0C}:

$$I_0 = I_{0C} \left(1 + 0.033 \times \cos\left(\frac{360N_j}{365}\right)\right) \qquad (2.48)$$

The factor by which is multiplied I_{0C} accounts for the ellipticity of earth's orbit around the sun (N_j is the Julian day).

The physical interpretation of T_L is that it represents the number of the clean dry atmospheres that reproduce the same atmospheric attenuation as a turbid atmosphere, it variates within the range $1 \leq T_L \leq 6$. It is said that Linke validated his formalism in a Swiss site with extremely clear and dry sky, but no actual records prove it (Iqbal, 1983).

The essential drawback of Line's turbidity factor T_L is its dependence upon the relative air mass, thus it varies at constant turbidities. The usual solution to bypass this difficulty is to normalize T_L for relative air mass value of 2. Most parameters, be it in Angstrom's formulation or Linke's one, generally need to be correlated basing on intensive measurements campaign. It is useful to note that Angstrom's coefficient β is a spectral parameter, while Line's turbidity factor T_L is a broadband one.

The relative air mass is the ratio between the atmospheric mass penetrated by the DNI at any time and the one it penetrates at solar noon with sun at zenith. At sea level with sun at zenith, $AM = 1$.

The optical mass, or in other words the mass of a substance in a column of unitary cross-section, is defined as (Iqbal, 1983):

$$m = \int_0^\infty \rho_{atm} dl \qquad (2.49)$$

dl is the element of the path l traversed through the atmosphere by the DNI until reaching the surface of reception. As refraction depends upon the wavelength, so does the path, and thus the aforementioned equation is applied to monochromatic radiation. When sun is at zenith, dl becomes dz, which is the unitary vertical distance, the relative air mass is then:

$$AM = \frac{\int_0^\infty \rho_{atm} dl}{\int_0^\infty \rho_{atm} dz} \qquad (2.50)$$

To solve this equation, one needs an actual variation in the atmosphere's density, which is an information that, apart from a standard atmosphere, is not available. According to (Iqbal, 1983; Kasten, 1965), after taking consideration of the curvature of earth, and the atmospheric non-homogeneity and refractiveness, equation 2.50 can be written as:

$$AM = \frac{1}{\rho_0 z_0} \int_0^\infty \left(1 - \left(\frac{R_E}{R_E + z_0}\right)^2 \left(\frac{n_0}{n}\right)^2 sin^2 Z\right) \rho dz \qquad (2.51)$$

Where z_0 is the height of homogenous atmosphere of which the density is ρ_0, the latter parameter is the density on the ground. R_E is the mean earth radius, n the refraction index at a height z, n_0 the refraction index at a height $z_0 \leq z$.

Kasten solved equation (2.51) from ground wide-range experimental data and provided the following formulation (Kasten, 1965):

$$AM = (cosZ + 0.15(93.885 - Z)^{-1.253})^{-1} \qquad (2.52)$$

At sea level, for the standard pressure condition of 1013.25 mbar, the absolute air mass m is:

$$m = AM \frac{P}{1013.25} \qquad (2.53)$$

P is the local pressure.

II. 3. 2. Optical phenomena of scattering and absorption

Scattering and absorption are complicated phenomena that take place within the atmosphere, dependently on the diameter of the particles D_p and the wavelength λ of the incident radiation, the assumptions and consequently the theories that govern these phenomena differ (n being the index of refraction, Iqbal, 1983):

- If $\frac{\pi D_p}{\lambda} \leq \frac{0.6}{n}$, then the governing theory is Rayleigh's scattering theory (the particles are too small to absorb radiation). In this mode, the scattering is identical in both directions, i.e., forwards and backwards. The assumptions here are that particles are of spherical shape and independently scatter.

- If $\frac{0.6}{n} \leq \frac{\pi D_p}{\lambda} \leq 5$, then the governing theory is Mie's particle theory which studies the scattering and continuous absorption by aerosols. In this case, the scattering is more intense in the forward direction. The complication of this theory is the high variability in atmospheric dust particles' size, shape, and distribution.

- $5 \leq \frac{\pi D_p}{\lambda}$, if particles are big enough to satisfy this condition, the light is reflected.

II. 4. Summary

In the present chapter, we have discussed physics behind the various phenomena of our interest, as well as the corresponding mathematical basis.

We hope that this chapter would be a starting point for students and researchers of soiling mechanisms of CSP fields' mirrors, photovoltaic panels, and dust deposition on flat surfaces in general, since the principles of dusting in the preceding cases are common Ghazi et al., 2014; Zereg et al., 2022).

It can be deduced that the theoretical -exact or approximate- prediction of the intensity of soiling is very delicate, this is due to the complicated theory and the numerous highly-variable included parameters, not to mention the not-so-real assumed simplifications often made (such as the spherical shape of dust particles, which is not always the case as will be clear in Chapter V), which would require multiple high-tech devices to obtain a detailed evaluation of soiling and turbidity levels.

Thus, the more usual trend in this research axis is to evaluate the intensity of soiling through in-situ outdoor measurements campaigns (Zereg et al., 2022), which is the approach that we will follow in our work.

Previous studies that investigated some aspects of the issue treated in our thesis are reviewed in the chapter to follow, it is the essential and an update of our recently published review paper (Zereg et al., 2022), which was the first paper to review the literature of dust-related issues and different approaches used for mitigation (unlike PV soiling which has beneficiated from many reviews).

References of Chapter II

Ahmadi, G., 2004. Van der Waals force. ME437 Class notes, London.

Ahmadi, G., Guo, S., 2007. Bumpy particle adhesion and removal in turbulent flows including electrostatic and capillary forces. *The Journal of Adhesion* 83, 289-311. https://doi.org/10.1080/00218460701239174

Al-Hasan, A.Y., 1998. A new correlation for direct beam solar radiation received by photovoltaic panel with sand dust accumulated on its surface. *Solar Energy* 63, 323-333. https://doi.org/10.1016/S0038-092X(98)00060-7

Al-Hasan, A.Y., Ghoneim, A.A., 2005. A new correlation between photovoltaic panel's efficiency and amount of sand dust accumulated on their surface. *International Journal of Sustainable Energy* 24, 187-197. https://doi.org/10.1080/14786450500291834

Angstrom, A., 1929. On the Atmospheric Transmission of Sun Radiation and on Dust in the Air. *Geografiska Annaler* 2, 156-166. https://www.tandfonline.com/doi/abs/10.1080/20014422.1929.11880498

Azad, F.H., Modest, M.F., 1981. Evaluation of the Radiative Heat Flux in Absorbing, Emitting and Linear-Anisotropically Scattering Cylindrical Media. *Journal of Heat Transfer* 103, 350-356. https://doi.org/10.1115/1.3244465

Ghazi, S., Sayigh, A., Ip, K., 2014. Dust effect on flat surfaces – A review paper. *Renewable and Sustainable Energy Reviews* 33, 742-751. http://dx.doi.org/10.1016/j.rser.2014.02.016

Hinds, W.C., 1999. Aerosol Technology: Properties, Behavior, and Measurement of Airborne Particles, second ed. Wiley-Interscience.

Iqbal, M., 1983. An introduction to solar radiation. Academic Press. https://www.elsevier.com/books/an-introduction-to-solar-radiation/iqbal/978-0-12-373750-2

Jacobson, M.Z., 2005. Fundamentals of Atmospheric Modeling, second ed. Cambridge University Press. http://refhub.elsevier.com/S0038-092X(18)30836-3/h0185

Kasten, F., 1965. A new table and approximation formula for the relative optical air mass. *Archiv für Meteorologie, Geophysik und Bioklimatologie, Serie B* 14, 206-223.

Khalil, S.A., Shaffie, A.M., 2016. Attenuation of the solar energy by aerosol particles: A review and case study. *Renewable and Sustainable Energy Reviews* 54, 363-375. http://dx.doi.org/10.1016/j.rser.2015.09.085

Lefevre, G., Jolivet, A., 2009. Calculation of Hamaker constants applied to the deposition of metallic oxide particles at high temperature. In: Proc. Int. Conf. Heat Exch. Fouling and Clean. VIII 2009, pp. 120-124.

https://heatexchanger-fouling.com/wp-content/uploads/2021/09/16_Lefevre_Hamaker_F.pdf

Li, L., Coventry, J., Bader, R., Pye, J., Lipinski, W., 2016. Optics of solar central receiver systems: a review. *Optics Express* 24, A985-A1007. https://doi.org/10.1364/OE.24.00A985

Linke, F., 1922. Transmission-Koeffizient und Trubungsfaktor. *Beitraege. Phys. fr. Atomos.* 10, 91-103.

Mejia, F.A., Kleissl, J., 2013. Soiling losses for solar photovoltaic systems in California. *Solar Energy* 95, 357-363. https://doi.org/10.1016/j.solener.2013.06.028

Modest, M.F., 2013. Radiative Heat Transfer, 3rd Edition. *Academics Express*.

Molineaux, B., Ineichen, P., Delaunay, J.J., 1995. Direct luminous efficacy and atmospheric turbidity improving model performance. *Solar Energy* 55, 125-137. https://doi.org/10.1016/0038-092X(95)00035-P

Picotti, G., Borghesani, P., Manzolini, G., Cholette, M.E., Wang, R., 2018. Development and experimental validation of a physical model for the soiling of mirrors for CSP industry applications. *Solar Energy* 173, 1287-1305. https://doi.org/10.1016/j.solener.2018.08.066

Seinfeld, J.H., Pandis, S.N., 1998. Atmospheric chemistry and physics: from air pollution to climate change. Wiley-Interscience, New York. http://refhub.elsevier.com/S0038-092X(18)30836-3/h0365

Sengupta, M., Wagner, M., 2012. Atmospheric attenuation in central receiver systems from DNI measurements. Presented at: SolarPACES, Conference proceedings. https://pdfs.semanticscholar.org/8abf/e7d0a121437a307ee786ca8b012d712964b8.pdf

Tahboob, Z., Oumbe, A., Hassar, Z., Obaidli, A., 2014. Modeling of irradiance attenuation from a heliostat to the receiver of a solar central tower. *Energy Procedia* 49, 2405-2413. https://doi.org/10.1016/j.egypro.2014.03.255

Zereg, K., Gama, A., Aksas, M., Rathore, N., Yettou, F., Panwar, N.L., 2022. Dust impact on concentrated solar power: A review. *Environmental Engineering Research* 27, 210345. https://doi.org/10.4491/eer.2021.345

Zhang, L., Gong, S., Padro, J., Barrie, L., 2001. A size-segregated particle dry deposition scheme for an atmospheric aerosol module. *Atmospheric Environment* 35, 549-560. https://doi.org/10.1016/S1352-2310(00)00326-5

CHAPTER III – LITERATURE REVIEW

III. 1. Optical losses due to soiling of solar mirrors

III. 1. 1. Correlations between deposited dust's weight and the corresponding losses

Some studies were interested in the relationship between the deposited dust's weight, and the consequent reflectance drop:

(Wu et al., 2020) evaluated the cleanliness of a parabolic trough collector in China, the material of the collector is the same as that used in CSP plants. The dust samples were collected from different tilt angles, and the reflectivity was evaluated with a spectrophotometer, the chemical properties were also determined. The results suggest that after a month of exposure, 1 g of deposited dust caused a decrease by 10% of the average reflectivity, as for the effect of the tilt angle on the soiling rate, it was found that the bottom edge of the collector was more soiled and lost more reflectivity than the top edge, the reflectivity dropped by 15% of the initial value, which was higher by 3% than the soiling rate of the top edge, also, 1.03 g was collected from the bottom edge, compared to 0.83 g from the top edge, in general, the reflectivity loss is in the range of 12-15%.

(Zhao et al., 2020) studied the soiling of Fresnel linear reflectors in China, the field is of north-south orientation and east-west tracking, with mirrors of 1820×300 mm^2 dimensions. After an exposure period of 48 days, a dust density of 2.5 g/m² caused 9.4% loss in average relative reflectivity. The soiling (average relative reflectivity loss) was maximal for the horizontal position (9.19%) and minimal for the vertical one (0.72%). the average increase in dust density was 0.16 g/m^2 every 3 days. A model for the cleanliness factor was developed with about 1% standard deviation.

More severe losses were reported in Morocco by (Azouzoute et al., 2020), an outdoor mirrors' exposure was performed for 3 months during the dry season, very precise meteorological station was available at the exposure site for records of various weather factors. The highest soiling loss rate was observed after two weeks of no-cleaning (the cleaning was done on a weekly basis), the dusting loss reached 39%, another high weekly value of 35% was measured. The corresponding deposition densities are respectively 0.8 g/m^2 and 1 g/m^2.

III. 1. 2. Effect of tilt angle on the optical losses

Factors such as the tilt angles of solar reflectors or their exposure direction have an impact on the intensity of the soiling.

(Griffith et al., 2014) assessed the intensity of soiling at a candidate CSP site in South Africa using a custom-made reflectometer. The soiling of horizontal mirrors was twice the +45° ones and the mean rate of reflectivity loss was 0.5% per day. The authors noted that the monitoring of Aerosols Optical Depth (AOD) around CSP sites should be done to assess soiling risk, especially for plants near industrial zones (AOD is proportional to the soiling rate of solar mirrors as noted by (Raillani et al., 2019)). The used reflectometer was based on a digital camera attached to a stainless-steel baseplate, along with a LED light with a collimating lens to simulate solar DNI.

Recently, (Wiesinger et al., 2021) investigated for one year the effect of both height and orientation of solar mirrors on their erosion under Moroccan climate. The variation of the height was between 1.2, 2.4, and 3.6 m (figure 3.1) for each of the four cardinal directions. The dimensions of the mirrors were 10x10 cm^2, the mirrors were inclined at angles of 45°, 90°, and 180° (ground facing). The apparatus used to measure the reflectance was the D&S 15R-USB portable reflectometer, widely used for this kind of studies. The erosion intensity (and consequently reflectance drop) decreased with increasing height and increased with the increasing tilt angle. Also, short, strong wind events caused more intense erosion than the more frequent, moderate events; and mirrors facing the dominant wind direction were damaged more than the rest.
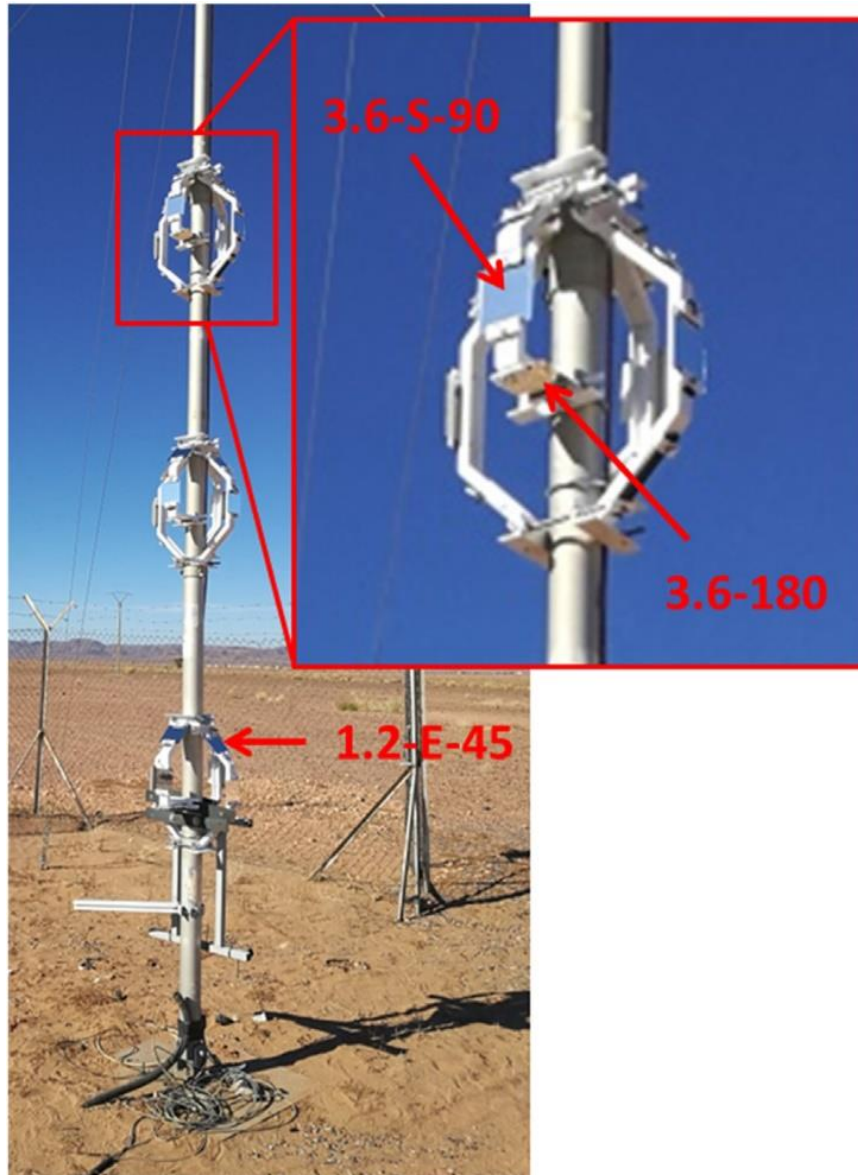
Figure 3.1. Experimental setup used by (Wiesinger et al., 2021).

(Matal et al., 2020) developed an experimental methodology for the sake of the experimentations of erosion simulations, with the different samples being homogeneously exposed to a uniform mass of sand. The loss in reflectivity increased with increasing velocity of airflow, the same trend was observed for the increasing tilt angle; indeed, at a perpendicular tilt, the reflectivity loss due to erosion was much more important than that at a 45° tilt, as an example, the respective decrease in reflectivity was 11.03% and 5.31% for 25 m/s.

(Alami Merrouni et al., 2015) evaluated soiling of different materials of solar reflectors during spring. The monthly cleanliness drops of the horizontal mirrors were 45%, while for +45° mirrors the drop was 14%, the 0° (vertical) and -45° (ground-facing) mirrors remained clean

(3% drop). An important soiling factor highlighted by the authors was the wind direction. The authors conducted X-ray diffraction analysis and found that the collected soil was composed mainly of quartz and calcite.

After an exposure of eight months in Morocco, (Karim et al., 2015) reported that mirrors at impact angle of 90° presented the lowest value of reflectivity (suffered the most intense erosion). Low wind speeds caused cracks that were ring-shaped, while high wind speeds caused normal cracks accompanied by the removal of materials. Furthermore, at an impact angle of 90° and wind speeds of 6.33 m/s the reflectivity loss was 1.7% in the ocean site and 1.5% in the desert sites. In desert sites, the wind speed was lower and the sand particles are harder and smoother, while in ocean sites, the wind speed was higher and the sand particles are smoother and sharper.

III. 1. 3. Coating application as a mitigation for soiling

Desert sites are very good for the installation of solar energy project, however, the usual scarcity of water in such regions, and the need to replace the mostly used water-based methods such as washing, pushed the research towards water-saving mitigation approaches such as anti-soiling coatings and Electrodynamic Screens (EDS); coatings are a very interesting water-saving solution for mirrors' dusting problems since less washing frequencies are used and coated mirrors usually restore their reflectance better (Wette et al., 2019b). The idea of using coatings to protect solar reflectors is older and more mature than that of using EDS (see for example (Bieg and Wischmann, 1980)).

(Dahlioui et al., 2022) studied the benefit of coating solar mirrors for soiling mitigation through one year of outdoor exposure in Morocco. The used coating was a hydrophilic one, applied on half of the exposed at three heights of 0.5 (S1), 1 (S2), and 1.5 m (S3, the first two heights are the same as the values used in our work, please see section IV.2), the application of the coating did not reduce significantly the initial reflectance of the coated mirrors. Monthly measurements of sample mirrors' cleanliness factor were taken, during one of the periods, strong winds and dust storms resulted in cleanliness values of 62% and 75% for the respective uncoated and coated mirrors exposed at 0.5 m height. The effect of coating reflectors for soiling mitigation was reported to be positive for all samples during the whole exposure period (figure 3.2), the maximum obtained average gain of cleanliness was as much as 7%, and a maximum soiling rate of 2.54%/day was reported for uncoated reflectors.
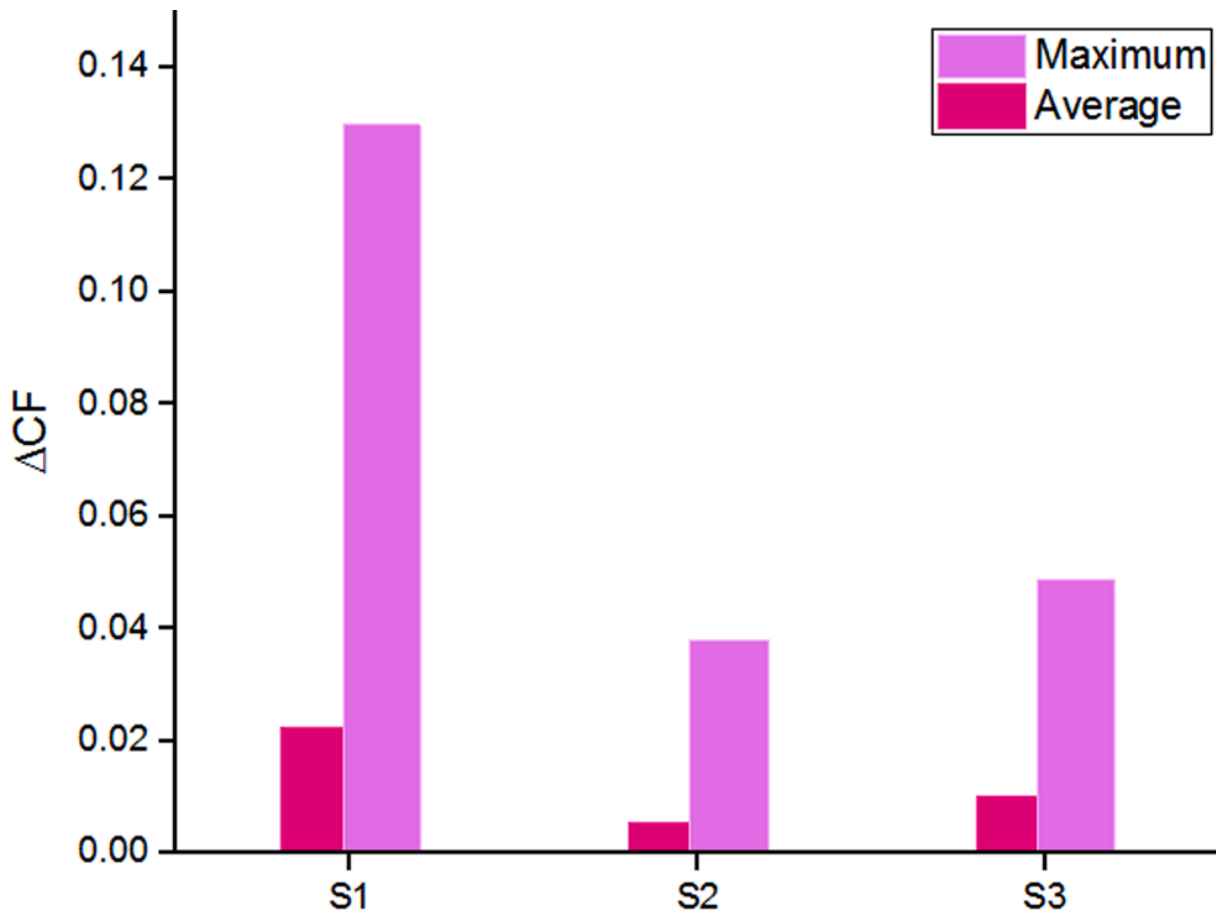
Figure 3.2. Gain in optical performance for coated mirrors (Dahlioui et al., 2022)

(Polizos et al., 2014) performed durability tests on anti-soiling coatings (spray) composed from multifunctional silica particles and polymeric binders, which are hydrophobic coatings with low surface energy and a high contact angle. The initial reflectivity was higher than 90%, and the accelerated aging showed that anti-soiling spray could maintain its performances for a period of 18 months to two years.

Similar investigations were conducted by (Hunter et al., 2014) and reported better results: 99% of initial solar weighted reflectance, and a range of two to three years of outdoor durability.

While most anti-soiling coatings are hydrophobic, (Aranzabe et al., 2018) tested a titania-based hydrophilic coating for CSP anti-soiling purposes in Spain for 43 months. Hydrophilic coatings have a high surface energy and a low contact angle, with a totally wet surface being the extreme case. The mirrors that were coated showed a higher average reflectance difference of 3.3% when compared to the uncoated ones, moreover, the highest reflectance difference was 9.5%. (Lorenz et al., 2014) studied the economic feasibility of a hydrophilic

coating with photo-catalytical functions, a 3% yearly energy yield gain is expected if the coating is applied.

(Wiesinger et al., 2018b) tested different anti-reflective coatings for the purpose of mitigating erosion; the coatings improved the optical performance of the tested glass by around 4.9%; however, if the CSP site often suffers extreme weather conditions, anti-reflective coatings would cause faster optical losses. Even though adding a hydrophobic coating to an anti-reflective one slightly reduced optical performance, it was reported to be very effective against sand erosion.

Since 2019, more recent papers reported innovative methods of water-saving mitigation by coatings:

(Wette et al., 2019a) tested a new hydrophilic coating under real outdoor conditions in PSA, Spain during 22 months; the effect of the coating was positive, lower soiling rates and higher cleanliness were observed for the coated mirrors in contrast to the uncoated ones. The optical properties and durability of this coating was studied by (Fernández-García et al., 2019), the coating did not cause significant change in the initial reflectance (-0.001 ±0.003). The assessment of the durability of the coating was done via accelerated aging tests and outdoor exposure, the same previous negligible values were observed, which denotes the expected durability of the anti-soiling coating and its reasonable applicability to reflectors in CSP plants.

(Matal and Naamane, 2020) conducted accelerated erosion tests of two types of coated solar reflectors: one with a hard coating, the other with an anti-soiling coating; the results suggest that the hard coating is better in terms of optical performance and resistance to mechanical stress.

(Wette et al., 2019b) conducted 6 years of outdoor exposure, as well as laboratory abrasion test, to evaluate anti-soiling coatings. One of the tested coatings improved the initial reflectance while the other one did not change much the sample's initial reflectance; this advantageous behavior diminishes for biweekly-cleaned coatings (2 years) faster than the monthly-cleaned ones (4 years), which confirms that coatings are water saving. Coated mirrors are more vulnerable to mechanical stress than uncoated ones as suggested by abrasion tests.

(Lopes et al., 2019) studied horizontal and tilted coated mirrors in Portugal. The coatings' effect was positive, especially for the tilted samples, while the horizontal ones presented almost similar soiling rates, coated or not.

(Pescheux et al., 2020) performed five extreme accelerated aging tests on different types of coatings (including a commercialized one), the tests simulated extreme conditions of salination, humidity, temperature, UV radiations and solar radiation. Hydrophobic SiO_2 nanoparticles-based coatings performed better than the other ones, including the commercial one.

(Sutter et al., 2020) studied the impact of dust on tube receivers of the parabolic trough technology for 5 years in Morocco and Spain. Anti-reflective coatings reduced the impact of dust to only -0.014 transmittance loss in Spain, while in Morocco, severe dust events resulted in a transmittance loss of 0.05; accelerated aging tests were also conducted and the highest degradation rate was -0.041. (Wette et al., 2020) tested two newly developed anti-soiling coatings during 2 years of exposure in Spain, the coatings were cleaned with pressurized water and a brush; the results suggest that the coatings perform differently and dependently on the cleaning technique: for one type, the pressurized water resulted in a cleanliness gain, for the other type it was vice-versa (poor washability).

(Yilbas et al., 2021) presented a comprehensive analysis of dust characterization techniques, soiling mechanisms, and dust mitigation by hydrophobic surfaces for solar energy applications.

III. 1. 4. Effect of climate on soiling intensity

The severity of dust deposition does not only vary with the solar mirror's material type, but also with the different climates and regions hosting the CSP plants:

(Sansom et al., 2017) studied and compared the deposition of airborne dust on CSP mirrors in different arid regions, namely: Algeria, Libya and Iran. They reported that the only aerosols to adhere to the surface of mirrors and cause reflectance loss were the ones smaller than 250 μm (maybe because much smaller particles aren't heavy enough to settle on the mirrors, and larger ones do not adhere due to rebounding or gravity), dust particles up to 1 mm or even more can be lifted by strong wind (up to 20 m/s) and damage the mirrors, thus, particles larger than 250 microns should also be used in laboratory simulations of glass mirrors erosion by

airborne sand (unlike the usual research trend of using only particles smaller than 250 microns).

(Guerguer et al., 2017) compared soiling between seaside and desert sites (Morocco, 3 years): mirrors exposed in the seaside were more soiled than those in the desert. The reflectivity losses were up to 80% (August) for seaside site and 23% (March) for desert site. More than 80% of the deposited particles were smaller than 30 microns. One of the main reasons that caused higher dusting in the seaside site in comparison to the desert one is the higher humidity recorded in the former (figure 3.3.a), since it enhances the adhesion of dust particles to the reflective surfaces of the mirrors. As for the effect of wind speed (which had similar behavior in both sites) on the intensity of soiling, a proportional correlation was confirmed, especially in the seaside site where stronger wind increased the salinity of the deposited particles, especially starting from 2.5 m/s (figure 3.3.b).
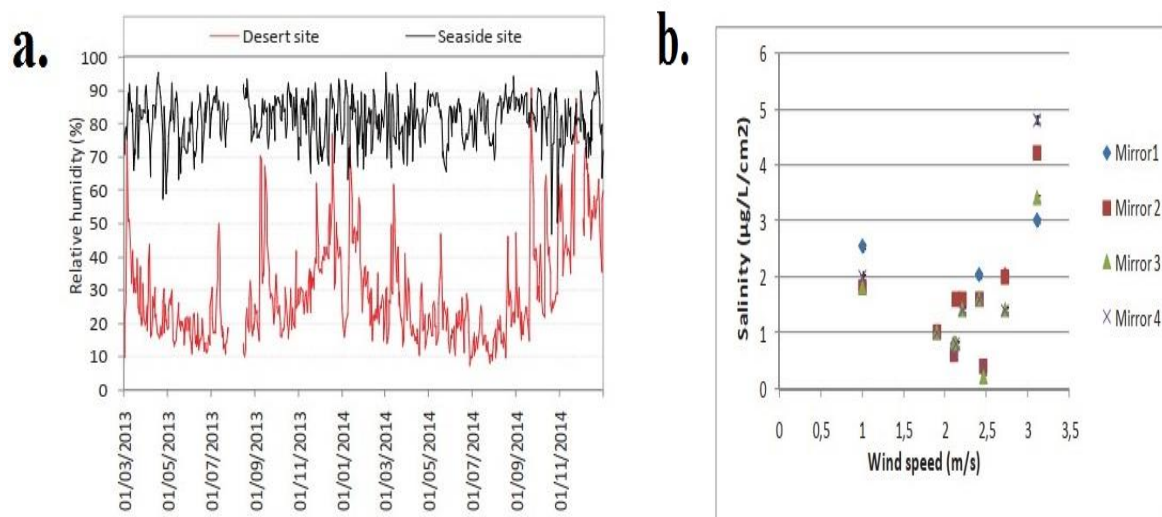
Figure 3.3. (a) Comparison of the relative humidity between the two sites. **(b)** Effect of wind speed on the salinity of particles in the seaside site (Guerguer et al., 2017).

In a similar coast/desert comparison, (Endaya et al., 2019) simulated -by accelerated tests- the impact of dust on a CSP reflector in Libya. The fine coastal dust caused more optical losses than the desert's one: the reflectivity losses were 8% and 4% respectively. The coastal dust had more silica than the desertic sand, however, the later was richer in calcium, which gave it more hardness. Since the reflectivity losses due to the coastal sand were double the desertic one, it can be safe to say that the effect of humidity, as a soiling factor, is more important the hardness of dust particles.

Long-range aerosols-transport can also cause soiling,(Conceição et al., 2019) compared soiling of mirrors in Portugal and Morocco during five months of the dry season, the daily dirtiness rates were 0.013 in Morocco and 0.004 in Portugal, this was due to the Saharan dust presence with higher quantities in Morocco in comparison with Portugal, for the later, the presence of dust is due to long-range transport phenomena, the general trend was that dirtiness in Morocco was higher than that of Portugal by factor of 3. Red rain in Morocco caused reflectance drop by 19.7% in one day. the mirrors dirtiness is measured with a Tracking Cleanliness Sensor (called TraCS), which components are a rotating mirror and 2 pyrheliometers, one is directed towards the sun and measures the solar irradiance, and the other measures the irradiance reflected from the mirror.

Similarly, (Alami Merrouni et al., 2020) reported, after about six months of exposure, higher soiling rates of 10 to 21% in Morocco compared to 3 to 7% in Portugal. An intense dust event caused severe cleanliness loss in Morocco by 39%, the long-range transport of the phenomenon reached Portugal and caused less severe but still important cleanliness loss of 18%.

In a wider comparison, (Wiesinger et al., 2020) run one year of outdoor exposure at six CSP potential sites in Spain, Morocco and Chile. In order to study mirrors' erosion, their reflectivity was measured first by taking images by 10-fold magnification objective after exposure, and comparing them with a new reflector of the same type, the difference in pattern is used to evaluated the reflectivity loss; this method is compared to measurements of a reflectometer. Also, for the purpose of reproducing outdoor exposure aging, laboratory accelerated aging experiments were conducted with an open-loop setup for better control of experiment conditions. Erosion potential risk matrix is proposed and validated in 5 CSP candidate sites to study erosion factors, the matrix has 6 meteorological and geological parameters as inputs.

Likewise, (Wiesinger et al., 2018a) studied the erosion risk of sandstorms on CSP reflectors, the experiments were carried out at two sites in Morocco for 25 months, as well as additional experiments in Kuwait. Glass was used as a reflecting material, soil samples were collected from two arid sites which are favorable for hosting CSP plants, the diameter of the collected sand range from 0.25 to 1200 μm, however, only particles of diameter up to 31 μm were kept in order to keep sampling accuracy, different meteorological (wind speed, Rh) parameters were also measured at sampling sites. The maximum loss of specular reflectance of glass mirrors exposed in Kuwait was 42.5% in just 9 months, however in Morocco, the maximum

specular reflectance loss was 5.9% in 25 months. The authors noted that an estimation of potential damage in a site can be done by artificial erosion setup, using the site's soil at different test velocities.

(Matal et al., 2020) performed erosion simulations, with the different samples being homogeneously exposed to a uniform mass of sand mass. The reflectivity loss is proportional to air velocity and tilt angle, the reflectivity loss due to erosion at an angle of 90° -for example- was much higher for an air velocity of 25 m/s (11.03%) than for velocities of 10 m/s and 5 m/s (about 3% and 0.9% respectively). The effect of particles shape was studied as well, sharp sand particles are more likely to stick to the mirrors' surfaces and/or cause more erosion.

III. 1. 5. Soiling effect on different types of mirrors

(Bouaddi et al., 2017) analyzed soiling's effect on different types of CSP mirrors; glass reflectors recover perfectly their reflectivity after rain, better than aluminum ones; however, glass mirrors tend to lose their reflectivity faster. Also, clean mirrors were soiled faster than unclean ones, especially for humid areas, as low humidity boosts the cleanliness by weakening adhesion between dust and mirrors' surfaces. The highest soiling rate was recorded for glass mirrors in August: -2.3% per day, by the summer's end, the mirrors lose up to 73% of cleanliness.

A similar study was done by (Wiesinger et al., 2017) through an exposure of two years at two sites in Morocco, and the average losses in the reflectance of the mirrors were 36.9% for aluminum and 10.8% for glass. Single Particle Momentum Distribution -which connects the speed of wind to the concentration of particle- was used for the sake of assessing the risks of erosion. In addition, the authors conducted indoor, laboratory investigations of accelerated aging.

(Azouzoute et al., 2019a) evaluated the effect of soiling on different solar mirrors, namely glass and aluminum, in Morocco during 18 weeks. The reflectivity of different mirrors is measured with the widely used portable specular reflectometer (D&S, 15R-USB, see figure 3.4). Aluminum mirrors were found to be less affected by dust than glass mirrors, their maximum soiling rate was 25% in comparison with 35% for glass mirrors. The authors recommended and noted that aluminum mirrors might be more suitable for CSP plants, especially if the plant project is in an arid region and is dedicated for industrial procedures with low temperature needs.

Figure 3.4. D&S 15R-USB Reflectometer used to measure reflectivity (Azouzoute et al., 2019a).

(Bouaddi and Ihlal, 2016) studied dusting of glass and aluminum solar mirrors in Morocco during 4 months of outdoor exposure, the average relative humidity and wind speed were 79% and 3.5 m/s respectively. Similarly to most reviewed studies, the authors reported that glass CSP mirrors are more susceptible to soiling than aluminum ones. However, raining events were reported to have a more efficient cleaning effect on glass mirrors, manual washing is expected to have a similar effect, and it could be concluded thus that aluminum mirrors encourage water saving and/or that it would be of benefit to use such type of mirrors for regions with water scarcity.

III. 1. 6. Modeling soiling losses in CSP

An efficient way to bypass the aforementioned experimental studies is by developing models -on physical bases- that evaluate the soiling of CSP reflectors.

(Picotti et al., 2018) developed a physical model to evaluate the soiling rate of CSP solar mirrors, the model was validated using 4 months of experimental data in Brisbane, Australia. The model takes into account dry dust deposition rate, gravity, diffusion and turbulence,

Brownian motion, aerodynamic drag and van der Waals forces, the model considers in addition to dust deposition, dust shading and blockage effects; model details can be found in (Picotti et al., 2018). The input parameters of the model are: aerosols concentration and size distribution, solar mirrors' position, wind speed and ambient air temperature. To validate the model, mirrors at different tilt angles were exposed and had their reflectivity measured by a 15R-USB D&S reflectometer, dust concentration was measured by the mean of an E-sampler dust-monitor, and a weather station provided meteorological parameters. The average relative error is reported to be 15% for 45° tilt angles which reflects a good agreement between modeled and measured data. Furthermore, the model was used to evaluate different scenarios in 3 candidate sites in order to display trends of reflectivity loss under variable conditions.

(Heimsath and Nitz, 2019) developed an optical model that evaluates incidence angles' impact on the reflectance and attenuation of solar radiation by dust. the model was developed and validated using laboratory experiments with both artificial and desert dust types. Incidence angle variated between 8° and 80°. The results showed that the reflectance of soiled mirrors depends upon light incidence angle, the same observation was made for light scattering. The model showed proportionality between incidence angles and the intensity of scattering by aerosols, and inverse proportionality to specular reflectivity, which indicates that CSP optical models should take into account irradiance angle. When applying this model to simulations, it was found that the optical efficiency of parabolic trough reflectors in southern Spain was overestimated by 1.5%. Similarly, (Wu et al., 2020) proposed a model to predict dust characteristics and tilt angles' influence on the soiling rate. The model was validated, with less than 3% standard deviation, by the measured cleanliness of a parabolic trough collector in China.

Similarly, (Heimsath et al., 2020) proposed a model that considers the effects of variable reflectance angles and soiling rates. They suggest that the reduction of the optical efficiency of second glass silvered solar mirrors occurs via two optical phenomena: shading and blockage (figure 3.5). For the former, the deposition of dust particles on the surface of the glass layer blocks the solar irradiation and prevents it from being reflected by the silver layer as can be seen in figure 3.5 hereafter. A for blockage, the light that escapes shading by some particles and gets reflected afterwards by the silver layer might be blocked by other deposited particles, the losses due to blockage are either by scattering or absorption. The intensity of the optical losses is proportional to incidence angles (relatively to the normal). It would be good to note that this consideration simplifies real-life conditions, as in reality the two phenomena

overlap, furthermore, the deposition of soil particles and their size distribution are more likely to be inhomogeneous, adding that to the fact that the considered round shape of particles, the proposed model is significantly simplifying but still useful, as a try in this research axis at least.
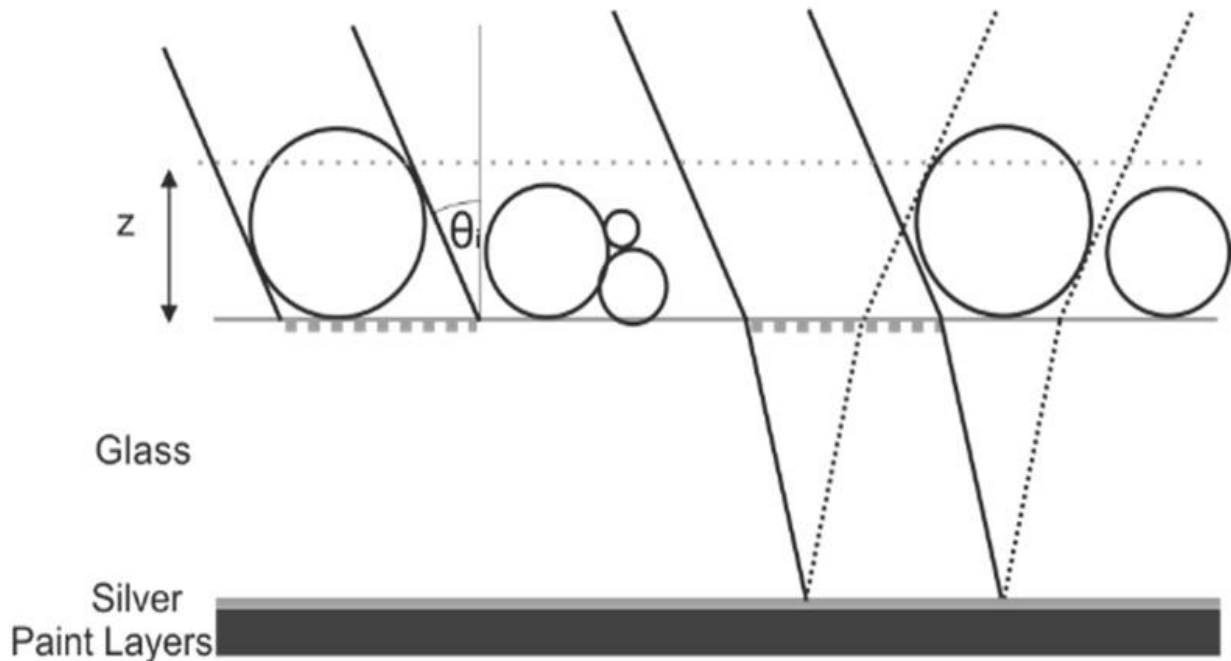
Figure 3.5. Consideration of the optical losses caused by dust particles via shading (left) and blockage (right) (Heimsath et al., 2020).

(Bouaddi et al., 2015) modeled the cleanliness of CSP reflectors with Dynamic Linear Models, then compared it with that of exposed 45° tilted mirrors. The dust distribution was homogenous (since there's one row of mirrors, this confirms that fist row mirrors are soiled uniformly as noted also by (G. Singh et al., 2015; Z. Guan et al., 2015)). The lowest measured cleanliness was around 20% after 3 months. The local linear trend described most accurately the cleanliness factor, intervention variables should be included to account for rain episodes or cleaning operations.

(Sansom et al., 2015) conducted experimental simulations of reflective surfaces' erosion in a laboratory erosion rig, using dust samples collected from Libya and climate conditions recorded in Egypt near a CSP project. They reported that sandstorm would be characterized by 4 g of airborne sand particles at a speed of 10m/s. A computational prediction of the sand's impact on the reflectivity was developed basely on meteorological data in CSP sites. The

reflectance loss was due to the adhesion of fine particles rather than surface damage, the loss was up to 23%.

(Deffenbaugh et al., 1986) proposed, after one year of outdoor exposure in the United States, a model to simulate soiling through combination of different data sets and models, the model considers real-world degradations of parabolic trough collectors. Optimal washing frequencies were predicted and found to be 20 and 45 days, in New Mexico and Texas respectively. The maximum measurements of the soiling rate were in the range between 1.3% and 0.7%.

Recently, (El-Boujdaini et al., 2022) studied the outdoor soiling of a sample solar mirror for six months in Morocco, the selected experimental data included soiling rate (measured with a TraCS setup), global, diffuse, and direct solar irradiance, precipitations, ambient temperature, relative humidity, wind speed and direction, all recorded by a meteorological station. The highest soiling rate was 63% resulting from 20 days without natural nor manual cleaning, then it fluctuated due to occasional precipitations. The optical performance was modeled by the mean of neural network approaches, the best neural network model -which showed very low root mean square error- depended upon wind speed, relative humidity, temperature, and Aerosols' Optical Depth (please refer to subsections II.3.1.a and II.3.1.b for more details about the later parameter and its impact on optical losses). Authors noted that heavy rain served as natural cleaning, while light rain enhanced soiling because of the coagulation it caused.

III. 1. 7. Soiling effect on the energy yield of a CSP plant

To assess the impact of dust deposition on the CSP plant's energy output, (Alami Merrouni et al., 2020) used Ebsilon software to simulate energy yield with and without consideration of mirrors' soiling. Without taking soiling into account, the energy yield in Morocco and Portugal was 1.4 GWeh and 1.3 GWeh respectively, but with consideration of soiling losses, both sites produce comparable electricity supply of 1.25 GWeh during the exposure period, this is expected given the higher soiling in Morocco compared to Portugal (Conceição et al., 2019).

(Azouzoute et al., 2019b) evaluated the impact of soiling on energy production of a 5 MW plant. The cleanliness index was measured by TracCS system and dropped by up to 30% in just 8 days. In addition to evaluating the cleanliness of the mirrors, different meteorological parameters were measured throughout the year, the data were then implanted in System

Advisor Model (SAM) software used to predict the effect of dust on a linear Fresnel plant, the consequent impact of two weeks without cleaning was a daily production loss of 22% in average.

While (Hachicha et al., 2019) investigated the impact of soiling on CSP optical and thermal performance in UAE through 5 months of outdoor experimentation. After 3 months of exposure, the reflectivity dropped by 63% and led to 36% decrease in thermal efficiency of parabolic trough collectors. Dust deposition was reported to cause more loss in performance of CSP than PV by a factor of 3 to 5, the deposition rate was correlated to wind speed and direction parameters.

(Bellmann et al., 2020) investigated soiling losses in Portugal during 9 weeks, through studying cleanliness using samples mounted on a solar tracker (figure 3.6), as well as solar mirrors of various directions and tilts (0° to 90°). Soiling rate of CSP was reported to be 8 to 14 times higher than that of PV for an identical quantity of soiling. Based on Mie-scattering and the wide-range incidence angle measurements, authors developed a model that evaluates the optical losses due to soiling for both CSP and PV, the model has for inputs: the gravimetric density (g/m^2), refraction's complex index, size distribution and spectral and acceptance angle responses. For mitigation, monthly cleaning frequency ensured reflectivity of -at least- about 90%.

Figure 3.6. Solar Tracker (Bellmann et al., 2020).

To evaluate the impact of dust on solar tower plants, (Singh et al., 2015) investigated the soiling of heliostats and Open Volumetric Air Receivers (OVAR), the tests were done with single and double heliostat set-ups, the heliostats were inclined at 25° and the inlet velocity was 16 m/s. Dust blocked 20% of the OVAR's pores, which caused reduction of the convective heat transfer and the overall efficiency. For the single heliostat and the first one of the double-heliostat set-ups, the deposition of dust was uniform, for the second heliostat, the deposition was localized due to the turbulent flow generated by the presence of the first heliostat.

(Niknia et al., 2012) developed a method to evaluate dust deposition effect on parabolic trough collectors, the measured effect of soiling was 44% and 60% reduction of reflectance after 44 days and two months without cleaning, respectively; while 1 g/m² and 1.5 g/m² of dust caused 45% and 60% reduction consecutively. The custom-made instrument (figure 3.7) consists of a bottomless black box divided by a black separating wall into two partitions, in one partition there is a laser light source, in the other a reflectometer, the role of the black separation is preventing scattered light from noising the reflectometer's measurements, the

mirror is placed under the bottomless box and is opposite to the devices. The authors gave the following empirical loss correlation as a function of the deposited dust thickness "y", in a parabolic trough power plant in Iran:

$$\Delta Q / Q = 0.367 * lny + 0.7249 \qquad (3.1).$$

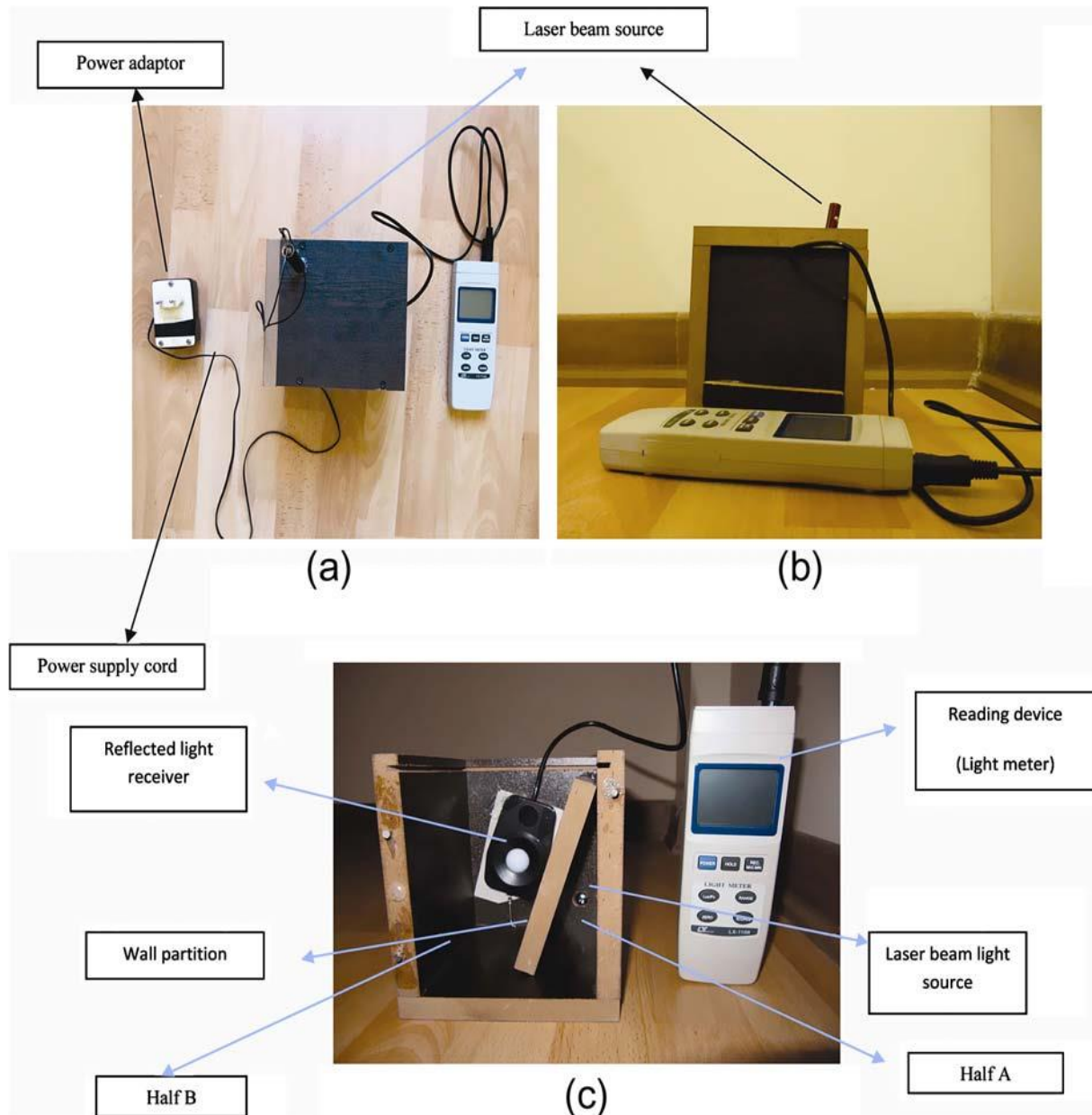**Figure 3.7.** The proposed method for reflectivity measurement (Niknia et al., 2012): **(a)** Top view. **(b)** Right-side view. **(c)** Bottom view.

Recently, (Abraim et al., 2022) evaluated the techno-economic impact of soiling on solar power applications (CSP and PV). Used data included one year of meteorological, soiling, and dust quantity measurements under semi-arid Moroccan climate, using respectively a

meteorological station, a TraCS system, and DustIQ soiling sensor (technical details on setups and devices can be found in the aforementioned study). Optical losses for CSP were reported to be five to six times more important when compared to PV, with a daily average of 1.21%/day 0.24%/day respectively over the studied year between March 2018 and March 2019. With these measured values as inputs, the simulated yearly energy losses were - logically- higher for Fresnel linear 1MWe plant (17.76%) in contrast to the 1MWe PV panels plant, these losses were obtained considering a monthly cleaning frequency. As for the economic impact of cleaning frequencies, the analysis concluded that the optimal cleaning would be at a three-weeks-frequency for both technologies, with an annual economic gain of 230.16 x10^3\$ for CSP and 278.51 x10^3\$. The simulations were performed with EBSILON software and the economic assessment with the Levelized Cost of Energy, commonly used for such studies.

III. 1. 8. Soiling mitigation by washing solar mirrors

The usual mitigation of solar mirrors' soiling is by washing their reflective surfaces, even though this mitigation approach is not water economic (Wette et al., 2019b).

(Niknia et al., 2012) studied and presented tabulation of the impact of cleaning frequencies' programs on the yielded energy of parabolic troughs in Iran. The extremums of cleaning frequencies were 7 and 42 days, which resulted in consuming 398.9 and 69.0 m^3/year of water and losing 11% and 38%/year of the mirrors' optical efficiency, respectively. While the monthly cleaning resulted in yearly efficiency losses of 27% and the consequent water consumption was 99.7 m^3/year.

(Ashley et al., 2019) used a heuristic approach to determine a solar field's cleaning sub-routing that optimizes a solar tower plant's optical performance. It was highlighted that the true profit of this approach would be during planning and design of CSP plants. The authors concluded that for cleaning schedules, regular cleaning approach appears to be the most optimal.

For precise simulations of soiling losses of frequently cleaned plants, (Bouaddi et al. 2018) proposed the application of Markov switching regime that allows to consider different soiling regimes instead of constant soiling rate, and this through the inclusion of site-dependent climatic variables.

(Fernández-García et al., 2014) assessed a diversity of washing techniques for two years at a semi-desertic site, the most efficient technique was the association of a brush with

demineralized water, which resulted in an excellent restoration of optical performances (average reflectivity of 98.8%), while detergents' addition didn't result in considerable profits. The use of a steam device along with a soft issue wasn't enough as reported by the study.

(Conceição et al., 2020) studied soiling's economic impact on solar tower in semi-arid climates, during rainy periods (November to May) washing operations are not economic nor efficient. As for the methodology followed to obtain the reported results, TraCS system recorded 18 months of reflectivity, and different data were inputs for simulations of the energy yield, then the plant profitability was plotted versus cleaning price of various frequencies.

(Picotti et al., 2020) studied the optimization of cleaning schedules in solar tower plants. The authors established a model to compute the economic feasibility of different schedules. The model was developed according to the theoretical attitude of dusting of reflectors and is tested on solar tower plants in UAE and Australia, the reports suggest potential economic profit of total cleaning that can be up to 15%.

(Bourdan et al., 2020) suggested water-economic mitigation for dusting issues of CSP plants. The authors proposed dust-barriers that were able to stop 47% of particles of sizes larger than 25 microns; an economic portable dusting detector was also developed, and this in order to perform cleaning operations only when needed. An ultrasonic equipment was tested as well, it resulted in an up-to-99% cleanliness factor.

III. 1. 9. Electrodynamic screens' potential for soiling mitigation

Electrodynamic screens (EDS, Mazumder et al., 2005) are an emerging mitigation to prevent CSP mirrors' soiling, EDS consist of a transparent dielectric film in which alternated electrodes are deposed, when activated with phased voltage pulses, the electrodynamic field prevents dust particles from depositing on solar mirrors and removes the already deposed ones, by charging the particles, lifting them, and propelling them off the reflector (Mazumder et al., 2013). (Mazumder et al., 2014) reported high EDS dust removal efficiency and highlighted its high potential as a low-cost self-cleaning method for CSP reflectors.

(Stark et al., 2014) conducted experimental and numerical investigation of the efficiency of EDS in preventing CSP mirrors' soiling, it was reported that even though EDS application caused initial reflectivity loss of 3%, EDS integrated mirrors kept specular reflectivity >90% without any cleaning operation. (Mazumder et al., 2019) reported similar experimental results

and highlighted the low energy consumption and cost of EDS, namely 0.2 Wh and $0.005 per m^2 per cleaning cycle respectively.

(Chan et al., 2019) proposed a model of a new EDS configuration to study the usability of EDS for parabolic trough collectors, the model was validated by comparison to published experiments under similar conditions; they noted that the new EDS configuration offered improved cleaning.

After 3 years of study (2017-2020), (Mazumder et al., 2020) reported that EDS' dust removal efficiency and specular reflectivity restauration are both higher than 90%, it was proved that EDS can operate under all solar fields' temperatures and for relative humidity between 20% to 95%; the authors concluded after economic analysis that EDS technology is in a commercial level.

III. 2. Optical losses due to atmospheric extinction

III. 2. 1. Relationship between Aerosols' Optical Depth (AOD) and reflectivity losses

The optical losses in CSP plants is the outcome of the overlapped cumulus of two attenuative phenomena: in addition to drops in reflectance due to solar reflectors' soiling, another factor that should be considered is the attenuation of solar irradiance due to suspended aerosols particles, the suspension of aerosols particles generally originates from wind lifting up particles of dust, while the deposition of soiling on solar mirrors is the consequence of the settlement of aerosols particles. The overlapping of these two soiling factors implies that the atmospheric attenuation of solar irradiance at CSP sites ought to be put into consideration as we have recommended in our review paper (Zereg et al., 2022).

Even though this is not the general trend in CSP mirrors' soiling papers, the results reported by few studies confirm the relationship (simultaneity/causations?) of Aerosols' Optical Depth (AOD) trends and drops in reflectance, this is the case of the conference paper of (Raillani et al., 2019) who confirmed the inverse proportionality between AOD and reflectance, through measurements of one year of meteorological data by the mean of a weather station, in addition to reflectivity drop measurements. Besides the inverse proportionality, and after studying the volume distribution of aerosols, the authors concluded also that the coarse particles are much more responsible for the attenuation than other particles.

These findings confirm what (Griffith et al., 2014) remarked: supervising AOD and wind speed and direction near CSP plants is necessary to evaluate dusting risks, this is particularly mandatory for sites around active industrial zones/mines.

III. 2. 2. Importance of AOD assessment for the evaluation of extinction in solar tower plants

Precise modeling and prediction of the incident DNI is essential for CSP plants in general and solar tower plants in particular, the precision of this prediction depends greatly upon the assessment of the atmospheric extinction and attenuation of solar irradiance, one of the key parameters for this assessment is AOD.

(Polo et al., 2016) proposed a model for the evaluation of the atmospheric extinction in solar tower plants, the model outputs the attenuation (in %) as a third order polynomial dependance upon the plant's slant range, furthermore, the coefficients of the polynomial are a third order linear dependence upon the AOD as well. This model was improved using two years of atmospheric extinction data measured -at PS Almeria, Spain- by CIEMAT system for measuring extinction levels in solar tower plants, using two cameras with high-resolution, the cameras are 742 m apart, which is a distance representative of solar tower plants range (generally inferior to 1 km). The improved model (Polo et al., 2020) was validated by comparing the measured extinction with the simulations based on AOD data of the nearby AERONET station, which resulted in 6.1% of Root Mean Square Error (RMSE) in comparison to 10.9% for the original model.

For the same purpose of predicting precisely the attenuation levels between the heliostats and receiver in solar tower plants, (Carra et al., 2020) used one year of extinction data measured by the before-mentioned CIEMAT system to validate the "extinction atmospheric optical thickness model" anteriorly developed by the authors (Carra et al., 2018), the measured data were also used to validate the datasets of AERONET, MERRA2, as well as MODIS Aqua and Terra satellites. As for the extinction levels recorded by the four datasets compared to that of CIEMAT, it can be observed that the four datasets underestimated the mean extinction levels and overestimated the minimum ones. While for the maximum extinction levels, the datasets obtained from the satellites overestimated the extinction levels, unlike the other datasets. At PSA, the mean, maximum, and minimum extinction levels measured by CIEMAT system are: 5.80%, 13.20%, and 1.50% respectively.

(Hanrieder et al., 2019) evaluated the attenuation in solar tower plants too, they used a dataset of 35 months recorded in Morocco and Spain to validate their model (Hanrieder et al., 2016) for a plant's slant range of one kilometer. Three different approaches were used to estimate aerosols' quantities: The Boundary Layer Height (Berrisford et al., 2011), the Homogenous distribution, and finally the Vertical aerosols profiles of LIVAS database (Amiridis et al., 2015). For the Spanish site (PSA), the mean level of the broadband transmittance was 89%, while for the Moroccan sites, it was 87%, and 86%. The model had less than 5% of Mean Bias Error (MBE) and less than 8% of RMSE, which is a reflection of the good precision of the model.

(Singh et al., 2005) measured the levels of extinction of solar energy due to aerosols in India, the measured parameters were AOD and Global Horizontal Irradiance (GHI) using, respectively, a solar light spectrometer (MICROTOPS II) and a Kipp & Zonen CM-21 pyranometer, for the spectrometer, the measurements were taken at 340, 500, 675, 870, and 1020 nm. The authors reported that the high content of aerosols resulted in hazy skies, and as a consequence, extremely high values of AOD were measured during the period between April and June, the mean measured AOD was as high as 1.17 ±0.65 and the highest daily AOD was 3.08 ±0.55 which denotes the intense turbidity at the region during the study. The low corresponding values of Ångström exponent (average α was around 0.328) indicate that coarse particles were responsible for the haziness of the sky more than fine particles, the lowest α was -0.06 (negative values of α are correlated with the existence of particles that are water-insoluble). The average extinction level was about -13.6 W/m^2 for each 0.1 increase in AOD.

(Papadimas et al., 2012) evaluated numerically the effect of aerosols on solar energy over the Mediterranean basin using seven years dataset, the data were obtained from different databases. It was reported that, under clear sky, the surface reception of solar energy was reduced by a yearly average of 22.9 W/m^2 and by a monthly average of 31.7 W/m^2 for July. The main parameter characterizing the attenuation is AOD, aerosols' radiative impact is reported to be most important for clear skies, it's strongly dominated by a latitudinal gradient, and its seasonal variation is mainly due to the seasonal variation of solar irradiance reaching Earth, since the radiative summer/winter loss ratio is 4.8 while the AOD summer/winter ratio is 1.8. The Middle Eastern and North African region seems to present an important amount of absorption by aerosols > 30-40 W/m^2, AOD in desert areas is very high and up to 0.4 (compared to 0.25 in Europe).

(Cardemil et al., 2014) evaluated the use of three clear sky irradiance models for the sizing of a solar tower plant in Brazil, while "Pitman & Vant-Hull" model was in agreement with "Sengupta & Wagner", DELSOL didn't agree with both (as shown in figure 3.8), the Power Tower Generator (PTGen) program that was used for the sizing and optimization of the plant is based on -besides Fortran code- DELSOL3 code, which resulted in the underestimation by 4% of the irradiance attenuation between the receiver and the heliostats field due to the presence of aerosols and water vapor, as a consequence, the heliostats field should be 4% larger in order to avoid significant long-term losses. In fact, DELSOL model was developed for the specific elevation of 0.7 km of Barstow, California, USA and thus, necessary corrections should be introduced to the model before applying it to sites with different elevations.
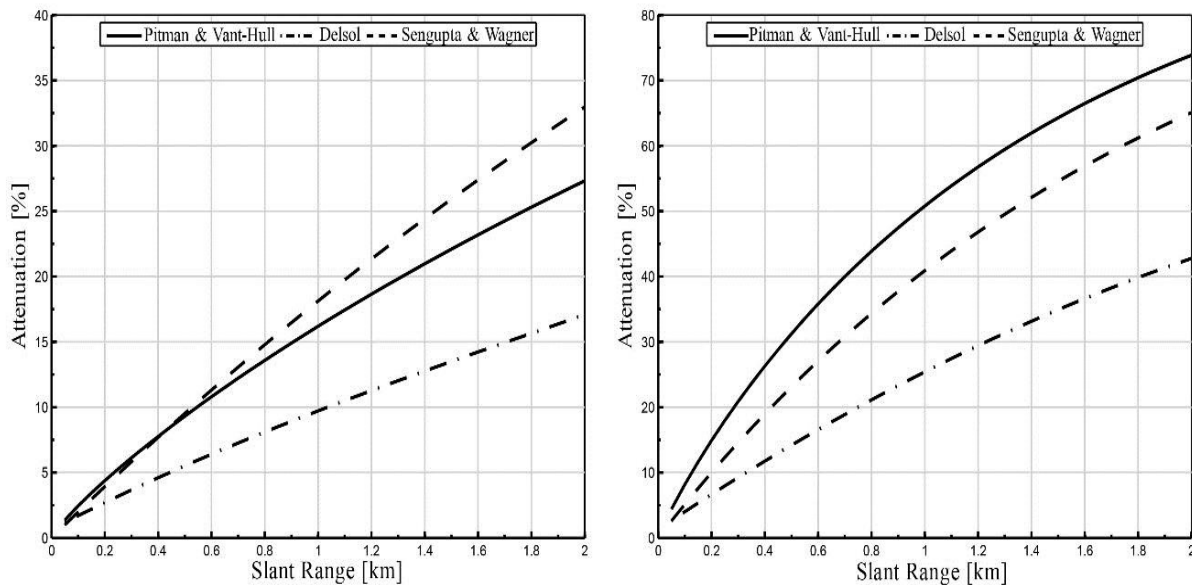
Figure 3.8. Atmospheric attenuation from the heliostat to the receiver over the slant range for the three models (Cardemil et al., 2014): clear day **(left)**, hazy day **(right)**.

III. 2. 3. Turbidity parameters for the prediction of direct normal irradiance

In addition to AOD, there are other turbidity parameters that are primordial to prediction of the incident solar radiation, namely: the Turbidity factor of Linke T_L, Ångström exponent α, and Ångström coefficient β. An accurate estimation of the solar radiation would give good energy yield assessment for solar energy applications such as concentrating systems and photovoltaic ones (Pérez-Burgos et al., 2017; Zereg et al., 2022).

For the purpose of improving numerical prediction of DNI in sites where no turbidity measurements are available, (Pérez-Burgos et al., 2017) compared eight solar direct irradiance models using 32-years-data of measured meteorological parameters at Madrid, Spain. An accuracy improvement of 4% can be achieved when the models' parameters are adapted to the local site. The best performing models in Madrid were: Louche (Louche et al., 1991), European Solar Radiation Atlas "ESRA" 2, and Robledo-Soler (Robledo and Soler, 2000), unlike the other two models, the T_L-dependent model ESRA 2 did not need any empirical coefficient to be adjusted to the site, and the accurate data of T_L were sufficient to obtain precise results. The authors reported also that models that depend upon the solar altitude angle as the solely input variable can be very efficient when adapted to the site through locally-adjusted coefficients, this is the case of the Robledo-Soler model. As for Louche model, it was selected because it is a widely used model that depends upon clearness index.

Atmospheric turbidity parameters -namely T_L, AOD, α, and β- were found to have the most important impact on the accuracy of numerical simulations of solar irradiance according to (Benkaciali et al., 2018) who studied the performance of 18 clear sky irradiance models under two years of Algerian climate, the measurements were taken in two sites: one is Algiers with its moderate Mediterranean climate and the other one is Ghardaia with semi-arid desert climate. The best performing models were: ESRA, Dogniaux, MAC and Yang. Formulations of the different parameters as well as models were given by the authors. Apparently, simple models over-estimated dramatically the DNI, while others underestimated it. Moreover, SMARTS code (which is commonly used as a comparison reference) was used to evaluate models, after it was compared -and in agreement- with the measured data, ESRA again, in addition to Dogniaux model, were found to provide good consistency with the SMARTS code.

(Behar et al., 2019) proposed a simplified methodology to estimate solar irradiance and atmospheric turbidity derived from ambient temperature and relative humidity. They also proposed a simple and accurate expression for precipitated water with a Mean Bias Error (MBE) of 4.19%, better than the 8.06% MBE of REST2v5 model (which is the fifth version of Reference Evaluation of Solar Transmittance). The proposed expression for the precipitated water depends upon the dew point temperature, which is a function of relative humidity and ambient temperature. The methodology is validated through one-year data of one-minute time step, measured in Atacama Desert in Chile, the recorded data include DNI, RH and ambient temperature, while Pw was retrieved from NASA's Modern-Era

Retrospective-analysis for Research and Applications (MERRA). The MBE of DNI, T_L and Pw are respectively: 0.91%, 1.31% and 4.19% which show the accuracy of the model despite its simplicity.

(Marif et al., 2019) studied the atmospheric turbidity in Algeria, using Linke turbidity factor and Ångström coefficient as main inputs for the purpose of developing a CSI model that is based on 31 months of radiometric and meteorological measured data. The authors confirmed that T_L and β are highly dependent upon wind speed, ambient temperature and relative humidity. Seasonal dependence of aerosols presence was reported, with aerosols' load being high in summer and low in winter. The highest T_L and β were 5.07 and 0.159, respectively, from data measured during July 2014. Capdero's formula for Linke turbidity factor (Capderou, 1987) was validated in this study and reported to be suitable for low altitudes.

(Ineichen and Perez, 2002) provided an air-mass independent formulation for T_L, so that the main disadvantage of the widely used T_L -which is its dependence upon solar geometry- is bypassed. Previously to this work, the most used solution was the normalization of T_L for an air mass value of 2. The authors developed an empirical formulation of T_L that's independent of the altitude and the air mass, yet still coherent with the previous studies for AM=2, formulations for Global Horizontal Irradiance (GHI) and DNI are given as well, the T_L formulation is:

$$T_L = (11.1 * \ln(b * I_0/DNI) /AM) + 1 \qquad (3.2),$$

where I_0 is the solar constant, b is a multiplicative factor and AM=2.

(Mikofski et al., 2017) used data of DNI, AOD, temperature, relative humidity, and precipitated water measured for ten years in USA (Seven locations) to compare the precision of three models, namely Bird, simplified Solis (sSolis), and Ineichen-Perez; the last model takes T_L as an input, unlike the other two which depend directly upon AOD and precipitations. No accuracy improvement was reported after using real-time AOD and Pw measurements as inputs. Ineichen-Perez model had the lowest errors for DNI, closely followed by sSolis. The highest T_L was 4.8, derived from measurements at Bondville, IL (altitude: 213 m).

(Paulescu and Schlett, 2003) (Romania, three years of measurements) suggested a simple yet accurate model which performed better than ESRA and Yang's hybrid model. The model needs only surface meteorological data. Ångström's coefficient and exponent in particular,

and turbidity factors in general, were reported to have a major impact on the model's accuracy.

(Molineaux et al., 1995) proposed an empirical formulation for T_L using the method of least squares fitting of measured one-year data at two sites in Switzerland and USA. The authors also presented a comparison of T_L and β (Ångström's coefficient), physically speaking, β speaks for the amount of aerosols contained in a vertical atmospheric column, it generally varies in the range between 0.01 and 0.5 (the lowest value stands for clear skies, while the second one stands for an extremely turbid atmosphere or a long traveled optical path near the northern and southern poles), while Linke's turbidity factor, proposed by (Linke, 1922), is an expression of the number of the clear skies needed to reproduce an extinction equal to the turbid sky. T_L is a broadband parameter, while β is a spectral one and is derived in from the visibility. More details in regard to the theory of physics behind extinction can be found in section II. 3.

III. 2. 4. Clear sky irradiance models

(Tahboub et al., 2014) derived from ground measurements a model that evaluates irradiance attenuation between heliostats and solar tower receiver in UAE. Four pyrheliometers at different altitudes ranging from 340 m to more than 1000 m recorded data during one year at a resolution of 10 min, then the obtained data were filtered, the reasons of selection were: night data, relative error higher than the mean absolute error, cloud passages (nonclear-sky) and shading of pyrheliometers by the surrounding landscape of the Hafeet mountain (highest in UAE) on which measurements took place. 55.8% of the recorded data were selected, the model is based on the Beer-Lambert equation and the attenuation of the irradiance is as follows:

$$DNI_n = DNI_4 * \exp\left(-X * d\right) \tag{3.3}$$

DNI_n is measured by stations 1, 2, or 3, "X" and "d" are, respectively, the extinction coefficient and distance between station n and 4 (figure 3.9). This model is similar to the one proposed by (Sengupta and Wagner, 2012) although the later hadn't been validated at a specific location according to the authors.
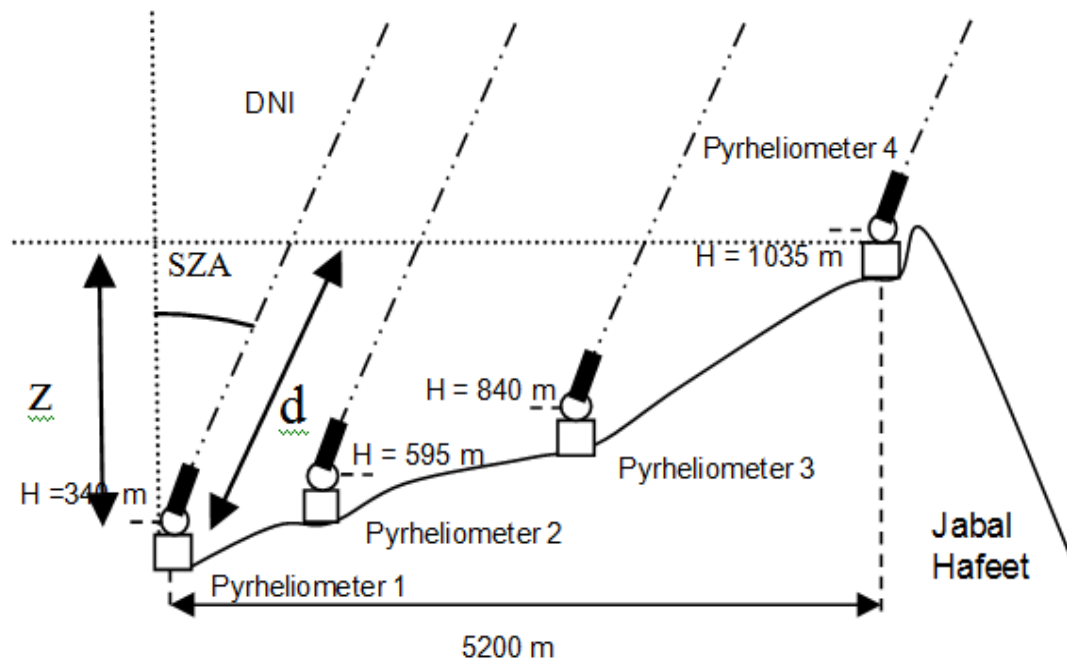
Figure 3.9. Representative scheme of placement of the four pyrheliometers on Jabal Hafeet (Tahboub et al., 2014).

(Rathore et al., 2019) generated a solar map of India under clear-sky conditions, they validated the r.sun model -which was developed in a C program- by comparison to eight years of measured data. The solar global, direct and diffuse radiation components were calculated with low MBE values, under the recommendation of ±10% MBE given by (Badescu et al., 2012), which makes the r.sun model qualified to compute irradiation in India for very hazy atmospheres. The T_L values were up to 5.8.

(Bright et al., 2020) suggested a new global clear sky detection model (Bright-Sun) and validated it with three years of meteorological data recorded at five Baseline Surface Radiation Network (BSRN) sites. The model performed well under five different climatic zones, it was tested at zones with each of the following characteristics: frequent, high dust loads (Tamanrasset), severe cloudiness, high rainfall (tropics), high solar zenith angles (low sun at the southern pole), as well as a reference zone. The Bright-Sun model overcame the limitations observed in other models, namely: poor performance under high zenith angles, short/long-term false positive/negative; the authors determined such limitations after testing 22 widely used models at the same five zones. The model is freely available and coded in Matlab.

(Ineichen, 2016) conducted a validation of seven CSI models over eight years at 22 locations in Europe, Mediterranean basin and south-east of Africa. They highlighted that atmospheric parameters other than AOD and precipitated water have minor effects on irradiation, so AOD and precipitations are the main input variables, precipitations were obtained from ground measurements of temperature and relative humidity (RH), AOD was obtained from MACC-II project, AERONET network, or by retrofit of DNI measurements. The three best models with low biases are: Solis, REST2 and McClear, furthermore, Solis is the only model that did not show any kind of inconsistencies. All models underestimated high DNI values, their performance did not present a seasonal dependence, and the biases of CSI predictions decreases with AOD for all models and at every location. The wide spatial-temporal range of measurements (22 sites, 8 years) and the restrictive selection of data ensured the clarity and stability of the kept clear-sky data and resulted in reasonable, acceptable biases.

(Engerer and Mills, 2015) validated nine CSI models with wide spatial and temporal range of data at high temporal resolution of 1 minute, ten years of data were measured at 14 sites in Australia which are representative for the different climatic regions of Australia. The meteorological input data included: solar zenith angle, Linke's T_L, Ångström's β, atmospheric content of water vapor, ozone, and nitrogen. The best performing model was ESRA, followed by REST2.

(Yang et al., 2001) with the help of two years of data at 16 meteorological stations in Japan, proposed a hybrid model to incorporate the direct and diffuse components for the sake of estimating the global solar radiation, the model is simple and takes into account different physical processes that affect the radiation.

(Alam, 2006) compared four CSI models, namely REST, Yang, Multi-Layer-Weighted Transmittance model, version 2 (MLWT2), and the Code for Physical Computation of Radiation, two bands (CPCR2). The models were compared using solar radiation data at four sites in India during eight years. Results suggested that REST model outperformed other models under Indian climate. The data used for the validation of REST model are comprised of monthly mean hourly global and diffuse solar radiation, recorded by a thermoelectric pyranometer with and without a shade ring for diffuse and global radiation respectively. Monsoon months are not considered since Ångström exponent α was considered constant and equal to 1.3, and during monsoon months Ångström exponent differs from this value either due to larger particles' size or due to aerosols being washed which means much smaller particles' size.

In a similar study, (Antonanzas-Torres et al., 2016) compared three models (sSolis, REST2, and ESRA) using six months of meteorological data in Canary Islands. The data were obtained from BSRN and AERONET networks at Tenerife Canary Islands (2373 m of elevation and 14 km away from the ocean). The authors studied the effect of elevation on the precision of the models too, this was done by comparison to a 156 m-high station which is only 11.5 km away from the first site. At the higher station, and using the data provided by the previously mentioned networks, sSolis model performed better than REST2 and ESRA, at the lower station however, ESRA performed better than the other, maybe thanks to its simplicity, despite the fact that all studied models overestimated solar radiation in the site with the lower altitude.

(Badescu et al., 2013) compared, using one year of data in Romania, 54 clear sky solar radiation models. The data were obtained from various sources, and were either measured at meteorological stations or derived from satellite data. The data included -but weren't limited to- solar irradiance (including DNI), ambient temperature, wind speed, ozone column, precipitable water, surface albedo. The statical parameters that were used in the evaluation are the widely used MBE and RMSE. Models that had $|MBE| < 5\%$ and $RMSE < 15\%$ were considered "good models". The best performing models -equally- were: ESRA3, METSAT, REST2v5, and Ineichen.

III. 3. Summary

The literature of studies in the focus of our thesis has been reviewed in the present chapter, in the first part, we highlighted the experimental and numerical papers that studied the different parameters affecting the deposition of dust on solar mirrors, the consequent loss in energy output, and coatings as a mitigation approach.

The deposition of dust on solar reflectors is mainly due to gravity more than diffusion (Griffith et al., 2014). Since AOD is proportional to the soiling rate of solar mirrors (Raillani et al., 2019), monitoring AOD in the surroundings of CSP plants ought to be done, in order to gauge the risk of soiling (Griffith et al., 2014). Intense, rare soiling events cause much more important reflectivity drops than the frequent, moderate dust deposition (Wiesinger et al., 2021; Conceição et al., 2019).

The tilt angle and material of solar reflectors have a crucial impact on the soiling rate: horizontal mirrors are always more soiled than tilted ones, thus a tilt angle, no matter how slight it is, can reduce the deposition of dust; also, glass mirrors are soiled faster than

aluminum ones, and restore their reflectivity faster and better after being washed (Alami Merrouni et al., 2015; Griffith et al., 2014). Soiling rates can reach high values (-2.3% per day (Bouaddi et al., 2017)), it would be of benefit to keep the factors controlling dust deposition under observation; other than the exposure direction, multiple meteorological factors are directly related to soiling events, namely: wind speed and direction, relative humidity and atmospheric pressure; low pressure is associated with rainy days, while high relative humidity values intensify dust deposition (Griffith et al., 2014), the effect of humidity, as a soiling factor, is more important the hardness of dust particles (Endaya et al., 2019). Monitoring these factors would help program efficient cleaning operations.

Many authors developed and validated soiling models for CSP applications (eg: (Heimsath et al., 2020; Wu et al., 2020)). The consideration of soiling when modeling the performance of CSP plants resulted in considerable losses of the yielded energy (Alami Merrouni et al., 2020). The weight of the deposited dust can also be used to develop correlations for assessment of optical -reflectivity- losses (Azouzoute et al., 2020; Zhao et al., 2020; Wu et al., 2020).

Other than the deposition of dust on the reflective surfaces, the optical losses are also caused by the erosion of the solar reflectors, mainly due to sandstorms (Matal et al., 2020; Wiesinger et al., 2021, 2018a). Erosion intensity varies from site to site, as a result of the variation of particles' composition and shapes that cause different microscopic cracks. The erosion's intensity is affected by the shape of particles more than their hardness (Sansom et al., 2017; Endaya et al., 2019; Guerguer et al., 2017). The general trend of erosion simulations is to use particles smaller than 250 microns, but larger particles should also be used to avoid erosion underestimation (Sansom et al., 2017).

Coatings of solar mirrors enhance water saving since less cleaning frequencies are required; the coated reflectors restore their reflectance better than the uncoated ones (Wette et al., 2019b). Furthermore, the coatings' anti-soiling effect will be more significant when the soiling is more intense (Wette et al., 2019a). Coatings can be associated with cleaning methods to enhance the optical performance of the reflectors; however, this association of mitigation approaches must be done dependently on the type of coating, different anti-soiling coatings perform differently for cleaning methods, the wrong association can lead to losses in the mirrors' reflectance instead of restoring it (Wette et al., 2020).

The amounts and composition of dust -and the consequent losses- relate to the geography and climate of each region in the world, thus the appropriate mitigation approaches are site-dependent, this explains the recent R&D trends of evaluating experimentally the factors controlling soiling losses in different regions of the world rather than standardizing those losses. The evaluation of the amount of dust is very important to assess the cost of cleaning tasks, and thus assess the viability of CSP projects around the world. The cost of cleaning solar fields must be optimized by adapting the cleaning method to the factors governing the deposition of dust at the plant's site, the careful association of different mitigation approaches can lead to more efficient cleaning operations. The usual scarcity of water in areas with high DNI potential urges the necessity of more research on water-economic solutions.

In the second part, the presented literature review indicates that the aerosols radiative effect must be accurately assessed for a better long-term thermal solar energy exploitation, furthermore, no model performs globally better than others, inter-models' differences -when estimating DNI- are high and spatially broad (Ruiz-Arias and Gueymard, 2018). To consider the particularities of sites, it is better to build models for sites potentially suitable to host CSP projects (eg: (Wu et al., 2020)). The performance of models shows spatial variations, as a result, adequate corrections are to be necessarily introduced for better precision (as noted by many authors such as (Cardemil et al., 2014)).

The major parameter characterizing the attenuation of solar radiation is Aerosols' Optical Depth (AOD) (Papadimas et al., 2012), it is found to be the particular input with the most crucial effect on CSI models predictions (Benkaciali et al., 2018; Ineichen, 2016; Ruiz-Arias and Gueymard, 2018). High AOD values are correlated with low Ångström exponent α (Liu et al., 2011; Singh et al., 2005), which means that very hazy atmospheres are a result of the presence of large aerosols particles.

Generally, models underestimate high DNI and present a poor performance for low solar zenith, this should be considered when developing or applying CSI models to areas with either of those climate conditions, in addition, due to the propagation of errors, complex models are not always a guaranty for accuracy and precision when compared to simple models (Ruiz-Arias and Gueymard, 2018). All these factors ought to be considered to minimize DNI estimation errors, especially when planning CSP projects.

To finalize this chapter, aerosols and soiling problems still remain in need for further research. The resulted decrease in the solar power plant's overall performance might increase the cost of cleaning operations and therefore increasing the cost of the produced kWh.

In Chapter IV, the description and data records of the climatology of the exposure site will be provided, as well as the detailed description of the experimental setup used to study the soling of solar mirrors, also, the followed methodology of measuring reflectivity loss and dust weight will be explained.

References of chapter III

Abraim, M., Salihi, M., El Alani, O., Hanrieder, N., Ghennioui, H., Ghennioui, A., El Ydrissi, M., Azouzoute, A., 2022. Techno-economic assessment of soiling losses in CSP and PV solar power plants: A case study for the semi-arid climate of Morocco. *Energy Conversion and Management* 270, 116285. https://doi.org/10.1016/j.enconman.2022.116285

Alami Merrouni, A., Conceição, R., Mouaky, A., Silva, H. G. Ghennioui, A. 2020. CSP performance and yield analysis including soiling measurements for Morocco and Portugal. *Renewable Energy* 162, 1777–1792. https://doi.org/10.1016/j.renene.2020.10.014

Alami Merrouni, A., Wolfertstetter, F., Mezrhab, A., Wilbert, S., Pitz-Paal, R., 2015. Investigation of soiling effect on different solar mirror materials under Moroccan climate. *Energy Procedia* 69, 1948–1957. https://doi.org/10.1016/j.egypro.2015.03.194

Alam, S., 2006. Prediction of direct and global solar irradiance using broadband models: Validation of REST model. *Renewable Energy* 31, 1253–1263. https://doi.org/10.1016/j.renene.2005.06.009

Amiridis, V., Marinou, E., Tsekeri, A., Wandinger, U., Schwarz, A., Giannakaki, E., Mamouri, R., Kokkalis, P., Binietoglou, I., Solomos, S., Herekakis, T., Kazadzis, S., Gerasopoulos, E., Proestakis, E., Kottas, M., Balis, D., Papayannis, A., Kontoes, C., Kourtidis, K., Papagiannopoulos, N., Mona, L., Pappalardo, G., Rille, O.L., Ansmann, A., 2015. LIVAS: a 3-D multi-wavelength aerosol/cloud database based on CALIPSO and EARLINET. *Atmospheric Chemistry and Physics* 15, 2247–2304. http://dx.doi.org/10.5194/acpd-15-2247-2015

Antonanzas-Torres, F., Antonanzas, J., Urraca, R., Alia-Martinez, M., Martinez-de-Pison, F.J., 2016. Impact of atmospheric components on solar clear-sky models at different elevation: Case study Canary Islands. *Energy Conversion and Management* 109, 122–129. https://doi.org/10.1016/j.enconman.2015.11.067

Aranzabe, E., Azpitarte, I., Fernández-García, A., Argüelles-Arízcun, D., Pérez, G., Ubach, J., Sutter, F., 2018. Hydrophilic anti-soiling coating for improved efficiency of solar reflectors. *AIP Conference Proceedings* 2033, 220001. https://doi.org/10.1063/1.5067223

Ashley, T., Carrizosa, E., Fernández-Cara, E., 2019. Heliostat field cleaning scheduling for Solar Power Tower plants A heuristic approach. *Applied Energy* 235, 653-660. https://doi.org/10.1016/j.apenergy.2018.11.004

Azouzoute, A., Merrouni, A. A., Garoum, M., 2020. Soiling loss of solar glass and mirror samples in the region with arid climate. *Energy Reports* 6, 693–698. https://doi.org/10.1016/j.egyr.2019.09.051

Azouzoute, A., Merrouni, A. A., Garoum, M., Bennouna, E. G., 2019a. Comparison of soiling effect of two different solar mirrors in mid-south of Morocco. *AIP Conference Proceedings* 2126, 190002. https://doi.org/10.1063/1.5117699

Azouzoute, A., Merrouni, A. A., Garoum, M., Bennouna, E. G., Ghennioui, A., El-Ydrissi, M., 2019b. The impact of optical soiling losses on the electrical production of CSP power plant. *AIP Conference Proceedings* 2123, 020090. https://doi.org/10.1063/1.5117017

Badescu, V., Gueymard, C.A., Cheval, S., Oprea, C., Baciu, Dumitrescu, A., Iacobescu, F., Milos, I., Rada, C., 2013. Accuracy analysis for fifty-four clear-sky solar radiation models using routine hourly global irradiance measurements in Romania. *Renewable Energy* 55, 85–103. https://doi.org/10.1016/j.renene.2012.11.037

Badescu, V., Gueymard, C.A., Cheval, S., Oprea, C., Baciu, M., Dumitrescu, A., Iacobescu, F., Milos, I., Rada, C., 2012. Computing Global and Diffuse Solar Hourly Irradiation on Clear Sky: Review and Testing of 54 Models. *Renewable and Sustainable Energy Reviews* 16, 1636–1656. https://doi.org/10.1016/j.rser.2011.12.010

Behar, O., Sbarbaro, D., Moran, L., 2019. A simplified methodology to estimate solar irradiance and atmospheric turbidity from ambient temperature and relative humidity. *Renewable and Sustainable Energy Reviews* 116, 109310. https://doi.org/10.1016/j.rser.2019.109310

Bellmann, P., Wolfertstetter, F., Conceição, R., Silva, H. G., 2020. Comparative modeling of optical soiling losses for CSP and PV energy systems. *Solar Energy* 197, 229–237. https://doi.org/10.1016/j.solener.2019.12.045

Benkaciali, S., Haddadi, M., Khellaf, A., 2018. Evaluation of direct solar irradiance from 18 broadband parametric models: Case of Algeria. *Renewable Energy* 125, 694–711. https://doi.org/10.1016/j.renene.2018.02.108

Berrisford, P., Dee, D., Poli, P., Brugge, R., Fielding, K., Fuentes, M., Kallberg, P., Kubayashi, S., Uppala, S., Simmons, A., 2011. *The ERA-Interim archive Version 2.0 (Technical).* ECMWF, UK. http://www.ecmwf.int/publications/library/do/references/show?id=90276

Bieg, K. W., Wischmann, K. B., 1980. Plasma-polymerized organosilanes as protective coatings for solar front-surface mirrors. *Solar Energy Materials* 3, 301–316. https://doi.org/10.1016/0165-1633(80)90068-4

Bouaddi, S., Fernández-García, A., Ihlal, A., Ait-El-Cadi, R., Álvarez-Rodrigo, L., 2018. Modeling and simulation of the soiling dynamics of frequently cleaned reflectors in CSP plants. *Solar Energy* 166, 422-431. https://doi.org/10.1016/j.solener.2018.03.070

Bouaddi, S., Ihlal, A., Fernández-García, A., 2017. Comparative analysis of soiling of CSP mirror materials in arid zones. *Renewable Energy* 101, 437–449. http://dx.doi.org/10.1016/j.renene.2016.08.067

Bouaddi, S., and Ihlal, A., 2016. Monthly soiling comparison of CSP candidate mirrors exposed in southwest Morocco. *Materials Today: Proceedings* 3, 2556–2561. https://doi.org/10.1016/j.matpr.2016.04.002

Bouaddi, S., Ihlal, A., Fernández-García, A., 2015. Soiled CSP solar reflectors modeling using dynamic linear models. *Solar Energy* 122, 847–863. http://dx.doi.org/10.1016/j.solener.2015.09.044

Bourdan, D., Wolfertstetter, F., Fernández-García, A., Sansom, C., Azpitarte, I., Bouaddi, S., Pérez, G., Maccari, A., Van-Nijnatten, P., Surquin, E., Perrotta, F., 2020. Saving water on concentrated solar power plants: The holistic approach of the WASCOP project. *AIP Conference Proceedings* 2303, 210002. https://doi.org/10.1063/5.0029639

Bright, J.M., Sun, X., Gueymard, C.A., Acord, B., Wang, P., Engerer, N.A., 2020. Bright-Sun A globally applicable 1-min irradiance clear-sky detection model. *Renewable and Sustainable Energy Reviews* 121, 109706. https://doi.org/10.1016/j.rser.2020.109706

Capderou, M., 1987. Modèles Théoriques et Expérimentaux, in : *Atlas Solaire de l'Algérie*. Algeria, p. 375.

Cardemil, J. M., Starke, A. R., Scariot, V. K., Grams, I. L., Colle, S., 2014. Evaluating solar radiation attenuation models to assess the effects of climate and geographical location on the heliostat field efficiency in Brazil. *Energy Procedia* 49, 1288–1297. https://doi.org/10.1016/j.egypro.2014.03.138

Carra, E., Marzo, A., Ballestrin, J., Polo, J., Barbero, J., Alonso-Montesinos, J., Monterreal, R., Abreu, E.F.M., Fernández-Reche, J., 2020. Atmospheric extinction levels of solar radiation using aerosol optical thickness satellite data. Validation methodology with measurement system. *Renewable Energy* 149, 1120–1132. https://doi.org/10.1016/j.renene.2019.10.106

Carra, E., Ballestrín, J., Polo, J., Barbero, J., Fernández-Reche, J., 2018. Atmospheric extinction levels of solar radiation at Plataforma Solar de Almería. Application to solar thermal electric plants. *Energy* 145, 400–407. https://doi.org/10.1016/j.energy.2017.12.111

Chen, C.Y., Chesnutt, J.K.W., Chien, C.H., Guo, B., Wu, C.Y., 2019. Dust removal from solar concentrators using an electrodynamic screen. *Solar Energy* 187, 341-351. https://doi.org/10.1016/j.solener.2019.05.044

Conceição, R., Lopes, F.M., Tavares, A., Lopes, D., 2020. Soiling effect in second-surface CSP mirror and improved cleaning strategies. *Renewable Energy* 158, 103-113. https://doi.org/10.1016/j.renene.2020.05.054

Conceição, R., Merrouni, A. A., Lopes, D., Azouzoute, A., Silva, H. G. Bennouna, E. G., Collares-Pereira, M., Ghennioui, A., 2019. A comparative study of soiling on solar mirrors in Portugal and Morocco Preliminary results for the dry season. *AIP Conference Proceedings* 2126, 220001. https://doi.org/10.1063/1.5117760

Dahlioui, D., Wette, J., Fernández-García, A., Bouzekri, H., Azpitarte, I., 2022. Performance assessment of the anti-soiling coating on solar mirrors soiling in the arid climate of Ouarzazate-Morocco. *Solar Energy* 241, 13–23. https://doi.org/10.1016/j.solener.2022.05.063

Deffenbaugh, D. M., Green, S. T. Svedeman, S. J., 1986. The effect of dust accumulation on line-focus parabolic trough solar collector performance. *Solar Energy* 36, 139–146. https://doi.org/10.1016/0038-092X(86)90118-0

El-Boujdaini, L., Mezrhab, A., Moussaoui, M.A., Lopez, J.A.C., 2022. The effect of soiling on the performance of solar mirror materials: Experimentation and modeling. *Sustainable Energy Technologies and Assessments* 53, 102741. https://doi.org/10.1016/j.seta.2022.102741

Endaya, E., Sansom, C., Comley, P., Almond, H., Dekam, E. I., Abdunnabi, M. J. R., 2019. Simulation of The Effect of Libyan Sand on The Reflectance Surface of CSP. *Solar Energy and Sustainable Development* 8, 33–46. http://jsesd.csers.ly/images/pdf/vol-008-02/vol-008-02-04.pdf

Engerer, N.A., Mills, F.P., 2015. Validating nine clear sky radiation models in Australia. *Solar Energy* 120, 9–24. https://doi.org/10.1016/j.solener.2015.06.044

Fernández-García, A., Aranzabe, E., Azpitarte, I., Sutter, F., Martínez-Arcos, L., Reche-Navarro, T. J., Pérez, G., Ubach, J., 2019. Durability testing of a newly developed hydrophilic anti-soiling coating for solar reflectors. *AIP Conference Proceedings* 2126, 160002. https://doi.org/10.1063/1.5117665

Griffith, D. J., Vhengani, L., Maliage, M., 2014. Measurements of mirror soiling at a candidate CSP site. *Energy Procedia* 49, 1371–1378. https://doi.org/10.1016/j.egypro.2014.03.146

Guan, Z., Yu, S., Hooman, K., Gurgensi, H., Barry, J., 2015. Dust characterisation for solar collector deposition and cleaning in a concentrating solar thermal power plant. Presented at

the Proceedings of *International Conference on Heat Exchanger Fouling and Cleaning*.

https://heatexchanger-fouling.com/wp-content/uploads/2021/09/40_Guan_F.pdf

Guerguer, M., Karim, M., Naamane, S., Edfouf, Z., Raccurt, O., Delord, C., 2017. Soiling deposition on solar mirrors exposed in Morocco. *AIP Conference Proceedings* 1850, 130005.

http://dx.doi.org/10.1063/1.4984499

Hachicha, A. A., Al-Sawafta, I., Hamadou, D. B., 2019. Numerical and experimental investigations of dust effect on CSP performance under United Arab Emirates weather conditions. *Renewable Energy* 143, 263–276. https://doi.org/10.1016/j.renene.2019.04.144

Hanrieder, N., Ghennioui, A., Merrouni, A. A., Wilbert, S., Wiesinger, F., Sengupta, M., Zarzalejo, L., Schade, A., 2019. Atmospheric Transmittance Model Validation for CSP Tower Plants. *Remote Sensing* 11, 1083. https://doi.org/10.3390/rs11091083

Hanrieder, N., Sengupta, M., Xie, Y., Wilbert, S., Pitz-Paal, R., 2016. Modeling beam attenuation in solar tower plants using common DNI measurements. *Solar Energy* 129, 244–255. http://dx.doi.org/10.1016/j.solener.2016.01.051

Heimsath, A., Sutardhio, C., Schöttl, P., Nitz, P., 2020. Soiling of solar mirrors-impact of incidence angles on CSP plant performance. *AIP Conference Proceedings* 2303, 210003. https://doi.org/10.1063/5.0029067

Heimsath, A., Nitz, P., 2019. The effect of soiling on the reflectance of solar reflector materials - Model for prediction of incidence angle dependent reflectance and attenuation due to dust deposition. *Solar Energy Materials and Solar Cells* 195, 258–268. https://doi.org/10.1016/j.solmat.2019.03.015

Hunter, S. R., Smith, D. B., Polizos, G., Schaeffer, D. A., Lee, D. F., Datskos, P. G., 2014. Low cost anti-soiling coatings for CSP collector mirrors and heliostats. Presented at the Proc. SPIE 9175, *High and Low Concentrator Systems for Solar Energy Applications IX*, 91750J. https://doi.org/10.1117/12.2061845

Ineichen, P., 2016. Validation of models that estimate the clear sky global and beam solar irradiance. *Solar Energy* 132, 332–344. http://dx.doi.org/10.1016/j.solener.2016.03.017

Ineichen, P., Perez R, 2002. A new air mass independent formulation for the Linke turbidity coefficient. *Solar Energy* 73, 151–157. https://doi.org/10.1016/S0038-092X(02)00045-2

Karim, M., Naamane, S., Delord, C., Bennouna, A., 2015. Study of the surface damage of glass reflectors used in Concentrated Solar Power Plants. *Energy Procedia* 69, 106–115. http://dx.doi.org/10.1016%2Fj.egypro.2015.03.013

Linke, F., 1922. Transmission-Koeffizient und Trubungsfaktor. *J. Beitraege. Phys. fr. Atomos.* 10, 91–103.

Liu, Y., Huang, J., Takamura, T., Khatri, P., Bi, J., Shi, J., Wang, T., Wang, X., Zhang, B., 2011. Aerosol optical properties and radiative effect determined from sky-radiometer over Loess Plateau of Northwest China. *Atmospheric Chemistry and Physics* 11, 11455. https://doi.org/10.5194/acp-11-11455-2011

Lopes, D., Conceição, R., Silva, H. G., Aranzabe, E., Pérez, G., Pereira, M. C., 2019. Anti-soiling coating performance assessment on the reduction of soiling in 2nd-surface solar mirror. *Solar Energy* 194, 478–484. https://doi.org/10.1016/j.solener.2019.10.059

Lorenz, T., Klimm, E., Weiss, K. A., 2014. Soiling and Anti-soiling Coatings on Surfaces of Solar Thermal Systems – Featuring an Economic Feasibility Analysis. *Energy Procedia* 48, 749. https://doi.org/10.1016/j.egypro.2014.02.087

Louche, A., Notton, G., Poggi, P., Simonnot, G., 1991. Correlations for direct normal and global horizontal irradiation on a French Mediterranean site. *Solar Energy* 46, 261–266. http://dx.doi.org/10.1016/0038-092X(91)90072-5

Marif, Y., Bechki, D., Zerrouki, M., Belhadj, M.M., Bouguettaia, H., Benmoussa, H., 2019. Estimation of atmospheric turbidity over Adrar city in Algeria. *Journal of King Saud University - Science* 31, 143–149. http://dx.doi.org/10.1016/j.jksus.2017.06.002

Matal, A., Karim, M., Naamane, S., 2020. Development and calibration of an experimental test bench simulating solar reflectors erosion. *Solar Energy* 201, 724–731. https://doi.org/10.1016/j.solener.2020.03.028

Matal, A., Naamane, S., 2020. Accelerated erosion of coated solar glass reflectors. *AIP Conference Proceedings* 2303, 150012. https://doi.org/10.1063/5.0029153

Mazumder, M., Horenstein, M., Joglekar, N., Yellowhair, J., Ellinger, C., Eriksen, R., Garner, S., Bernard, A.R., 2020. Enhancement of Optical Efficiency of CSP Mirrors for Reducing O&M Cost via Near-Continuous Operation of Self-Cleaning Electrodynamic Screens (EDS). Report of Boston University. https://doi.org/10.2172/1644255

Mazumder, M., Ellinger, C., O'Connor, K., Eriksen, R., Bernard, A., Horenstein, M., Yellowhair, J., Joglekar, N., Garner, S., Bones, J., Morales, C., Acuña, H., 2019. Industrial Production and Field Evaluation of Transparent Electrodynamic Screen (EDS) Film for Water-Free Cleaning of Solar Collectors. Presented at the 2019 IEEE 46th Photovoltaic Specialists Conference (PVSC), Chicago, USA. https://doi.org/10.1109/PVSC40753.2019.8980599

Mazumder, M., Yellowhair, J., Stark, J., Heiling, C., Hudelson, J., Hao, F., Gibson, H., Horenstein, M., 2014. Optical and adhesive properties of dust deposits on solar mirrors and their effects on specular reflectivity and electrodynamic cleaning for mitigating energy-yield

loss. Presented at the proceedings of *SPIE 9175, High and Low Concentrator Systems for Solar Energy Applications IX, 91750K.* https://doi.org/10.1117/12.2066328

Mazumder, M. Horenstein, M., Stark, J., Erickson, D., Sayyah, A., Jung, S., Hao, F., 2013. Development of self-cleaning solar collectors for minimizing energy yield loss caused by dust deposition. Presented at the proceedings of the *ASME 2013 7th International Conference on Energy Sustainability*, Minneapolis, USA. https://doi.org/10.1115/ES2013-18365

Mazumder, M. K., Sims, R. A., Wilson, J. D., June 28th 2005. Transparent self-cleaning dust shield. US patent N°: US 6,911,593 B2. https://patents.google.com/patent/US6911593B2/en

Mikofski, M.M., Hansen, C.W., Holmgren, W.F., Kimball, G.M., 2017. Use of measured aerosol optical depth and precipitable water to model clear sky irradiance. Presented at the *2017 IEEE 44th Photovoltaic Specialist Conference (PVSC)*, IEEE, Washington, DC. https://doi.org/10.1109/PVSC.2017.8366314

Molineaux, B., Ineichen, P., Delaunay, J.J., 1995. Direct luminous efficacy and atmospheric turbidity improving model performance. *Solar Energy* 55, 125–137. https://doi.org/10.1016/0038-092X(95)00035-P

Niknia, I., Yaghoubi, M., Hessani, R., 2012. A novel experimental method to find dust deposition effect on the performance of parabolic trough solar collectors. *International Journal of Environmental Studies* 69, 233–252. http://dx.doi.org/10.1080/00207233.2012.664810

Papadimas, C.D., Hatzianastassiou, N., Matsoukas, C., Kanakidou, M., Mihalopoulos, N., Vardavas, I., 2012. The direct effect of aerosols on solar radiation over the broader Mediterranean basin. *Atmospheric Chemistry and Physics* 12, 7165–7185. https://doi.org/10.5194/acp-12-7165-2012

Paulescu, M., Schlett, Z., 2003. A simplified but accurate spectral solar irradiance model. *Theoritical and Applied Climatology* 75, 203–212. http://dx.doi.org/10.1007/s00704-003-0731-y

Pescheux, A. C., Raccurt, O., Bourdon, D., Le-Baron, E., 2020. Accelerated aging tests and characterizations of innovated anti-soiling coatings for solar receiver glasses. *Materials Chemistry and Physics* 256, 123646. https://doi.org/10.1016/j.matchemphys.2020.123646

Pérez-Burgos, A., Díez-Mediavilla, M., Alonso-Tristán, C., Rodríguez-Amigo, M., 2017. Analysis of solar direct irradiance models under clear-skies: evaluation of the improvements for locally adapted models. *Journal of Renewable and Sustainable Energy* 9, 023703. https://doi.org/10.1063/1.4981798

Picotti, G., Moretti, L., Cholette, M.E., Binotti, M., Simonetti, R., Martelli, E., Steinberg, T.A., Manzolini, G., 2020. Optimization of cleaning strategies for heliostat fields in solar tower plants. *Solar Energy* 204, 501-514. https://doi.org/10.1016/j.solener.2020.04.032

Picotti, G., Borghesani, P., Manzolini, G., Cholette, M.E., Wang, R., 2018. Development and experimental validation of a physical model for the soiling of mirrors for CSP industry applications. *Solar Energy* 173, 1287–1305. https://doi.org/10.1016/j.solener.2018.08.066

Polizos, G., Schaeffer, D. A., Smith, D. B., Lee, D. F., Datskos, P. G., Hunter, S. R., 2014. Enhanced Durability Transparent Superhydrophobic Anti-Soiling Coatings for CSP Applications. Presented at the Proceedings of *the ASME 2014 8th International Conference on Energy Sustainability*, ES2014, Boston, Massachusetts, USA. https://doi.org/10.1115/ES2014-6505

Polo, J., Ballestrin, J., Carra, E., 2020. Assessment and improvement of modeling the atmospheric attenuation based on aerosol optical depth information with applicability to solar tower plants. *Energy* 208, 118399. https://doi.org/10.1016/j.energy.2020.118399

Polo, J., Ballestrin, J., Carra, E., 2016. Sensitivity study for modelling atmospheric attenuation of solar radiation with radiative transfer models and the impact in solar tower plant production. *Solar Energy* 134, 219–227. https://doi.org/10.1016/j.solener.2016.04.050

Raillani, B., Ouali, H. A. L., Amraqui, S., Moussaoui, M. A., Jeyar, M., Mezrhab, A., 2019. The Impact of Aerosol Optical Depth (AOD) On Decreasing the Optical Efficiency of CSP Solar Power Plants-A case study Eastern Morocco. Presented at the *2019 International Conference on Intelligent Systems and Advanced Computing Sciences* (ISACS), IEEE, Taza, Morocco. https://doi.org/10.1109/ISACS48493.2019.9068909

Rathore, N., Panwar, N.L., Gama, A., Yettou, F., 2019. Solar map of India under clear sky conditions. *International Journal of Sustainable Energy* 38, 415–446. https://doi.org/10.1080/14786451.2018.1527334

Robledo, L., Soler, A., 2000. Luminous efficacy of direct solar radiation for clear skies. *Energy* 25, 689–701. https://doi.org/10.1016/S0360-5442(00)00017-7

Ruiz-Arias, J.A., Gueymard, C.A., 2018. Worldwide inter-comparison of clear-sky solar radiation models: Consensusbased review of direct and global irradiance components simulated at the earth surface. *Solar Energy* 168, 10–29. https://doi.org/10.1016/j.solener.2018.02.008

Sansom, C., Almond, H., King, P., Endaya, E., Bouaichaoui, S., 2017. Airborne sand and dust soiling of solar collecting mirrors. *AIP Conference Proceedings* 1850, 130011. https://doi.org/10.1063/1.4984505

Sansom, C., Comley, P., King, P., Almond, H., Atkinson, C., Endaya, E., 2015. Predicting the effects of sand erosion on collector surfaces in CSP plants. *Energy Procedia* 69, 198–207. http://dx.doi.org/10.1016/j.egypro.2015.03.023

Sengupta, M., Wagner, M., 2012. Atmospheric attenuation in central receiver systems from DNI measurements. Presented at the *SolarPACES*, Conference proceedings. https://pdfs.semanticscholar.org/8abf/e7d0a121437a307ee786ca8b012d712964b8.pdf

Singh, G., Saini, D., Sarma, R., Chandra, L., Shekhar, R., 2015. Dust deposition mechanism and cleaning strategy for open volumetric air receiver based solar tower sub-systems. *Energy Procedia* 69, 2081. https://doi.org/10.1016/j.egypro.2015.03.222

Singh, S., Nath, S., Kohli, R., Singh, R., 2005. Aerosols over Delhi during pre-monsoon months: Characteristics and effects on surface radiation forcing. *Geophysical Research Letters* 32, L13808. https://doi.org/10.1029/2005GL023062

Stark, J., Yellowhair, J., Hudelson, J., Horenstein, M., Mazumder, M., 2014. Optical Modeling of Reflectivity Loss Caused by Dust Deposition on CSP Mirrors and Restoration of Energy Yield by Electrodynamic Dust Removal. Presented at Proceedings of *the ASME 2014 8th International Conference on Energy Sustainability,* Boston, Massachusetts, USA. https://doi.org/10.1115/ES2014-6506

Sutter, F., Reche-Navarro, T. J., Vicente, G. S., Fernández-García, A., 2020. Durability of anti-reflective coatings for parabolic trough receivers. *AIP Conference Proceedings* 2303, 150015. https://doi.org/10.1063/5.0028751

Tahboub, Z., Oumbe, A., Hassar, Z., Obaidli, A., 2014. Modeling of irradiance attenuation from a heliostat to the receiver of a solar central tower. *Energy Procedia* 49, 2405–2413. https://doi.org/10.1016/j.egypro.2014.03.255

Wette, J., Sutter, F., Buendía-Martínez, F., Fernández-García, A., 2020. Effect of long term outdoor exposure on anti-soiling coatings for solar reflectors. *AIP Conference Proceedings* 2303, 150016. https://doi.org/10.1063/5.0028960

Wette, J., Fernández-García, A., Sutter, F., Buendía-Martínez, F., Argüelles-Arízcun, D., Azpitarte, I., Pérez, G., 2019a. Water Saving in CSP Plants by a Novel Hydrophilic Anti-Soiling Coating for Solar Reflectors. *Coatings* 9, 739. https://doi.org/10.3390/coatings9110739

Wette, J., Sutter, F., Fernández-García, A., 2019b. Evaluation of anti-soiling coatings for CSP reflectors under realistic outdoor conditions. *Solar Energy* 191, 574–584. https://doi.org/10.1016/j.solener.2019.09.031

Wiesinger, F., Sutter, F., Fernández-García, A., Wette, J., Hanrieder, N.,2021. Sandstorm erosion on solar reflectors: A field study on height and orientation dependence. *Energy* 217, 119351. https://doi.org/10.1016/j.energy.2020.119351

Wiesinger, F., Sutter, F., Fernández-García, A., Wette, J., Wolfertstetter, F., Hanrieder, N., Pitz-Paal, R., 2020. Sandstorm erosion on solar reflectors: Highly realistic modeling of artificial aging tests based on advanced site assessment. *Applied Energy* 268, 114925. https://doi.org/10.1016/j.apenergy.2020.114925

Wiesinger, F., Sutter, F., Wolfertstetter, F., Hanrieder, N., Fernández-García, A., Pitz-Paal, R., Schmücker, M., 2018a. Assessment of the erosion risk of sandstorms on solar energy technology at two sites in Morocco. *Solar Energy* 162, 217–228. https://doi.org/10.1016/j.solener.2018.01.004

Wiesinger, F., Vicente, G. S., Fernández-García, A., Sutter, F., Pitz-Paal, R., 2018b. Sandstorm erosion testing of anti-reflective glass coatings for solar energy applications. *Solar Energy Materials and Solar Cells* 179, 10–16. https://doi.org/10.1016/j.solmat.2018.02.018

Wiesinger, F., Sutter, F., Wolfertstetter, F., Hanrieder, N., Wette, J., Fernández-García, A., Pitz-Paal, R., 2017. Sandstorm erosion simulation on solar mirrors and comparison with field data. *AIP Conference Proceedings* 1850, 130014. http://dx.doi.org/10.1063/1.4984508

Wu, Z., Yan, S., Wang, Z., Ming, T., Zhao, X., Ma, R., Wu, Y., 2020. The effect of dust accumulation on the cleanliness factor of a parabolic trough solar concentrator. *Renewable Energy* 152, 529–539. https://doi.org/10.1016/j.renene.2020.01.091

Yang, K., Hwang, G.W., Tamai, N., 2001. A hybrid model for estimating global solar radiation. *Solar Energy* 70, 13–22. https://doi.org/10.1016/S0038-092X(00)00121-3

Yilbas, B. S., Hassan, G., Al-Qahtani, H., Al-Sharafi, A., Sahin, A. Z., 2021. Dust mitigation by rolling water droplets from hydrophobic surfaces. *Surfaces and Interfaces* 22, 100825. https://doi.org/10.1016/j.surfin.2020.100825

Zereg, K., Gama, A., Aksas, M., Rathore, N., Yettou, F., Panwar, N. L., 2022. Dust impact on concentrated solar power: A review. *Environmental Engineering Research* 27, 210345. https://doi.org/10.4491/eer.2021.345

Zhao, X., Chen, Z., Yan, S., Ming, T., Wu, Z., Ma, R., 2020. Influence of Dust Accumulation on the Solar Reflectivity of a Linear Fresnel Reflector. *Journal of Thermal Science* 30, 1526-1541. https://doi.org/10.1007/s11630-020-1379-y

CHAPTER IV –
METHODOLOGY

IV. 1. Site description

IV. 1. 1. Climatologic description

The solar mirrors were exposed at Laghouat city (33°47'50.118" N, 2°52'9.863" E, figure 4.1), which is the capital of the province of Laghout that hosts Hassi R'mel Gas Field, tenth largest Africa natural gas reserve, as well as the first hybrid solar-gas power plant in Algeria and a candidate site for future CSP projects (Khaldi, 2012).

Figure 4.1. Location of Laghouat city (Source: ©Google maps).

The mean DNI received in summer can be as high as 930 W/m^2, with the variation range of the temperature being between 21 °C and 50 °C during summer and between -10 °C and 20 °C during winter; the highest temperatures were recorded during July, the monthly mean: minimum, maximum, and daily temperatures are respectively 22.6 °C, 38.8 °C, and 31.5 °C, while the lowest values were recorded during January: 3.4 °C, 14.9 °C, and 9.0 °C respectively. with respect to the yearly DNI and the mean 9.5 hours of daylight, the province receives 7140 Wh/m^2/day of DNI (Houyou et al., 2016; Khaldi, 2012). The site where the outdoor exposure is carried out is at an altitude of 750 m (Gourine et al., 2010). According to

(Houyou et al., 2016) who recorded the meteorological data of wind speed, relative humidity, and precipitations near Laghouat city for two and a half years, the variation of the mean daily wind speed is within the range of 2-12.5 m/s, it exceeded 6 m/s and 7 m/s during less than 5% and 2% of the recording period respectively. While the daily maximum 15-min values were over 6 m/s, 7 m/s, and 10 m/s during the respective percentage of 49%, 35% and 13% of the recorded days, without exceeding the value of 17.6 m/s according to the study. As for wind direction, two dominant directions were determined: *southwest* and northwest during 24% and 49% of the recording period respectively, which would be a problem for fix solar energy applications in general and CSP ones in particular, because their preferable exposure direction is south in the northern hemisphere, and southwestern wind (second dominant direction) would increase critically soiling and erosion risks. As for the Relative Humidity (RH), it was reported to be lowest during the space of time from June to August (monthly value in the range of 20 to 30%) and highest during the period from December to March (monthly value about 45-55%). The mean annual precipitations were 140 mm with a monthly-averaged value of 12 mm, as for the extremums during the measurements campaign, the wettest month was September with a value of 93.5 mm of precipitations, and the driest one was October with a monthly value of 1 mm; the authors highlighted the absence of any clear seasonally trend in rainfall for the period of record at Laghouat as can observed in figure 4 in the beforementioned reference.

Previous measurements of weather parameters at a time resolution of one hour during summer and their daily-averaged values are presented in figures 4.2 and 4.3, namely Global Horizontal Irradiance (GHI), wind speed, and relative humidity. In figure 4.2, the daily-averaged data can be visualized: 66.67% and 93.33% of the daily mean GHI exceeded 570 and 500 Wh/m^2 respectively (figure 4.2-a), the maximum daily GHI was on June 14th reaching up to 8193 Wh/m^2/day. In figure 4.3-a, the hourly GHI of the representative day -of which the daily value is the closest to the monthly averaged one- is provided, the daily GHI was around 7767 Wh/m^2/day and the hourly values were superior to 500 Wh/m^2 during 8 of the 11 daylight hours, which denotes the important potential of the exposure site for hosting solar projects in general and CSP ones in particular.
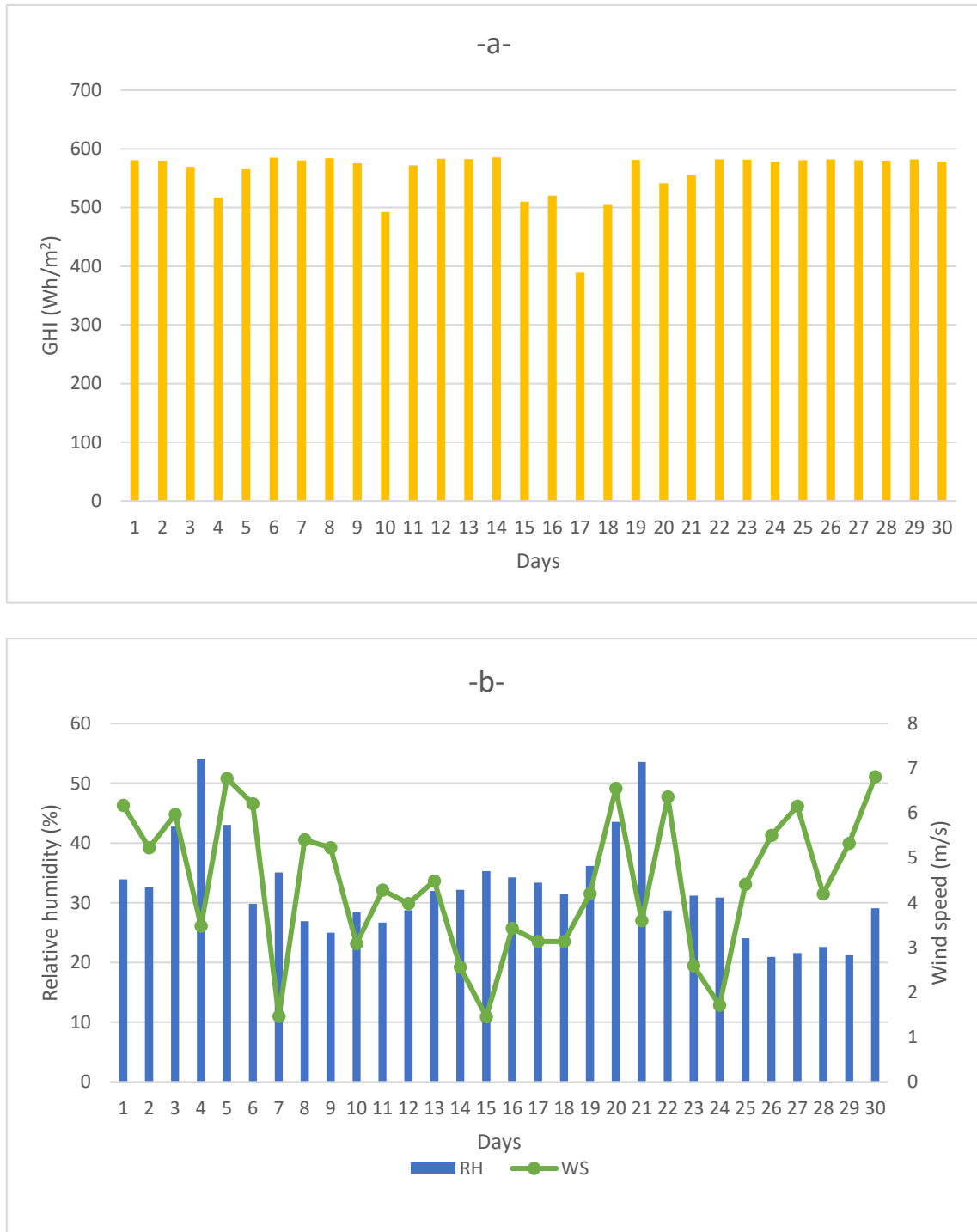
Figure 4.2. Daily global horizontal irradiance (a), wind speed, and relative humidity (b) at the exposure site during June 2017.

As for wind speed, the values rose above 6 m/s for 23.33% and 25% of the daily data (figure 4.2-b) and the hourly data of the representative day (June 13th figure 4.3-b) respectively, which is an indication for potential erosion risks of solar mirrors and/or their protective coatings. The monthly averaged relative humidity was 32.29% which is expected given the dry period of the year, the daily values did not exceed 40% except for 5 days (16.67 % of

data) and the highest daily relative humidity was 54.08% (June 4th), the daily behavior of the relative humidity can be observed in figure 4.2-b. The humidity was more important during nighttime and early morning, which maximizes soiling risk in this span of a day, especially that it coincides with strong wind as can be seen from the hourly data of the representative days in figure 4.3-b.
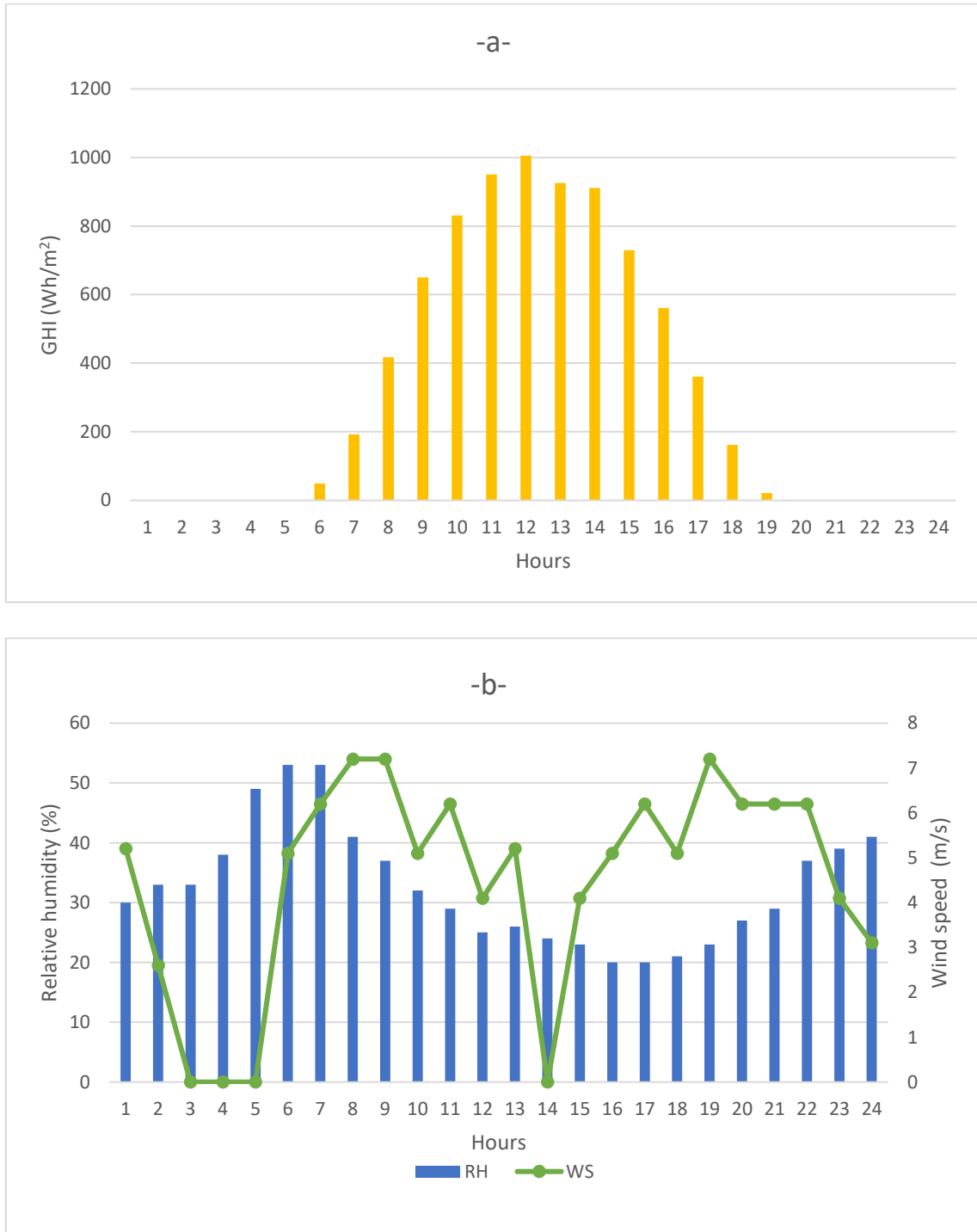

Figure 4.3. Hourly measurements for the representative day of: global horizontal irradiance (June 21st, **a**), wind speed and relative humidity (June 13th & 2nd respectively, **b**).

IV. 1. 2. Geologic description

Laghouat is 400 km away from the Mediterranean coast, situated at the limits between the Saharan region and the high steppe plateaus, and extending over 400 km^2 of land (Benkouider et al., 2019), thus, its geographical structure is composed of the Saharan Atlas (north, primarily limestones and sandstones) and the Saharan Platform (south, mainly Hamada sand ergs), which causes the topography of the region to considerably vary, going - respectively- from abrupt reliefs to sub-plain surfaces, and from elevation and slopes of 1000 to 1700 m, and 12.5 to 25 %, to values ranging between 700 to 1000 m and 0 to 3 % (Saadoud et al., 2017), who reported that large surfaces of the province of Lagouat present an extremely important wind-erosion profile, which is a condition where wind erosion is enhanced by poor vegetal coverage and bare soils sensitive to wind-erosion, the site of our study is included in this high wind-erosion class. This high risk of erosion in the site of concern is consequent to the overlap of multiple factors: for the topographic factor, the city is characterized by a gentle slope, making it exposable to wind, and highly affected by strong winds; another factor is the weak vegetal coverage and the dominant presence of sand and sandy soils. According to the topographic study of wind erosion in Laghouat province by (Saadoud et al., 2017) -in which they use data regarding remote sensing, vegetal cover, and soil analysis, as well as other climatic and topographic data to generate a regional wind-erosion risk map for the province of Laghouat-, wide areas of this province are identified with high to very high erosion risks, and these risks do not concern only the province of Laghouat, but could also affect its surrounding provinces because of its easily erodible sand particles.

The landscape of the province of Laghouat, its important solar potential, and the concentration of the population in three major urban zones, namely the cities of Laghouat, Hassi R'mel, and Aflou, leave wide areas which are appropriate for CSP plants as well as hybrid solar-gas power plants, thanks to the important reserves of Laghouat in terms of natural gas, the best example of the latter type of plants is the first Algerian integrated solar combined cycle power plant of Hassi R'mel of 150 MW with 20 MW of solar parabolic trough concentrators, where the solar field starts the concentration of solar irradiance as DNI is greater than 300 W/m^2, and operates so that the heat transfer fluid would keep a mass flow rate of 90 to 450 kg/s and an outlet-inlet temperature difference of 100 °C (Abdelhafidi et al., 2020). The results of our thesis could be useful to evaluate the losses for this plant (and the appropriate mitigation approach), since the principles of optical losses are the same for all CSP technologies.

IV. 2. Experimental set-up description

Gravity is the major force that is responsible for the deposition of aerosols and dust particles on the reflective surfaces of mirrors in the solar field, and the particles' attraction and attachment to the surface of the reflective mirror are owed to Van der Waals, capillary, and electrostatic forces. The intensity of the three phenomena -deposition, attraction, and attachment of soil- is directly and majorly affected by the tilt angle of the mirrors and their surfaces' state, because for inclined mirrors, the tangent component of gravity participates in the removal of particles (Zereg et al., 2022).

In order to study the optical losses due to the cumulative dust deposition on solar reflectors, eight 20x25 cm^2 mirror samples were south-exposed on a structure that we conceived, fabricated, and mounted (figure 4.4), and which is composed of two superposed rows with 50 cm of height difference and 1 m of height for the upper row (figure 4.4-a, sixteen mirrors in total, half of them were used in this study), the exposure setup is mounted next to the technical platform for physical and chemical analyzes within the campus of the University of Laghouat. To assess the effect of the variation of inclination angle, the lower four mirrors were fixed at inclinations of 0°, 15°, 30°, and 45° relatively to the horizontal plane on a rotation axis of east-west direction, since -as it is well known- the suitable exposure direction for fixed solar energy applications (i.e., in the absence of solar tracking systems) is south in the northern hemisphere and north in the southern one. The chosen inclinations are commonly found in the literature of CSP soiling issues (especially the horizontal (0°) and 45° inclinations), and have been investigated by many previous studies (such as: Alami Merrouni et al., 2015; Bouaddi et al., 2015; Griffith et al., 2014; Matal et al., 2020; Picotti et al., 2018). As for the upper four mirrors, two of them were fixed at the horizontal and the other two mirrors at 30°, a mirror of each inclination was coated and the other left uncoated to assess the benefit of coating solar reflectors as a mitigation for soiling. Also, the 50 cm difference in height between the upper row and lower one (figure 4.4-b, 4.5) provides an indication on the impact of this factor on soiling intensity and the resulted optical losses for the mirrors of similar tilt and state of surface, in other words, the mirrors which are uncoated and at inclinations of 0° and 30°.

The duration of the cumulative soiling campaign was 74 days of the dry season of the year (summer 2021), during which no operation of cleaning was performed for the aim of evaluating soiling in remote CSP locations where it is hard to clean solar reflectors (either due to scarcity of water or expensive cost of labor). By continuously checking local

meteorological predictions, the outdoor exposure campaign begun immediately after the last heavily rainy day in early summer and ended just before another similar meteorological event, providing 74 days with no cleaning, be it natural or manual. Light rainfalls occurred but did not clean the reflective surfaces and -instead- enhanced the soiling of mirrors, thus, it is safe to say that the present study is a very realistic outdoor simulation of dusting of solar mirrors in remote sites in the Algerian Sahara, as the solar mirrors were not subject to any kind of cleaning and the soiling campaign was conducted during summer which is the season with the most important solar potential, making this study very useful for decision makers to assess the benefit of CSP plants in particular and solar technologies in general, since the principle of dust deposition is similar for all surfaces, even though the consequent losses differs, with CSP technologies being the mostly affected as the needed component of solar radiation is the DNI, unlike PV -for example- which uses even the diffuse component.

IV. 3. Soiling rate measurements

The portable light meter VA8050 model from Environmental Instrument (figure 4.6) with 4% accuracy was used to measure the reflectivity. This device has a wide range of measurements of 0-30000 lux, and is able to operate under temperature conditions of 0-50 °C and relative humidity conditions of 0-80%. First of all, the illuminances of the sunlight and the light reflected by each mirror were measured, afterwards, the basic optical parameter needed for our study: the *reflectivity "ρ"* was determined from the ratio of the reflected luminosity divided by the luminosity of sunlight. This experimental protocol is similar to the commonly used dusting tracking system known as tracking cleanliness sensor (TraCS), which comprises of measuring the dusting of reflectors that are mounted on a solar tracker (in the present study the reflectors are immobile) by two pyrheliometers, one of them is directed towards the sky in order to measure the solar irradiance and the other one is directed towards the reflector for the aim of measuring the irradiance reflected from the dusted reflector, this procedure has been followed in many previously published papers, such as (Alami Merrouni et al., 2020; Bellmann et al., 2020).

Since the reflectivity can be derived either from solar irradiance or solar illuminance (the two parameters are related through the constant conversion factor: the luminous efficacy, Michael et al., 2020; Molineaux et al., 1995; Vartiainen, 2000), we chose to go with the latter option because the lux meter instrument available for us (figure 4.6) is not only portable but also light, which makes it advantageous when it comes to in-situ measurements at different locations and environments.
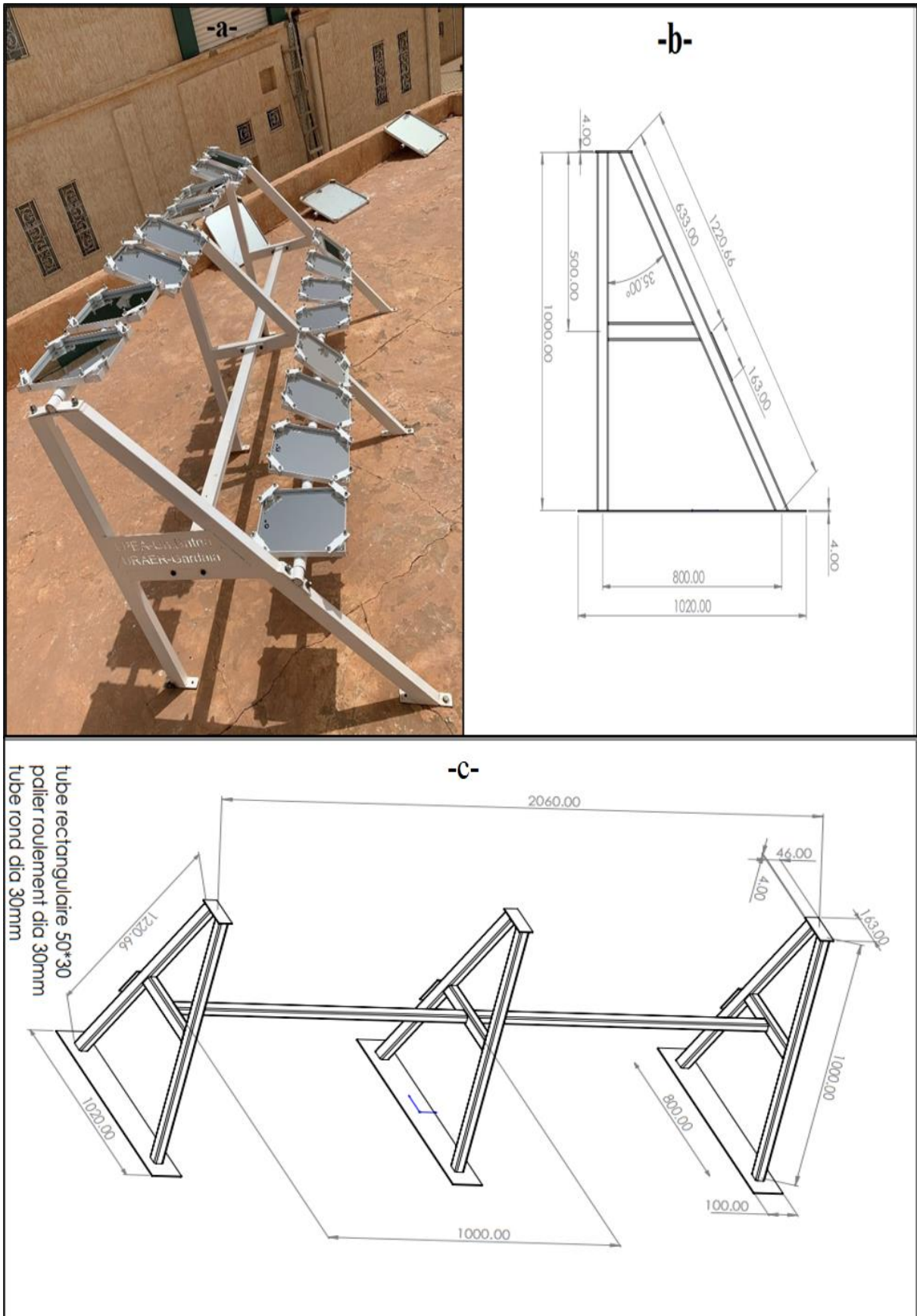
Figure 4.4. The experimental setup used in the study **(a)**, Schematic of the setup: side view **(b)**, 3D view **(c)**.

Figure 4.5. Close side view of the setup.

To show better the impact of soiling on the optical efficiency, the Cleanliness Index (CI) is more appropriate, the CI presents a comparison between the reflectivity of the mirror in its soiled -dusted- condition (ρ_s) to its clean -initial- state (ρ_c) in the light of the equation 4.1 (Alami Merrouni et al., 2020):

$$CI = {\rho_s}/{\rho_c} \qquad (4.1).$$

The initial reflectivity of the non-coated, clean reflector is of 96.61%, while that of the coated, clean reflector is of 96.01%, this denotes that coating the mirror had slenderly lowered the initial reflectivity, as one would logically predict.

In order to get a better grasp of the impact of the site's climatic condition (arid in this study) on the magnitude of dusting during the period of exposure, the Soiling Rate parameter (SR in %/day) ought to be used (Alami Merrouni et al., 2020). The SR speaks for the mirrors' cleanliness variation during the exposure time Δt (equation 4.2):

$$SR = {CI(t + \Delta t) - CI(t)}/{\Delta t} \qquad (4.2).$$

It should be highlighted that the sign of SR is usually negative, unless cleaning operation has been performed (CI(t+Δt) greater than CI(t)).

Figure 4.6. The VA8050 light meter from Environmental Instrument.

IV. 4. Dust weight measurements

The weight was measured with the Precision Balance OHAUS EX223 Explorer which has a precision of 10 µg (figure 4.7). First, we measured the weight of a clean wipe, in order to get more precision, we weighted a single wipe and compared the weight to that of ten wipes divided by ten; after confirming the weight of the wipe, we weighted the tissue one more time following the cleaning of the dusted reflector, the obtained difference in weight is the dust weight (M). The division of this later by the reflector's area (A) yields the dust density (in g/m^2), which, divided by the exposure time (Δt), gives the Dust Deposition Rate (DDR, in g/m^2/day) as clarified in equation 4.3:

$$DDR = {}^{M}\!/_{A * \Delta t} \qquad (4.3).$$

Figure 4.7. OHAUS EX223 Explorer Precision Balance used to measure the weight of the wipes.

IV. 5. Dust characterization

For the sake of enhancing our understanding of the optical losses due the deposition of soil on reflective mirrors, the physical and chemical properties of dust are characterized at Laghouat University by Scanning Electron Microscopy (SEM), energy dispersive X-ray spectroscopy (EDX), and X-Rays Diffraction (XRD).

Two high technologies are used for the characterization: the first device is the "Ultra versatile high resolution scanning electron microscope" from Quatro© company (figure 4.8), which associates different high techniques of imaging and analysis (including EDS) to permit the in-situ study of the samples in their natural state. This modern SEM uses a field emission gun and associates it with environmental mode (ESEM) to guarantee excellent imaging resolution; also, the low-vacuum allows charge-free characterization of non-conductive and/or hydrated specimens. Not to mention the wide coverage of information and the excellent abilities of analysis thanks to the simultaneous imaging by up to three EDX detectors. The temperature range of the in-situ analysis covers from -165 °C to 1400 °C.
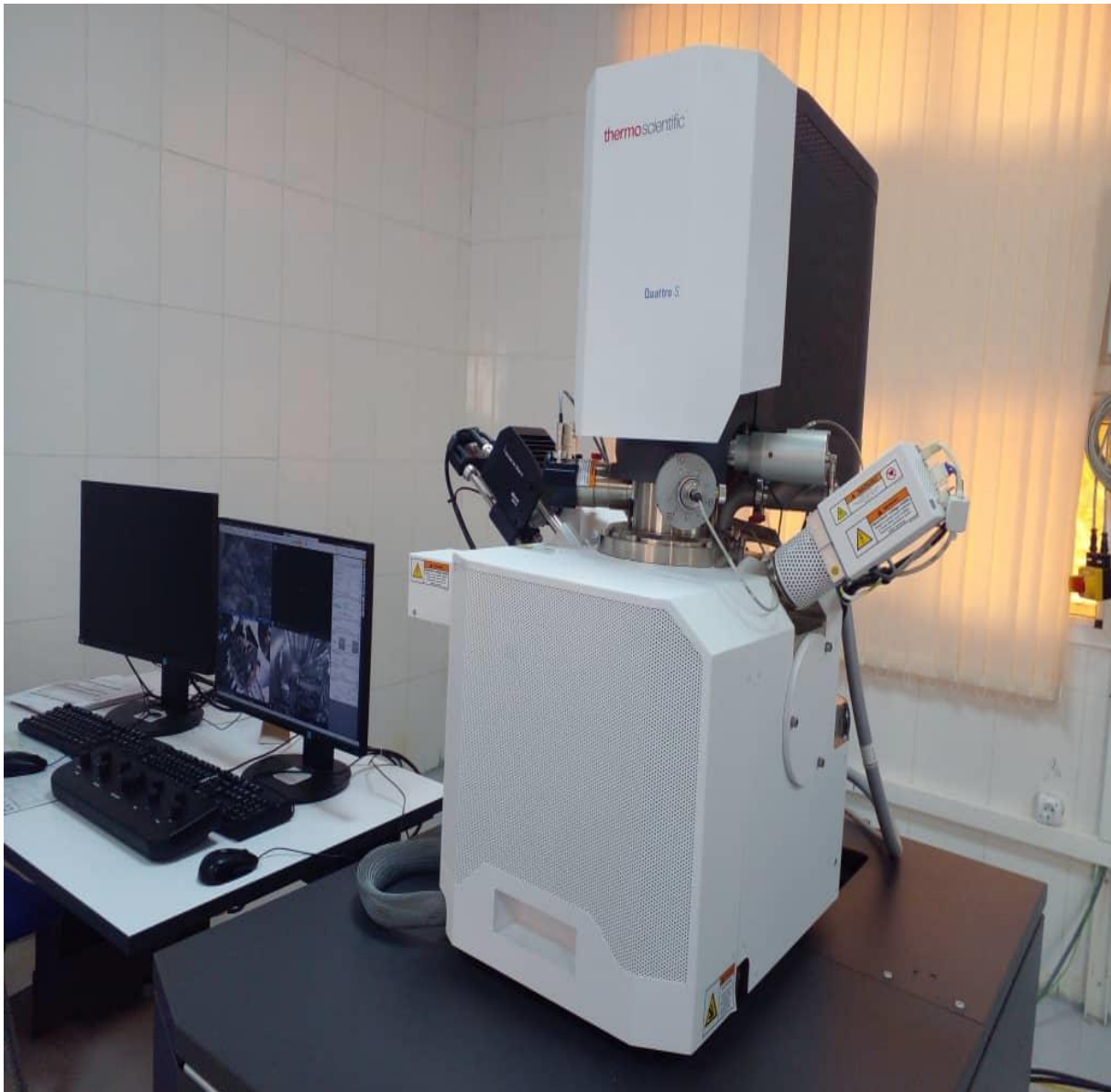
Figure 4.8. Thermos Scientific ^{TM} Quatro SEM.

The second used technology is the "Third generation Empyrean intelligent diffractometer" from Malvern Panalytical© (figure 4.9), with an X-ray generator of 4 kW (max 60 kV, max 100 mA). The maximum usable range of 2theta (theta is the angle of incidence) is between -111° and 168°, and the smallest step is about 0.0001°. X-ray diffraction determines the structure, composition, as well as other properties of materials by the emission of X-ray beams and the measurement of angles and intensities of beams' diffraction by the studied material.

Figure 4.9. Empyrean intelligent diffractometer from Malvern Panalytical.

IV. 6. Summary

The methodology of the experimental work -first one in Algeria- done in our thesis has been clarified in this chapter, such kind of studies is very site-dependent (Alami Merrouni et al., 2020), thus the motivation to conduct the outdoor soiling exposure campaign described here.

Previous meteorological data recorded during summer (period of interest) have been displayed, the data include hourly and daily-averaged values of: global horizontal irradiance,

wind speed, as well as relative humidity. The important amplitude of the recoded data of the global horizontal irradiance strongly suggests the high potential of the selected location (Lagouat city in particular, and Laghouat province in general) for solar energy projects, especially CSP plants. However, the analysis of the behavior of wind speed implies the high risks of soiling and erosion of solar reflectors and/or their protective coatings in case they are coated, especially that some strong wind events are preceded or coincide with high values of relative humidity, which means the surfaces of the mirrors are wetter and more susceptible to soiling, thus the necessity of in-situ studies.

The experimental setup supporting the exposed mirrors was described as well, two soiling factors were studied: inclination angle of the exposed mirrors and coating their reflective surfaces. For the first factor, the inclination values ranged from 0° to 45° by a step of 15°, for the second factor, the mirrors were fixed at two inclinations: 0° and 30°, and a mirror was coated at each inclination. The 50 cm of height difference between the upper and lower rows and the presence of mirrors of identical inclination and state of reflective surface (uncoated) at each inclination allows also the study of a third soiling factor which is the height difference, even though this was not a targeted factor in the present study.

The step-by-step calculations of the two characteristic quantities is detailed as well, namely: the soiling rate and the dust deposition rate.

In the last chapter, Results and Discussion, the optical losses and the corresponding dust quantities that resulted from the long-term uninterrupted soiling campaign (74 days with no precipitations nor manual or automated cleaning) are presented and discussed. Two factors affecting the intensity of soiling were studied, namely: tilting solar mirrors and coating their reflective surfaces.

References of chapter IV

Abdelhafidi, N., Yilmaz, I.B., Bachari, N.E., 2020. An innovative dynamic model for an integrated solar combined cycle power plant under off-design conditions. *Energy Conversion and Management* 220, 113066. https://doi.org/10.1016/j.enconman.2020.113066

Alami Merrouni, A., Conceição, R., Mouaky, A., Silva, H.G., Ghennioui, A., 2020. CSP performance and yield analysis including soiling measurements for Morocco and Portugal. *Renewable Energy* 162, 1777–1792. https://doi.org/10.1016/j.renene.2020.10.014

Alami Merrouni, A., Wolfertstetter, F., Mezrhab, A., Wilbert, S., Pitz-Paal, R., 2015. Investigation of soiling effect on different solar mirror materials under Moroccan climate. *Energy Procedia* 69, 1948-1957. https://doi.org/10.1016/j.egypro.2015.03.194

Bellmann, P., Wolfertstetter, F., Conceição, R., Silva, H.G., 2020. Comparative modeling of optical soiling losses for CSP and PV energy systems. *Solar Energy* 197, 229–237. https://doi.org/10.1016/j.solener.2019.12.045

Benkouider, F., Abdellaoui, A., Hamami, L., 2019. New and improved Built-Up Index using SPOT imagery: application to an arid zone (Laghouat and M'Sila, Algeria). *Journal of the Indian Society of Remote Sensing* 47, 185-192. https://doi.org/10.1007/s12524-018-0895-7

Bouaddi, S., Ihlal, A., Fernández-García, A., 2015. Soiled CSP solar reflectors modeling using dynamic linear models. *Solar Energy* 122, 847-863. http://dx.doi.org/10.1016/j.solener.2015.09.044

Gourine, N., Yousfi, M., Bombarda, L., Nadjemi, B., Stocker, P., Gaydou, E.M., 2010. Antioxidant activities and chemical composition of essential oil of Pistacia atlantica from Algeria. *Industrial Crops Production* 31, 203–208. https://doi.org/10.1016/j.indcrop.2009.10.003

Griffith, D.J., Vhengani, L., Maliage, M., 2014. Measurements of mirror soiling at a candidate CSP site. *Energy Procedia* 49, 1371-1378. https://doi.org/10.1016/j.egypro.2014.03.146

Houyou, Z., Bielders, C.L., Benhorma, H.A., Dellal, A., Boutemdjet, A., 2016. Evidence of strong land degradation by wind erosion as a result of rainfed cropping in the Algerian steppe: A case study at Laghouat. *Land Degradation Development* 27, 1788–1796. https://doi.org/10.1002/ldr.2295

Khaldi, F., 2012. Energy and exergy analysis of the first hybrid solar-gas power plant in Algeria. Presented at the Proceedings of ECOS 2012 – The 25th international conference on efficiency, cost, optimization, simulation and environmental impact of energy systems; June 26-29, 2012, Perugia, Italy.

Matal, A., Karim, M., Naamane, S., 2020. Development and calibration of an experimental test bench simulating solar reflectors erosion. *Solar Energy* 201, 724-731. https://doi.org/10.1016/j.solener.2020.03.028

Michael, P.R., Johnston, D.E., Moreno, W., 2020. A conversion guide: solar irradiance and lux illuminance. *Journal of Measurements in Engineering* 8, 153-166. https://doi.org/10.21595/jme.2020.21667

Molineaux, B., Ineichen, P., Delaunay, J.J., 1995. Direct luminous efficacy and atmospheric turbidity improving model performance. *Solar Energy* 55, 125-137. https://doi.org/10.1016/0038-092X(95)00035-P

Picotti, G., Borghesani, P., Manzolini, G., Cholette, M.E., Wang, R., 2018. Development and experimental validation of a physical model for the soiling of mirrors for CSP industry applications. *Solar Energy* 173, 1287-1305. https://doi.org/10.1016/j.solener.2018.08.066

Saadoud, D., Guettouche, M.S., Hassani, M., Peinado, F.J.M., 2017. Modelling wind-erosion risk in the Laghouat region (Algeria) using geomatics approach. *Arabian Journal of Geoscience* 10, 363. https://doi.org/10.1007/s12517-017-3139-1

Vartiainen, V., 2000. A comparison of luminous efficacy models with illuminance and irradiance measurements. *Renewable Energy* 20, 265-277. https://doi.org/10.1016/S0960-1481(99)00115-9

Zereg, K., Gama, A., Aksas, M., Rathore, N., Yettou, F., Panwar, N.L., 2022. Dust impact on concentrated solar power: A review. *Environmental Engineering Research* 27, 210345. https://doi.org/10.4491/eer.2021.345

CHAPTER V – RESULTS AND DISCUSSION

V. 1. Effect of tilt angle

Due to the arid, dry, and hazy weather of the chosen site during the long-term exposure, the soiling intensity and patterns' variations with different inclination angles are clear from the visual inspection of the mirrors: the soiling is most intense for the horizontal position and decreases with increasing inclination, and the bidimensional distribution of dust deposition is - generally- homogenous as can be observed in Figure 5.1.a. The outdoor soiling campaign started after the last heavy rain event in early summer and ended right before the following one, resulting in 74 days without any type of cleaning (natural, manual, or automated), on the day of measurements of cumulus soiling, the daily values of GHI, WS, and RH are respectively 388.86 Wh/m^2, 3.13 m/s, and 33.33%. Even though the main raison behind optical losses is the deposition of dust on the reflective surfaces, another contributing factor is bird droppings which were observed on one of the exposed mirrors (Figure 5.1.b), compared to soiling, bird droppings is much more localized and would cause more severe optical losses.

The resulting optical losses and the respective dust quantities of the outdoor exposure are presented in Figure 5.2, the dust deposition and soiling rates are calculated using equations 4.3 and 4.2 respectively. As expected, and in accordance with the literature, dust deposition rate and tilt angle are inversely proportional, while the latter is proportional to soiling rate; since the negative sign of SR stands for the losses in optical performances, the intensity of soiling rate is inversely proportional to tilt angles, similarly to DDR.

Indeed, the horizontal mirror position is characterized by the maximum dust deposition rate (8.65 10^{-2} g/m^2/day), which is logical given the absence of the tangent component of the gravity that would contribute to the removal of dust particles for tilted mirrors, as this contribution increases with increasing inclination, the minimal DDR is 2.16 10^{-2} g/m^2/day characterizing the maximum tilt of 45°. Since more dust deposition reduces more the reflected DNI via scattering, absorption, and shadowing, the cleanliness drop is maximal for the horizontal tilt (-0.99%/day) and minimal for 45° tilt (-0.90%/day). The large difference observed in SR and DDR between the horizontal position and tilted ones leads to the recommendation of sloping solar mirrors at an angle, no matter how slight it is, in order to avoid maximal soiling.
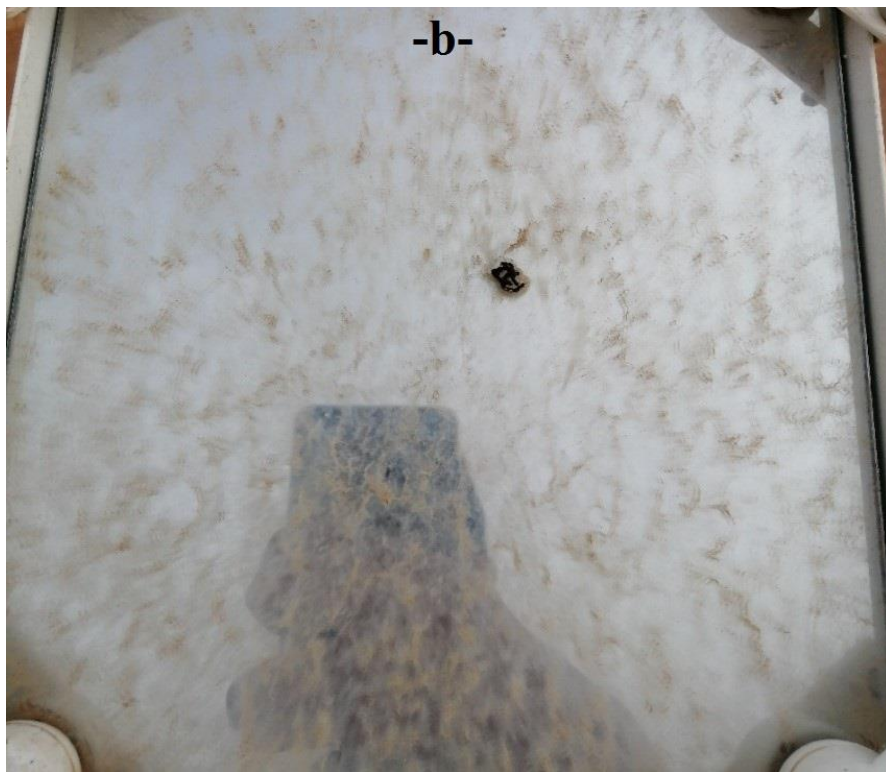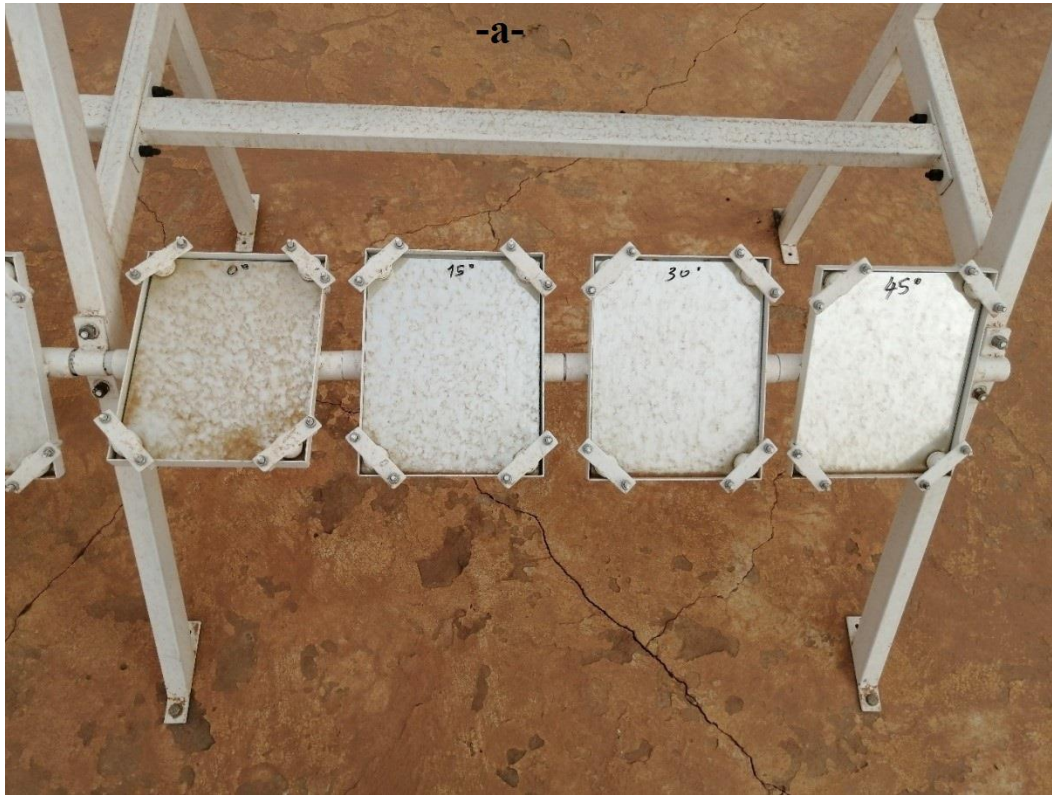
Figure 5.1. (a) Differently tilted mirrors in soiled state, **(b)** bird drops on an exposed mirror.
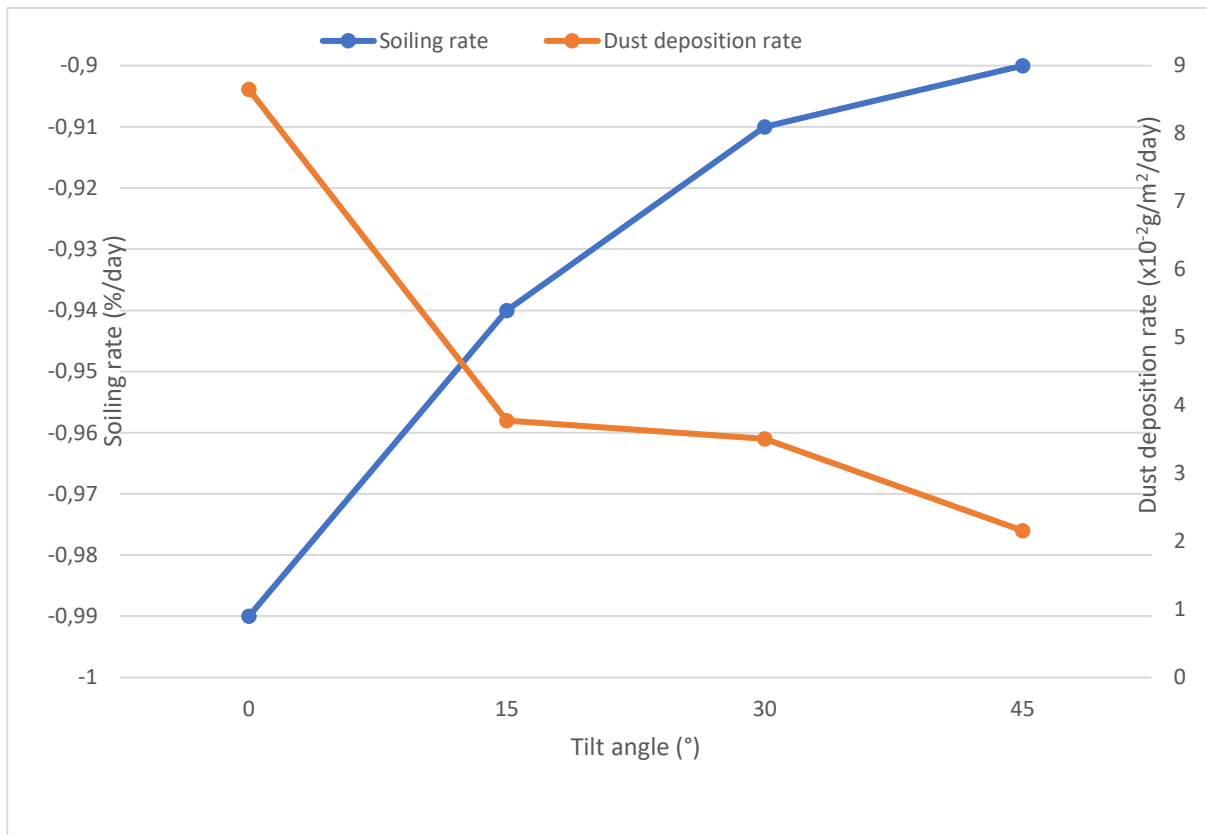
Figure 5.2. Effect of tilt angle on the long-term soiling and dust deposition rates of solar mirrors.

The variation of the cleanliness -which compares the reflectivity of the soiled mirror to its clean state- as function of the tilt angle is presented in Figure 5.3, losing 0.99% of its cleanliness per day, the horizontal mirror's cleanliness was as low as 26.6% after 74 days, while the soiling rate of -0.90%/day of the 45° mirror resulted in 33.18% cleanliness, these low cleanliness values were consequent to dust densities of 6.4 and 1.6 g/m^2 for the horizontal and 45° mirrors respectively (Figure 5.4), thus, the quantity of dust that soiled the horizontal mirror is four times the one that soiled the 45° one, and comparing the former to the 15° tilted mirror, a factor of 2.29 can be deduced, in other words, the deposition of dust on the horizontal mirror is at least double the less tilted mirror, which confirms that stowing mobile reflectors can be an efficient mitigation for dusting problems in CSP plants.

Since dust deposition mechanisms on CSP mirrors and PV modules are similar (Sarver et al., 2013), the reported DDRs are also valid for solar panels under similar climatic conditions.
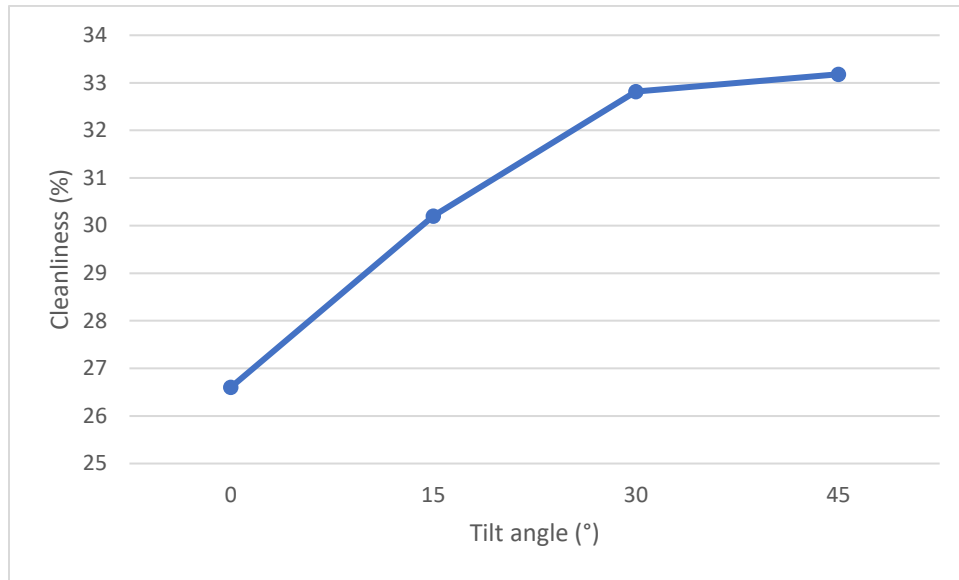
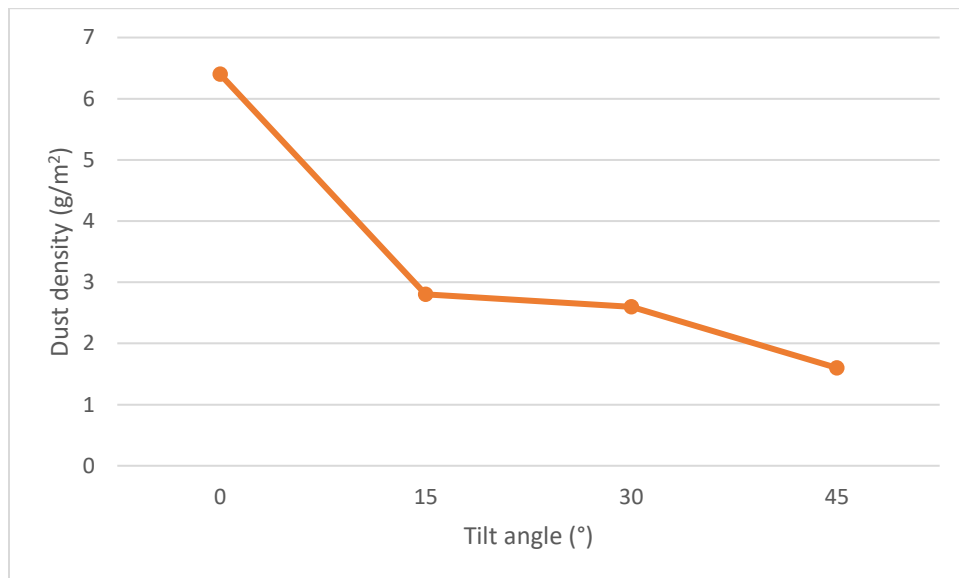**Figure 5.3.** Cleanliness index variation for different inclinations.

Figure 5.4. Dust density variation for different inclinations.

V. 2. Effect of coating application

Coating as a -sustainable and economic- mitigation for soiling issues of solar mirrors has been tested to evaluate its protective role, especially that the conventional mitigation for dusting problems in CSP plants is washing the mirrors, water, however, is usually a scarce resource in arid regions and should be preserved for local consumption. In addition, cleaning operations -

whether manual or automated- can be costly in remote sites, which makes coatings as a passive mitigation both a sustainable and an economic solution for solar reflectors' dusting problems.

A commercial coating has been used to protect the surfaces of two mirrors at tilts of 0° and 30°, which were exposed next to two uncoated mirrors at the same inclinations (Figure 5.5). The coating is acrylic based with supposed resistance to scratch, UV radiations, and weather parameters. 1 l of this coating would give approximatively 12 m^2 of 50 µm thick dry layer according to its technical note.

Figure 5.5. Mirrors exposed to study soiling mitigation by coating.

In Figure 5.6, we provide the dust deposition and soiling rates of the coated and uncoated mirrors after 74 days. It can be deduced that the coating's diminution of the intensity of dusting and the consequent cleanliness losses is more pronounced for the tilted mirrors than the horizontal ones. Certainly, the coating's application to the 30° tilted mirror resulted in a lesser soiling rate (-0.85%/day) than the uncoated identically tilted mirror (-0.93%/day), that is the equivalent of 0.08% cleanliness gain per day. This is expected since coating the reflective surfaces weakened the adhesion of dust particles to them, and the DDR diminution for the coated mirror was 1.62 10^{-2} g/m^2/day compared to the uncoated one, which is an important gain in optical performances (0.54 and 2.16 10^{-2} g/m^2/day of DDR for the coated and uncoated mirrors respectively). Whereas for the horizontal mirrors, coating one of them resulted in a slight 0.28 10^{-2} g/m^2/day DDR

diminution and consequently a 0.02%/day gain in SR, the coating is thus still of benefit even if it's not as important as for the 30° tilted mirror.
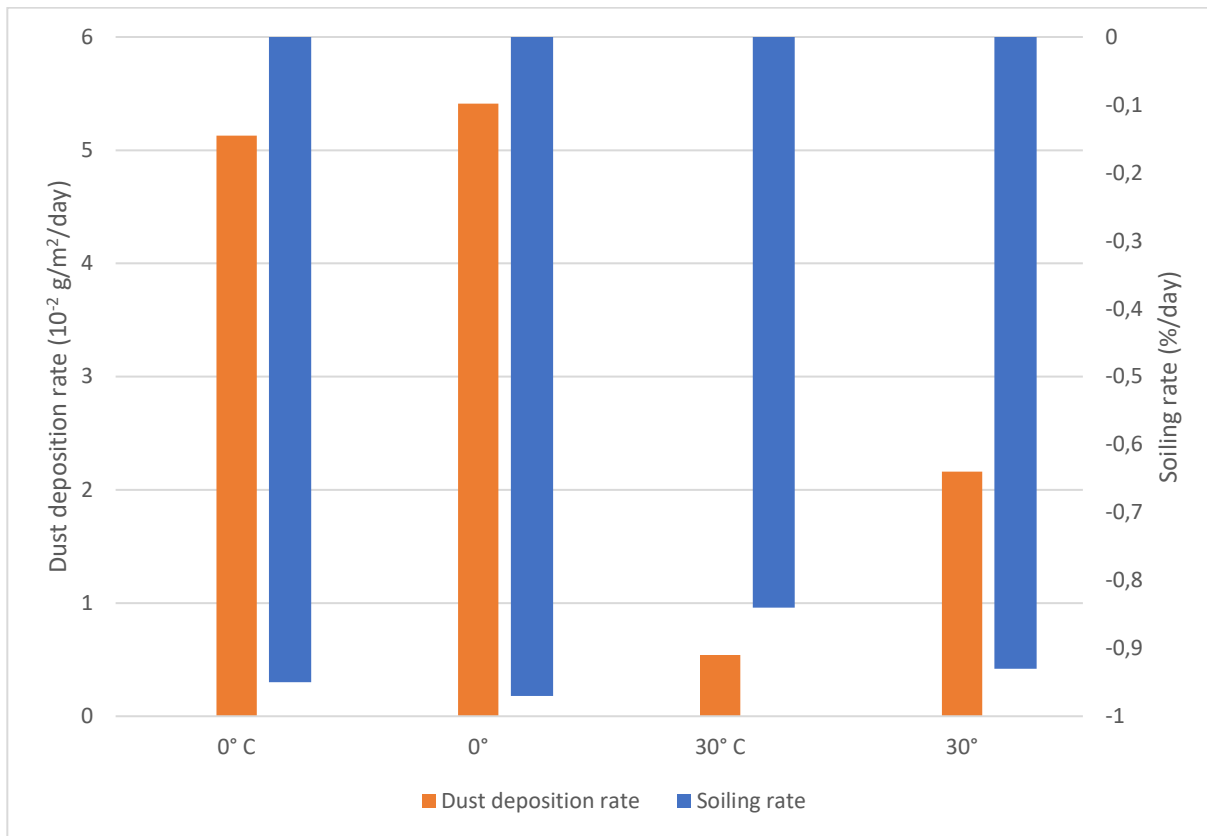

Figure 5.6. Effect of coating on the long-term soiling and dust deposition rates of solar mirrors.

The cleanliness index and dust density values for the different mirrors are displayed in Figures 5.7 and 5.8 respectively. After 74 days, the cleanliness index of the 30° coated mirror was 37.98% compared to 31.12% cleanliness for the 30° uncoated one, while for the horizontal position the values were 29.68% and 28.25% for the coated and uncoated mirrors respectively. Similarly, the dust density diminution was much more important for the tilted mirrors compared to the non-tilted ones: 1.2 and 0.2 g/m^2 respective differences between coated and uncoated mirrors. Physically speaking, this difference in optical behavior might be due to the fact that the soiling of horizontal mirrors is mainly due to gravity force (deposition of particles) much more than adhesive forces (attraction and attachment of particles), while for tilted mirrors, coating weakens the adhesive forces and the tangent component of gravity contributes to the removal as well.
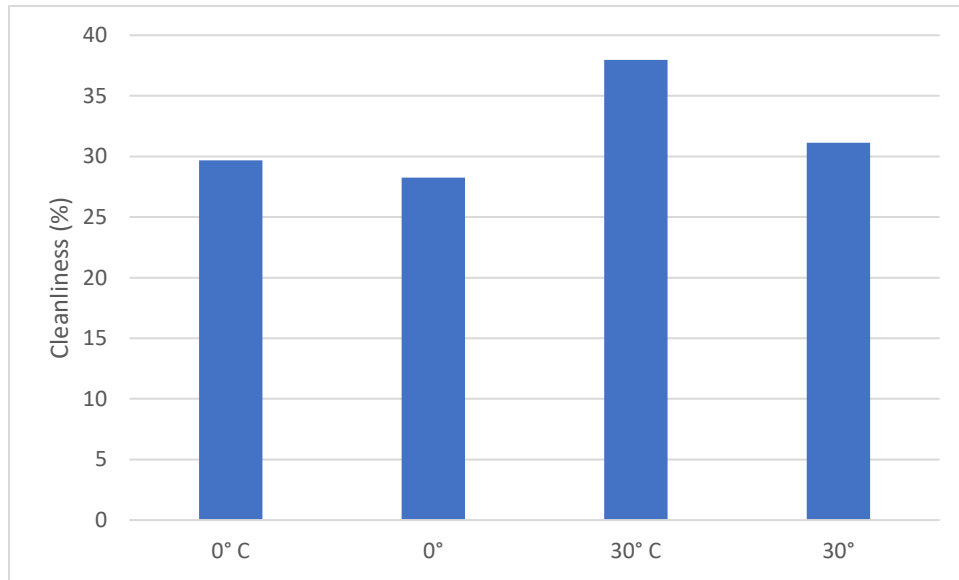
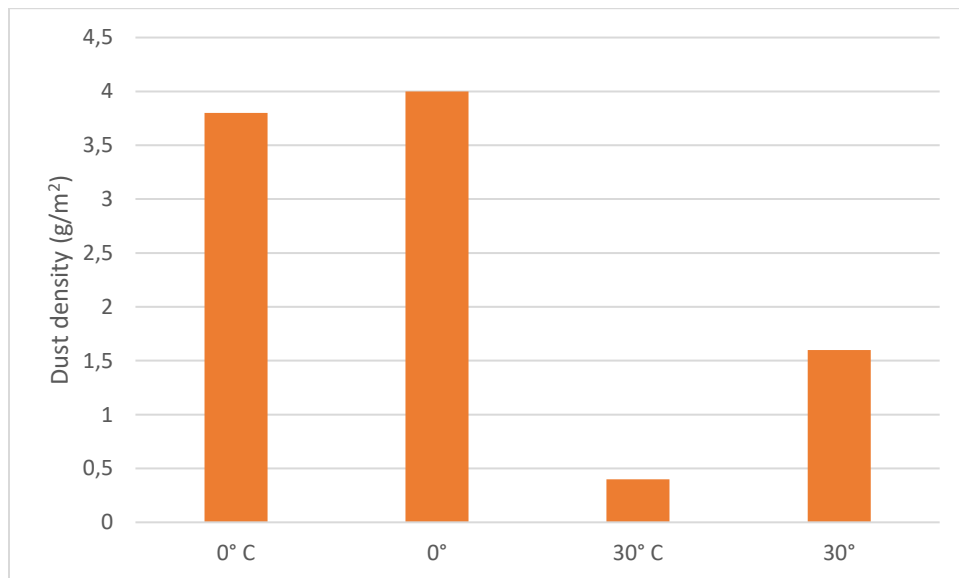**Figure 5.7.** Comparison of the cleanliness index for coated and uncoated mirrors.

Figure 5.8. Comparison of dust density for coated and uncoated mirrors.

V. 3. Effect of height difference

Very few works have studied this soiling factor (Wiesinger et al., 2021). As can be seen in Figure 4.4 of the experimental setup, the upper row was used to study the effect of coating and the lower row to study the effect of inclination, the height difference between the rows is 50 cm and thus it is expected that the upper row would accumulate less dust which is truly the case of the compared uncoated mirrors as shown in Figure 5.9. For the horizontal mirrors the DDR of the

bottom mirror was 8.65 against 5.41 10^{-2} g/m^2/day of the top one, while for the 30° tilted mirrors the DDR of the bottom and top mirrors were 3.51 and 2.16 10^{-2} g/m^2/day respectively. In regard to optical performance, the bottom horizontal mirror lost more cleanliness as a consequence of the more deposited dust on it, for the tilted mirrors however, the bottom mirror's cleanliness was slightly better than the top mirror's, this could be due to some unevenness in the distribution of dust particles which tend to pileup on the lower edge of tilted mirrors. The impact of height difference on soiling was not a principal objective of the present study, still, the expected greater accumulation of dust on the lower mirrors was confirmed.
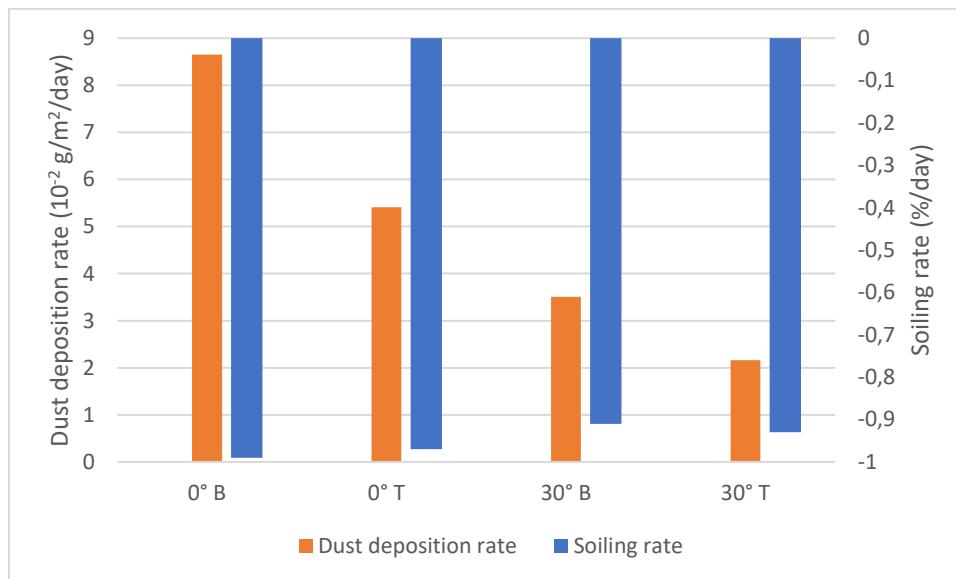

Figure 5.9. Effect of height on soiling and dust deposition rates (B: Bottom, T: Top).

## V. 4. Physical and chemical properties of deposited dust

In this section, the size, morphology, and chemical composition of random deposited dust particles obtained through characterization by scanning electron microscopy, energy dispersive X-ray spectroscopy, and X-rays diffraction are presented and analyzed.

Regarding dust particles' size, scanning electron microscopy images at scales of 350x, 1200x, and 6500x are shown in Figure 5.10. The range of the particles' diameter was smaller than 120 microns, this supports previous studies which reported that particles smaller than 200 microns should be used in laboratory soiling simulations since only particles in this range are found on

reflectors' surfaces, and confirms that particles bigger than 500 µm are lifted only by strong wind and rarely become airborne (Sansom et al., 2017; Wu et al., 2020).

As for the morphology of particles, angular, sharp particles are more numerous and bigger than round ones, which explains the considerable optical losses after 74 days, as sharper particles of Saharan dust would cause more damage to the reflective surface of solar mirrors than blunter, rounder particles. This confirms that the sharpness of particles has more negative impact than their hardness on the optical performances of solar mirrors as reported by previous studies such as (Endaya et al., 2019).

The results of the chemical composition analysis of the deposited dust by energy dispersive X-ray spectroscopy, and X-rays diffraction are provided in Figures 5.11, 5.12, and Table 5.1, the dominant elements are oxygen (O), carbon (C), silicon (Si), iron (Fe), calcium (Ca), and potassium (K), which indicates that the origin of dust is both natural and anthropogenic, that is expected given the exposure site is situated in the outskirts of Laghouat city (anthropogenic origin) near its surrounding mountains (natural origin).
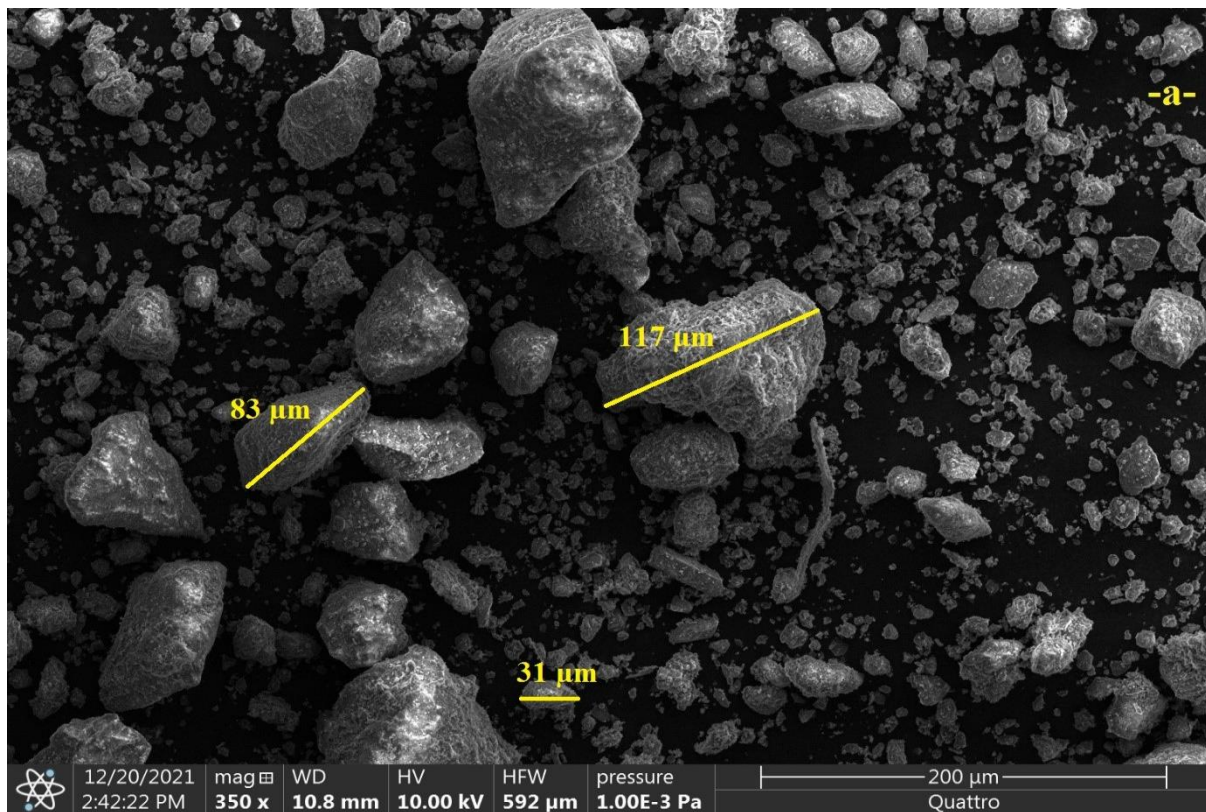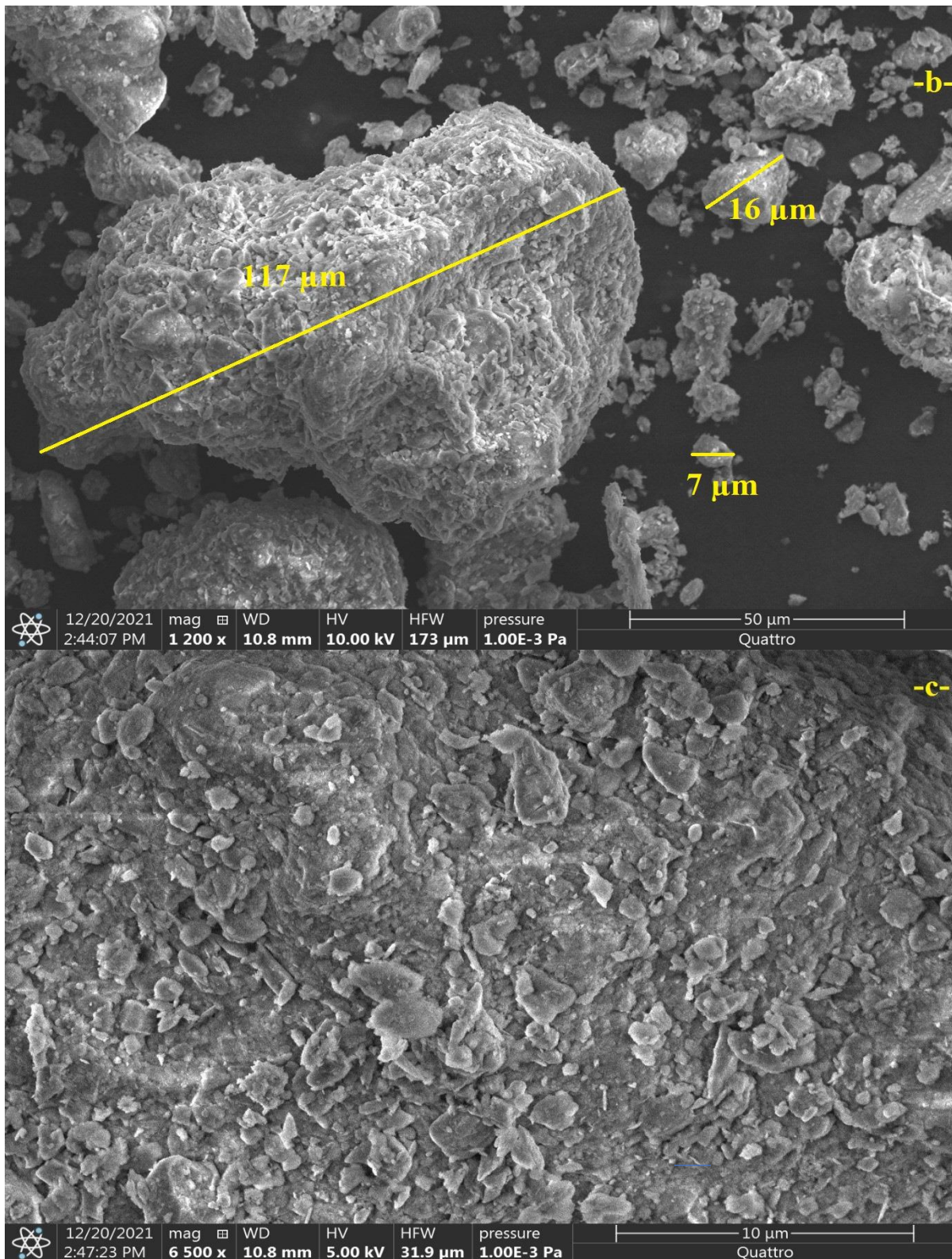
Figure 5.10. Scanning electron microscopic image of deposited dust: 350x **(a)**, 1200x **(b)**, 6500x **(c)**.
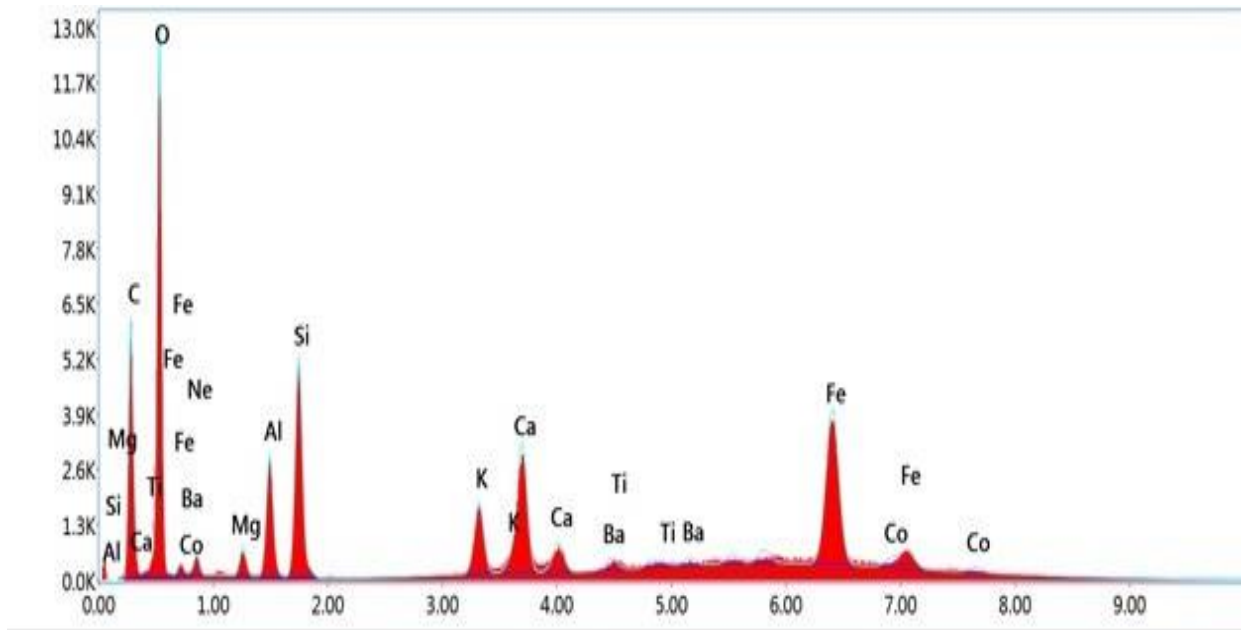
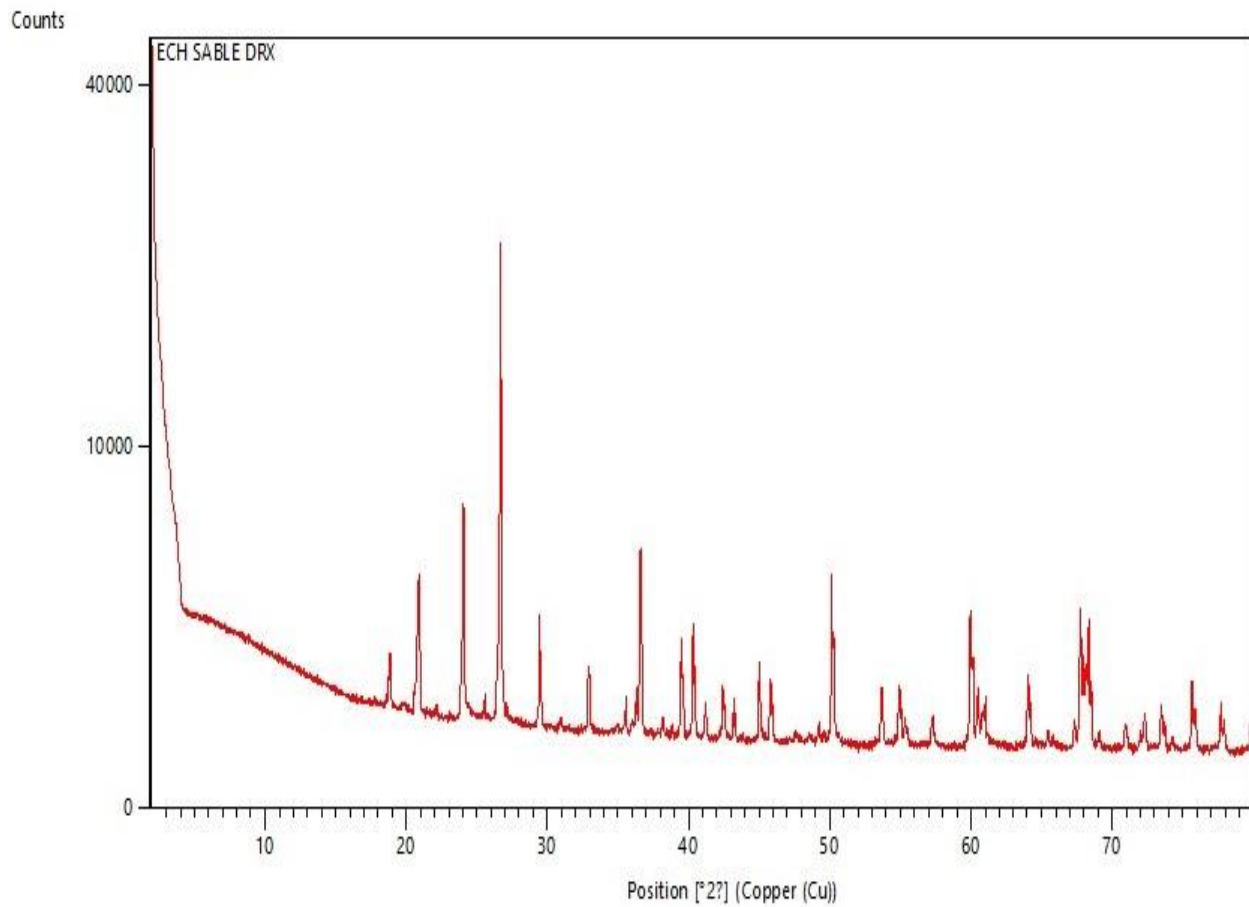**Figure 5.11.** Energy-dispersive X-ray spectroscopy of dust.

Figure 5.12. X-ray diffraction spectrum of dust.

Table 5.1: Chemical composition of Laghouat city's dust.

Element	Weight %	Atomic %
O K	50.39	53.13
C K	25.15	35.32
Fe K	7.47	2.26
Si K	4.69	2.82
Ca K	3.37	1.42
Al K	3.31	2.07
K K	1.61	0.69
Ne K	1.51	1.26
Mg K	1.11	0.77
Ba L	0.84	0.10
Co K	0.50	0.14
Ti K	0.06	0.02

V. 5. Summary

The results of the first outdoor study of solar mirrors' dusting under Algerian Sahara and factors affecting the intensity of soiling and dust deposition were presented and discussed in this chapter. Soiling of solar mirrors was pointed out as a confirmed source of reflectivity losses in Algerian Sahara, especially in remote sites.

The first studied factor was the tilt angle of solar mirrors, the widely reported inverse proportionality between soiling rate (as well as dust deposition rate) and inclination angles is confirmed. The range of reflective mirrors' soiling rate was between -0.90 and -0.99 %/day, the maximum value was recorded for the horizontal position and resulted in the lowest cleanliness (26.6 %) after 74 days without cleaning during the dry period of the year. The corresponding dust quantities were weighted as well and the dust deposition rate was in the range of 2.16 (45° tilt) to 8.65 (0° tilt) 10^{-2} g/m^2/day. The maximum optical loss and dust deposition on the horizontal reflectors led to the recommendation of tilting or stowing solar mirrors to avoid maximum soiling.

In order to assess water-economic, passive soiling mitigation, the second studied factor was coating reflective surfaces of mirrors. Coating as a preventive mitigation approach was proved to be of positive effect, especially for tilted mirrors for which coating resulted in gains of 0.08 %/day and 1.62 10^{-2} g/m^2/day in soiling rate and dust deposition rate respectively after 74 days, this makes coating application to solar reflectors both a sustainable and economic solution for dusting issues, especially in remote sites.

The physical and chemical properties of the collected dust were analyzed using scanning electron microscopy, energy dispersive X-ray spectroscopy, and X-rays diffraction. The particles were found to be sharp, smaller than 120 microns, and dominated by elements of both natural and anthropogenic origin.

The effect of height difference on the intensity of soiling was discussed as well and the deposition of dust (and the consequent cleanliness drop) was inversely proportional to height, as expected.

The achieved results are expected to be the subject of an eventual publication.

References of Chapter V

Endaya, E., Sansom, C., Comley, P., Almond, H., Dekam, I.E., Abdunnabi, M.J.R., 2019. Simulation of The Effect of Libyan Sand on The Reflectance Surface of CSP. *Solar Energy and Sustainable Development* 8, 33–46. http://jsesd.csers.ly/images/pdf/vol-008-02/vol-008-02-04.pdf

Sansom, C., Almond, H., King, P., Endaya, E., Bouaichaoui, S., 2017. Airborne sand and dust soiling of solar collecting mirrors. *AIP Conference Proceedings* 1850, 130011. https://doi.org/10.1063/1.4984505

Sarver, T., Al-Qaraghuli, A., Kazmerski, L.L., 2013. A comprehensive review of the impact of dust on the use of solar energy: History, investigations, results, literature, and mitigation approaches. *Renewable and Sustainable Energy Reviews* 22, 698-733. http://dx.doi.org/10.1016/j.rser.2012.12.065

Wiesinger, F., Sutter, F., Fernández-García, A., Wette, J., Hanrieder, N., 2021. Sandstorm erosion on solar reflectors: A field study on height and orientation dependence. *Energy* 217, 119351. https://doi.org/10.1016/j.energy.2020.119351

Wu, Z., Yan, S., Wang, Z., Ming, T., Zhao, X., Ma, R., Wu, Y., 2020. The effect of dust accumulation on the cleanliness factor of a parabolic trough solar concentrator. *Renewable Energy* 152, 529–539. https://doi.org/10.1016/j.renene.2020.01.091

CONCLUSION

The following research objectives were aimed: a) the publication of a literature review dedicated to the effects of dust on the performance of concentrated solar power plants, including solar tower plants; b) evaluation of optical losses in solar tower plants due to the deposition of dust, which was done through outdoor exposition of flat mirrors (assimilating heliostats), followed by in-situ measurements of the consequent optical losses and quantitative dust deposition; c) assessment of economic mitigation approach in the image of anti-soiling coating, very suitable for desertic sites with water scarcity.

The first chapter of the thesis' manuscript precised the motivation of our research, and introduced the reader to some basic notions required to grasp the essential of the work.

In *Chapter II*, we provided a comprehensive theoretical background of reflectivity losses due to soiling and extinction due to atmospheric turbidity, which are the two main sources of optical losses consequent to the presence of aerosols. This chapter is not limited to the context of the thesis and can be extended to the mechanisms of soiling of flat surfaces in general, as well as -in its second part- climatologic turbidity-related phenomena. The reason why the theoretical background preceded the literature review, which might seem unusual, is the necessity of the introduction of various parameters and phenomena which are mandatory to the understanding of the comprehensive literature review, which is why the reader was asked to refer to Chapter II multiple times in the literature review.

As already mentioned, the *Chapter III* consists of a literature review, presenting the essential of our previously published in-depth review of the studies related to dust and aerosols issues in concentrated solar power plants, the review paper is the first to review such issues for CSP technologies, and to the moment of the redaction of this chapter, it is the only one, and has been sited seven times.

The chapter to follow explained the methodology used to obtain the experimental evaluation of dust effect on solar mirrors, it includes climatologic and geologic description of the exposure site, the characterization of the experimental setup, as well as pursued methodology to measure the optical losses and the correlated dust quantities.

In *Chapter V*, the results of the first outdoor solar mirrors' soiling measurements' campaign in Algeria were presented and discussed. The effect of the inclination on the intensity of soiling and

the density of dust was assessed, as expected theoretically -and as reported by numerous previously published papers- the intensity of soiling is inversely proportional to tilt angle (with regards to the horizon), indeed, this is due to the fact that the main driving force of soiling is the perpendicular component of gravity, which is maximum at the horizontal position, thus the maximum soiling intensity characterizing this position. The application of an anti-soiling coating as mitigation to dusting issues was assessed, this dry mitigation method is promising, for that it is economic both in effort and water resources, which makes it suitable to desertic sites, especially remote ones. Even though it was not a primary object, the effect of height difference on soiling intensity was assessed as well, and the intensity of soiling is inversely proportional to height. The physical and chemical characterization of collected dust particles was performed as well, by means of scanning electron microscopy, energy dispersive X-ray spectroscopy, and X-rays diffraction. The obtained results are expected to be the subject of an eventual research paper.

We believe that the present thesis entitled "Evaluation of aerosols' effect on the efficiency ofsolar tower power plants in Algeria" achieved its aimed purposes, especially in the light of theabsence of support in terms of experimental means, which obliged the PhD candidate to resort tohis own means for most of the time. Not to mention that coronavirus (COVID19) pandemic andthe consequent lockdown took place shortly after the beginning of the thesis, which resulted inthe delay of the conducted -outdoor- experimental part of the thesis.

Future work is expected to be about the establishment of the first cartography of aerosols content in Algeria, as well as the assessment of the benefit of electrodynamic screens in mitigating-under Algerian Saharan climate- the intensity of soiling and, consequently, improving the optical efficiency of solar mirrors.